

Air Force Institute of Technology

AFIT Scholar

Theses and Dissertations

Student Graduate Works

6-2006

Effects of Frequency and Environment on Fatigue Behavior of an Oxide-Oxide Ceramic Matrix Composite at 1200°C

Griffin Hetrick

Follow this and additional works at: <https://scholar.afit.edu/etd>



Part of the [Ceramic Materials Commons](#), and the [Engineering Science and Materials Commons](#)

Recommended Citation

Hetrick, Griffin, "Effects of Frequency and Environment on Fatigue Behavior of an Oxide-Oxide Ceramic Matrix Composite at 1200°C" (2006). *Theses and Dissertations*. 3544.

<https://scholar.afit.edu/etd/3544>

This Thesis is brought to you for free and open access by the Student Graduate Works at AFIT Scholar. It has been accepted for inclusion in Theses and Dissertations by an authorized administrator of AFIT Scholar. For more information, please contact AFIT.ENWL.Repository@us.af.mil.



**EFFECTS OF FREQUENCY AND ENVIRONMENT ON FATIGUE BEHAVIOR
OF AN OXIDE-OXIDE CERAMIC MATRIX COMPOSITE AT 1200°C**

THESIS

Griffin Hetrick, Ensign, USN

AFIT/GAE/ENY/06-J05

**DEPARTMENT OF THE AIR FORCE
AIR UNIVERSITY**

AIR FORCE INSTITUTE OF TECHNOLOGY

Wright-Patterson Air Force Base, Ohio
APPROVED FOR PUBLIC RELEASE; DISTRIBUTION IS UNLIMITED.

The views expressed in this thesis are those of the author and do not reflect the official policy or position of the United States Air Force, Department of Defense, or the U.S. Government.

AFIT/GAE/ENY/06-J05

**EFFECTS OF FREQUENCY AND ENVIRONMENT ON FATIGUE BEHAVIOR
OF AN OXIDE-OXIDE CERAMIC MATRIX COMPOSITE AT 1200°C**

THESIS

Presented to the Faculty

Department of Aeronautical and Astronautical Engineering

Graduate School of Engineering and Management

Air Force Institute of Technology

Air University

Air Education and Training Command

In Partial Fulfillment of the Requirements for the
Degree of Master of Science in Aeronautical Engineering

Griffin Hetrick, B.S.M.E.

Ensign, USN

June 2006

APPROVED FOR PUBLIC RELEASE; DISTRIBUTION IS UNLIMITED

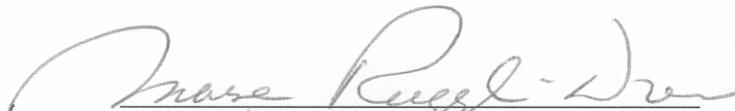
AFIT/GAE/ENY/06-J05

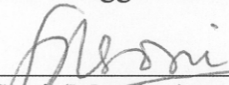
**EFFECTS OF FREQUENCY AND ENVIRONMENT ON FATIGUE BEHAVIOR
OF AN OXIDE-OXIDE CERAMIC MATRIX COMPOSITE AT 1200°C**

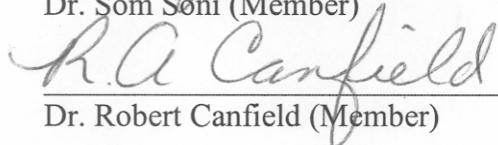
Griffin Hetrick, B.S.M.E.

Ensign, USN

Approved:


Dr. Marina B. Ruggles-Wrenn (Chairman)


Dr. Som Soni (Member)


Dr. Robert Canfield (Member)

1 JUN 2006
date

2 Jun 2006
date

1 Jun 06
date

Abstract

Advances in aeronautical engineering in the 21st century depend upon materials that can perform well in extreme environments such as high temperatures and oxidizing conditions. Nextel™720/Alumina (N720/A) is an oxide/oxide ceramic matrix composite with a porous alumina matrix that has been identified as a candidate material for such applications. This research investigated the effects of frequency on fatigue response of N720/A at 1200°C in both air and steam environment. Prior investigation of this material by Eber [8] in 2005 studied fatigue behavior at 1200°C in air and in steam environments at the frequency of 1.0 Hz. The current research focused on fatigue response at the frequencies of 0.1 Hz and 10 Hz.

Results of mechanical testing showed a significant decrease in fatigue performance in steam versus air. Specimens tested at 0.1 Hz exhibited shorter fatigue lives and smaller strains at failure than those tested at 10 Hz. Scanning Electron Micrographs of specimen fracture surfaces revealed higher degrees of fiber pull-out and greater variation in fiber failure locations in specimens tested at 10 Hz, indicating a weakening of the fiber/matrix interface. Qualitative assessment using Energy Dispersive Spectroscopy showed correlations between frequency and amount of silicon species migration between fiber and matrix.

Acknowledgments

I would like to offer my heartfelt thanks to the following individuals who aided in the completion of this research: Dr. Marina Ruggles-Wrenn for her sage advice and support throughout the entirety of this work, Dr. Joseph Zelina and Dr. Ruth Sikorski (AFRL/PRTC) for sponsoring this research, Dr. Seungsu Baek for his professional assistance with microscopy, Barry Page for set-up and servicing of test equipment, fellow students Capt. John Mehrman, Lt. Patrick Jackson, and Lt. Jennifer Ryba for their help with materials testing, ENS Gregory Siegert for his friendship and support, and to my family for their love and encouragement.

Griffin Hetrick

AFIT/GAE/ENY/06-J05

To my father and the Bulldogs of the 525th TFS.

Table of Contents

	Page
List of Figures.....	ix
List of Tables	xviii
1 Introduction.....	1
2 Applications and Background	3
2.1 Ceramic Matrix Composites	3
2.1.1 Introduction to continuous fiber ceramic composites	3
2.1.2 Traditional ceramic matrix composites.....	5
2.1.3 Oxide/oxide ceramic matrix composites.....	6
2.1.4 Nextel™ 720/Alumina CMC	7
2.1.5 Fatigue Performance of CMCs	10
2.2 Ceramic Matrix Composites in Aerospace Applications.....	12
3 Experimental Setup	16
3.1 Specimen Preparation	16
3.2 Test Equipment	18
3.3 Environmental Controls	20
3.4 Microstructural Characterization	22
4 Results and Discussion	28
4.1 Section Summary	28
4.2 Thermal Expansion	29
4.3 Fatigue in laboratory air at the frequency of 0.1 Hz	30
4.3.1 Strain and stiffness data	30
4.3.2 Residual Strength and Stiffness	33
4.4 Fatigue in steam environment at the frequency of 0.1 Hz	34
4.4.1 Strain and Stiffness Data.....	34
4.4.2 Energy Dissipation.....	37
4.5 Cyclic loading at the frequency of 10 Hz in steam at 1200 °C	40
4.6 Conclusions on the effects of frequency on fatigue in steam	43

	Page
5 Fracture Surface Investigation	45
5.1 Optical Microscopy	45
5.1.1 Tensile failure in air	45
5.1.2 Fatigue failure in steam at the frequency of 0.1 Hz	46
5.1.3 Effect of frequency on fracture surface characteristics	49
5.2 Scanning Electron Microscopy	51
5.2.1 General SEM observations	51
5.2.2 ESEM micrographs and discussion	52
5.2.3 Fracture surface observation in high vacuum SEM mode	57
5.3 Energy Dispersive X-ray Spectroscopy (EDS)	61
6 Conclusions and Recommendations	69
6.1 Conclusions	69
6.1.1 Mechanical testing in air	69
6.1.2 Mechanical Testing in Steam	69
6.1.3 Microscopy	70
6.1.4 Spectroscopy	71
6.1.5 Final Conclusions	71
6.2 Recommendations for Further Work	72
Appendix A Additional Micrographs	73
Bibliography	93
Vita	98

List of Figures

	Page
Figure 1. Strength to weight ratio versus temperature for various materials. From reference [38].	4
Figure 2. Surface of as-received Nextel 720/A specimen showing matrix cracking and matrix infiltration within fiber bundles. From reference [11;27].	9
Figure 3. Fracture surface of a Nextel 720/A specimen tested in fatigue at 1200°C in steam environment with the frequency of 0.1 Hz and maximum stress of 170 MPa showing crack deflection around 90° fibers.	9
Figure 4. Diagram highlighting time spent above a given stress level at different frequencies.	11
Figure 5. Pollutant emission as a function of combustion temperature. From reference [29].	13
Figure 6. Turbine components with potential for CMC applications. From reference [27].	14
Figure 7. Test specimen, dimensions in mm.	16
Figure 8. Tabbed N720/A CMC specimen.	17
Figure 9. MTS equipment setup.	18
Figure 10. Close-up view of extensometer during high-temperature testing.	19
Figure 11. AMTECO furnace with control thermocouples.	20
Figure 12. Photographs of alumina susceptor showing: (A) susceptor assembly and (B) susceptor with test specimen and furnace.	22
Figure 13. SEM and EDAX equipment.	23
Figure 14. Uncoated N720/A specimens prepared for SEM observation.	25
Figure 15. Diagram of load as a function of time over a span of 10 seconds for the frequencies of 0.1, 1.0, and 10 Hz. Figure is not to scale.	26
Figure 16. Typical test procedure.	27

Figure 17. Maximum and minimum strain versus cycle number for fatigue of N720/A in air at 1200°C with maximum stress level of 170 MPa. Data from reference [8:32] is also included.	31
Figure 18. Normalized stiffness as a function of cycle number for the specimen tested at 1200°C in air with the frequency of 0.1 Hz. Data from reference [8:26] is also included.	32
Figure 19. Maximum strain as a function of cycle number for N720/A specimens subjected to fatigue testing in steam at 1200°C with the frequency of 0.1 Hz and maximum stresses of 170, 150, 125, 100, and 75 MPa.	35
Figure 20. Normalized stiffness as a function of cycle number for N720/A specimens subjected to fatigue testing in steam at 1200°C with the frequency of 0.1 Hz and maximum stresses of 170, 150, 125, 100, and 75 MPa.	36
Figure 21. Illustration of typical quadrilateral used in hysteresis energy density calculations, including hysteresis loop for the initial cycle of the specimen tested in steam at 1200°C with the frequency of 0.1 Hz and maximum stress of 170 MPa.	37
Figure 22. Hysteresis energy density as a function of cycle number for N720/A specimens subjected to fatigue testing in steam at 1200°C with the frequency of 0.1 Hz and maximum stresses of 170, 150, 125, 100, and 75 MPa.	39
Figure 23. Maximum strain as a function of cycle number for N720/A specimens subjected to fatigue testing in steam at 1200°C with the frequency of 10 Hz and maximum stresses of 170 and 150 MPa.	41
Figure 24. Normalized stiffness as a function of cycle number for N720/A specimens subjected to fatigue testing in steam at 1200°C with the frequency of 10 Hz and maximum stresses of 170 and 150 MPa.	42
Figure 25. Times to failure for N720/A specimens subjected to fatigue in steam at 1200°C. Data from reference [8:43] is also included.	43
Figure 26. Maximum stress versus failure strain for N720/A specimens tested in fatigue at 1200°C in steam environment. Strains for specimens that achieved run-out are denoted by an arrow. Run-out strains are equivalent to the maximum strain at run-out. Note that no run-outs were achieved for the frequency of 0.1 Hz. Data from reference [8:43] is included.	44

- Figure 27. Fracture surfaces of Nextel 720/A specimens tested in tension following survival of 10^5 cycles at 1200°C in air environment (maximum stress = 170 MPa) at frequencies of: (a) 0.1 Hz, and (b) 1.0 Hz. Micrograph of specimen tested at 1.0 Hz is from reference [8]. 46
- Figure 28. Fracture surfaces of Nextel 720/A specimens tested in fatigue at 1200°C in steam environment at maximum stresses of: (a,d) 100 MPa, (b,e) 125 MPa, and (c,f) 150 MPa, and frequencies of: (a,b,c) 10 Hz, and (d,e,f) 0.1 Hz. Specimens tested at 1.0 Hz exhibit higher degrees of fiber pull-out than those tested at the frequency of 0.1 Hz. Micrographs (a,b,c) are from reference [8]. 47
- Figure 29. Fracture surfaces of Nextel 720/A specimens tested in fatigue at 1200°C in steam environment (frequency = 0.1 Hz) at maximum stresses of: (a) 150 MPa, (b) 125 MPa, (c) 100 MPa, and (d) 75 MPa. 48
- Figure 30. Fracture surfaces of Nextel 720/A specimens tested in fatigue at 1200°C in steam environment (maximum stress = 170 MPa) at frequencies of: (a) 0.1 Hz, (b) 1.0 Hz, and (c) 10 Hz. Damage zone size and fiber pullout increase with frequency. Micrograph (b) is from reference [8]. 49
- Figure 31. Fracture surfaces of Nextel 720/A specimens tested in fatigue at 1200°C in steam environment (maximum stress = 10 Hz) at frequencies of: (A) 0.1 Hz, and (B) 10 Hz. The specimen tested with the frequency of 10 Hz exhibits greater variation in fiber failure location. 50
- Figure 32. Fracture surface of a Nextel 720/A specimen tested in fatigue at 1200°C in steam environment (maximum stress = 75 MPa, frequency = 0.1 Hz) with emphasis placed on areas of: (A) crack deflection around fibers, (B) fiber pull-out, and (C) coordinated failure. 51
- Figure 33. Fracture surfaces of Nextel 720/A specimens tested in fatigue at 1200°C in steam environment (frequency = 0.1 Hz) at maximum stresses of: (a,b) 170 MPa, and (c,d) 150 MPa. All micrographs exhibit both areas of coordinated fracture and fiber pull-out. 52
- Figure 34. Fracture surfaces of Nextel 720/A specimens tested in fatigue at 1200°C in steam environment (frequency = 0.1 Hz) at maximum stresses of: (a,b) 125 MPa, (c,d) 100 MPa. All micrographs exhibit both areas of coordinated fracture and fiber pull-out. 53

- Figure 35. Fracture surfaces of Nextel 720/A specimens tested in fatigue at 1200°C in steam environment (frequency = 0.1 Hz) at maximum stresses of: (a) 170 MPa, (b) 150 MPa, (c) 125 MPa, and (d) 100 MPa. Micrographs show: (a) coordinated fiber failure, (b,c,d) fiber pull-out. 54
- Figure 36. Fracture surface of a Nextel 720/A specimen tested in fatigue at 1200°C in steam environment (maximum stress = 170 MPa, frequency = 10 Hz) showing extensive fiber pull-out. Damage zone is seen in Figures 30 (c) and 31 (B). .. 55
- Figure 37. Fracture surface of a Nextel 720/A specimen tested in fatigue at 1200°C in steam environment (maximum stress = 170 MPa, frequency = 10 Hz) showing pulled-out fibers of varying lengths. Note the large pieces of matrix material attached to some fibers (circled). 56
- Figure 38. Fracture surfaces of Nextel 720/A specimens tested in fatigue at 1200°C in steam environment (maximum stress = 170 MPa) at frequencies of: (a,b) 10 Hz, and (c,d) 0.1 Hz. Micrographs (b) and (d) exhibit small pieces of matrix attached to the exposed fibers. 57
- Figure 39. Fracture surface of a Nextel 720/A specimen tested in fatigue at 1200°C in steam environment (maximum stress = 170 MPa, frequency = 10 Hz) showing wooly fibers located deep within the specimen fracture surface..... 59
- Figure 40. Fracture surface of a Nextel 720/A specimen tested in fatigue at 1200°C in steam environment (maximum stress = 170 MPa, frequency = 10 Hz) showing: (a) crack deflection around 0° fibers, and (b) a magnified view of the same area. 60
- Figure 41. EDS spectra of fiber and matrix of N720/A composite tested in fatigue at 1200°C in steam environment with maximum stresses 170 MPa and frequency 63
- Figure 42. Fracture surfaces of Nextel 720/A specimens tested in fatigue at 1200°C in steam environment with maximum stresses and frequencies: (a) 170 MPa, 0.1 Hz, (b) 75 MPa, 0.1 Hz, (c) 170 MPa, 10 Hz. Areas analyzed with EDS are indicated on each micrograph as follows: T(a), T(b), and T(c) indicate matrix troughs left by pulled out fibers, while M(a), M(b), and M(c) indicate matrix interior. 64
- Figure 43. EDS spectra of matrix from three N720/A specimens tested in fatigue at 1200°C in steam environment with maximum stresses and frequencies of: 170 MPa and 0.1 Hz, 75 MPa and 0.1 Hz, and 170 MPa and 10 Hz. 65

Figure 44. EDS spectra of matrix near fiber edge from two N720/A specimens tested in fatigue at 1200°C in steam environment with maximum stress 170 MPa and frequencies of 0.1 Hz and 10 Hz.	66
Figure 45. EDS spectra of matrix near fiber edge from two N720/A specimens tested in fatigue at 1200°C in steam environment with the frequency of 0.1 Hz and maximum stresses of 170 MPa and 75 MPa.	67
Figure 46. Fracture surface of a Nextel 720/A specimen tested in fatigue at 1200°C in steam environment (maximum stress = 170 MPa, frequency = 0.1 Hz) showing 90° fiber bundle.	73
Figure 47. Fracture surface of a Nextel 720/A specimen tested in fatigue at 1200°C in steam environment (maximum stress = 170 MPa, frequency = 0.1 Hz) showing coordinated failure of a 0° fiber bundle.	73
Figure 48. Fracture surface of a Nextel 720/A specimen tested in fatigue at 1200°C in steam environment (maximum stress = 170 MPa, frequency = 0.1 Hz) showing 0° fibers at the edge of a 90° bundle.	74
Figure 49. Fracture surface of a Nextel 720/A specimen tested in fatigue at 1200°C in steam environment (maximum stress = 170 MPa, frequency = 0.1 Hz) showing matrix rich area.	74
Figure 50. Fracture surface of a Nextel 720/A specimen tested in fatigue at 1200°C in steam environment (maximum stress = 150 MPa, frequency = 0.1 Hz) showing 90° fibers with variation in failure location.	75
Figure 51. Fracture surface of a Nextel 720/A specimen tested in fatigue at 1200°C in steam environment (maximum stress = 150 MPa, frequency = 0.1 Hz) showing both pull-out and coordinated failure in a single tow.	75
Figure 52. Fracture surface of a Nextel 720/A specimen tested in fatigue at 1200°C in steam environment (maximum stress = 150 MPa, frequency = 0.1 Hz) showing matrix rich area with isolated fiber pull-out.	76
Figure 53. Fracture surface of a Nextel 720/A specimen tested in fatigue at 1200°C in steam environment (maximum stress = 150 MPa, frequency = 0.1 Hz) showing matrix rich area with matrix troughs from 0° fibers.	76

Figure 54. Fracture surface of a Nextel 720/A specimen tested in fatigue at 1200°C in steam environment (maximum stress = 125 MPa, frequency = 0.1 Hz) showing fiber pull-out.....	77
Figure 55. Fracture surface of a Nextel 720/A specimen tested in fatigue at 1200°C in steam environment (maximum stress = 125 MPa, frequency = 0.1 Hz) showing matrix rich area within 0° fiber bundle.	77
Figure 56. Fracture surface of a Nextel 720/A specimen tested in fatigue at 1200°C in steam environment (maximum stress = 125 MPa, frequency = 0.1 Hz) showing 0° fiber pull-out.	78
Figure 57. Fracture surface of a Nextel 720/A specimen tested in fatigue at 1200°C in steam environment (maximum stress = 125 MPa, frequency = 0.1 Hz) showing matrix rich areas with well-formed matrix troughs from 0° fibers.	78
Figure 58. Fracture surface of a Nextel 720/A specimen tested in fatigue at 1200°C in steam environment (maximum stress = 125 MPa, frequency = 0.1 Hz) showing 90° fiber bundle.	79
Figure 59. Fracture surface of a Nextel 720/A specimen tested in fatigue at 1200°C in steam environment (maximum stress = 125 MPa, frequency = 0.1 Hz) showing coordinated fracture.....	79
Figure 60. Fracture surface of a Nextel 720/A specimen tested in fatigue at 1200°C in steam environment (maximum stress = 125 MPa, frequency = 0.1 Hz) showing 0° fiber pull-out at high magnification.	80
Figure 61. Fracture surface of a Nextel 720/A specimen tested in fatigue at 1200°C in steam environment (maximum stress = 100 MPa, frequency = 0.1 Hz) showing 0° and 90° fiber bundles.	80
Figure 62. Fracture surface of a Nextel 720/A specimen tested in fatigue at 1200°C in steam environment (maximum stress = 100 MPa, frequency = 0.1 Hz) showing 0° fiber bundle with variation in fracture location.	81
Figure 63. Fracture surface of a Nextel 720/A specimen tested in fatigue at 1200°C in steam environment (maximum stress = 100 MPa, frequency = 0.1 Hz) showing 0° fiber bundles with matrix-rich area.....	81

Figure 64. Fracture surface of a Nextel 720/A specimen tested in fatigue at 1200°C in steam environment (maximum stress = 100 MPa, frequency = 0.1 Hz) showing well-formed matrix shape at high magnification.	82
Figure 65. Fracture surface of a Nextel 720/A specimen tested in fatigue at 1200°C in steam environment (maximum stress = 100 MPa, frequency = 0.1 Hz) showing 0° pulled-out fiber surfaces.	82
Figure 66. Fracture surface of a Nextel 720/A specimen tested in fatigue at 1200°C in steam environment (maximum stress = 75 MPa, frequency = 0.1 Hz) showing overall fracture surface.	83
Figure 67. Fracture surface of a Nextel 720/A specimen tested in fatigue at 1200°C in steam environment (maximum stress = 75 MPa, frequency = 0.1 Hz) showing separate 0° fiber tows.	83
Figure 68. Fracture surface of a Nextel 720/A specimen tested in fatigue at 1200°C in steam environment (maximum stress = 75 MPa, frequency = 0.1 Hz) showing 0° fiber tow with matrix-rich areas.	84
Figure 69. Fracture surface of a Nextel 720/A specimen tested in fatigue at 1200°C in steam environment (maximum stress = 75 MPa, frequency = 0.1 Hz) showing 0° pulled-out fibers.	84
Figure 70. Fracture surface of a Nextel 720/A specimen tested in fatigue at 1200°C in steam environment (maximum stress = 75 MPa, frequency = 0.1 Hz) showing separate 90° fiber tow with matrix rich area and pull-out.	85
Figure 71. Fracture surface of a Nextel 720/A specimen tested in fatigue at 1200°C in steam environment (maximum stress = 75 MPa, frequency = 0.1 Hz) showing matrix cavities from 0° fibers.	85
Figure 72. Fracture surface of a Nextel 720/A specimen tested in fatigue at 1200°C in steam environment (maximum stress = 170 MPa, frequency = 10 Hz) showing 90° fibers.	86
Figure 73. Fracture surface of a Nextel 720/A specimen tested in fatigue at 1200°C in steam environment (maximum stress = 170 MPa, frequency = 10 Hz) showing 90° fiber bundle.	86

Figure 74. Fracture surface of a Nextel 720/A specimen tested in fatigue at 1200°C in steam environment (maximum stress = 170 MPa, frequency = 10 Hz) showing 0° fiber bundle.	87
Figure 75. Fracture surface of a Nextel 720/A specimen tested in fatigue at 1200°C in steam environment (maximum stress = 170 MPa, frequency = 10 Hz) showing 0° fiber pull-out.	87
Figure 76. Fracture surface of a Nextel 720/A specimen tested in fatigue at 1200°C in steam environment (maximum stress = 170 MPa, frequency = 0.1 Hz) showing 0° fiber surface.	88
Figure 77. Fracture surface of a Nextel 720/A specimen tested in fatigue at 1200°C in steam environment (maximum stress = 170 MPa, frequency = 0.1 Hz) showing 90° fiber with pieces of matrix attached.....	88
Figure 78. Fracture surface of a Nextel 720/A specimen tested in fatigue at 1200°C in steam environment (maximum stress = 170 MPa, frequency = 0.1 Hz) showing matrix infiltration between fibers in a 0° fiber tow.....	89
Figure 79. Fracture surface of a Nextel 720/A specimen tested in fatigue at 1200°C in steam environment (maximum stress = 170 MPa, frequency = 10 Hz) showing matrix rich area.....	89
Figure 80. Fracture surface of a Nextel 720/A specimen tested in fatigue at 1200°C in steam environment (maximum stress = 170 MPa, frequency = 10 Hz) showing surface of a pulled out 0° fiber.	90
Figure 81. Fracture surface of a Nextel 720/A specimen tested in fatigue at 1200°C in steam environment (maximum stress = 170 MPa, frequency = 10 Hz) showing surface of pulled out 0° fibers.	90
Figure 82. Fracture surface of a Nextel 720/A specimen tested in fatigue at 1200°C in steam environment (maximum stress = 170 MPa, frequency = 10 Hz) showing surface of 90° fibers.	91
Figure 83. Fracture surface of a Nextel 720/A specimen tested in fatigue at 1200°C in steam environment (maximum stress = 170 MPa, frequency = 10 Hz) showing surface of a pulled out 0° fiber.	91

Figure 84. Fracture surface of a Nextel 720/A specimen tested in fatigue at 1200°C in steam environment (maximum stress = 170 MPa, frequency = 10 Hz) showing surface of pulled out 0° fibers.	92
Figure 85. Fracture surface of a Nextel 720/A specimen tested in fatigue at 1200°C in steam environment (maximum stress = 170 MPa, frequency = 10 Hz) showing surface of pulled out 0° fiber	92

List of Tables

	Page
Table 1. Physical Properties of the Nextel™ 720/Alumina Panels [5].....	8
Table 2. Summary of N720/A specimen data. All fatigue tests conducted at 1200°C....	28
Table 3. Thermal strains produced by N720/A CMC due to temperature expansions from 23 to 1200 °C. Results from prior studies are also included [11,23].....	29
Table 4. Results of tensile test for N720/A specimen at 1200°C following survival of 10 ⁵ cycles with the frequency of 0.1 Hz and maximum stress 170 MPa.....	33
Table 5. Results of fatigue testing of N720 CMC at 1200°C in steam with the frequency of 0.1 Hz.	34
Table 6. Results of fatigue tests of N720/A CMC at 1200°C in steam, 10 Hz.	40

EFFECTS OF FREQUENCY AND ENVIRONMENT ON FATIGUE BEHAVIOR OF AN OXIDE-OXIDE CERAMIC MATRIX COMPOSITE AT 1200°C

1 Introduction

Efforts dedicated to aeronautical engineering have brought about some of the most impressive feats in history. In less than a century, humans have progressed from a world where the dream of escaping the pull of gravity for a few moments above the dunes of Kitty Hawk was considered outlandish to a world where many take the use of satellites to navigate around the globe for granted. The realization of Mankind's dream of flight has also brought with it new challenges. As engineers have refined their craft over the decades, flying machines have become faster, safer, and more efficient. Some advances in aircraft performance can be attributed to improvements in areas such as design technique and manufacturing methods, but over the years the biggest factor influencing cutting-edge aeronautical technology has been the application of new materials.

One recent trend in aircraft design has been more extensive use of composite materials. Fighters produced in the late 1970s such as the F-15 and F-16 incorporated about 1-2% composites into the airframe of by weight [43]. The incorporation of composites increased greatly in the next generation of aircraft designed to fulfill the same role, so much that the F/A-18E/F and F-22A are approximately 25% composites by weight [32: 433]. Composites are now being considered for use in areas in which metals have traditionally been used, such as turbine engines.

One type of composites that shows promise for future aerospace applications is ceramic matrix composites (CMCs). Ceramic matrix composites are advantageous in that they exhibit strength and high temperature tolerance as well as decreased brittleness compared to monolithic ceramics. Unfortunately, CMCs are prone to strength degradation in oxidizing environments. Oxide/oxide CMCs, on the other hand, have high thermal shock resistance as well as reduced susceptibility to oxidation [4]. Nextel™ 720/Alumina composite (N720/A), combines the strength and creep resistance of a di-phase alumina/mullite fiber with the damage tolerance of a porous alumina matrix, and is being considered for various aerospace applications.

Recent efforts by Eber, Harlan, and Mehrman [8,11,23] have investigated the effects of oxidizing environments on the performance of N720/A. Eber and Harlan [8,11] studied the response to creep and cyclic loading, respectively, and showed that the presence of steam severely degrades performance at 1200°C [35]. Mehrman investigated the effects of prior fatigue on creep behavior, and concluded that a history of prior fatigue loading increases creep life of N720/A [23;83]. All cyclic tests by Eber and Mehrman were conducted at a frequency of 1 Hz. The focus of this research is to study the effects of frequency on fatigue response of N720/A in both air and steam environments by conducting additional fatigue testing at the frequencies of 0.1 and 10 Hz. In addition, damage mechanisms and microstructural changes at each loading rate will be investigated. Note that the terms fatigue and cyclic loading are used interchangeably in this document.

2 Applications and Background

2.1 Ceramic Matrix Composites

2.1.1 Introduction to continuous fiber ceramic composites

Humans have been making ceramic materials for over 24,000 years [24]. The advantageous properties of ceramics, such as strength, low reactivity, and high temperature capability have been known nearly since the inception of engineering. However, until the last several decades the use of this class of materials in load-bearing components has been limited due to inherent brittleness and low shock tolerance [24]. Early earthenware items such as terra cotta contained many different compounds and were subject to sudden failure under load. Recent technological advances have made it possible to isolate individual ceramic compounds and combine them in customized materials with improved mechanical properties. Purified ceramics offer many advantages over other classes of materials, such as high strength at extreme temperatures [4:4].

Most materials exhibit significant deformation in tension prior to complete structural failure. Ceramics, on the other hand, exhibit elastic behavior until the stress level reaches the ultimate tensile strength (UTS). Abrupt tensile failure in monolithic ceramics initiates at small stress concentrations and microcracks formed during processing. Minimization of such defects may improve performance, but thermal shock and cyclic loading can exacerbate any existing flaws in the structure [4:9]. The

introduction of ceramic matrix composites in the late 1970s may have been the first step towards solving the problem of the brittle behavior of ceramics.

Ceramic matrix composites are custom-made materials, designed to minimize the drawbacks of monolithic ceramics. Continuous fiber ceramic composites (CFCCs) are made of bundles of strong high aspect-ratio fibers (diameter $\sim 10 \mu\text{m}$) in a weaker ceramic matrix. Compared to monolithic ceramics, CFCCs exhibit reduced brittleness and decreased susceptibility to both flaws and shock, while maintaining excellent properties at high temperatures [31]. Figure 1 shows general trends of strength to weight ratio versus temperature for various types of materials, including CMCs [38].

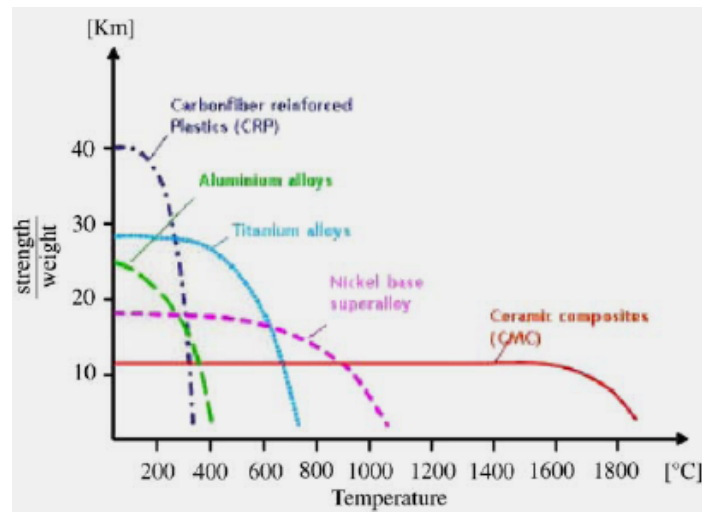


Figure 1. Strength to weight ratio versus temperature for various materials. From reference [38].

2.1.2 Traditional ceramic matrix composites

Damage tolerance mechanisms vary between CMCs based on the fiber and matrix materials in addition to the design of the composite [6,31]. Many early CMC designs had poor damage tolerance due to the strength of the interface between the fiber and the matrix. A strong fiber-matrix interface decreases composite strength because cracks in the matrix can propagate through nearby fibers, leading to fiber failure [4:302]. One way to prevent this phenomenon is to introduce a relatively weak interphase between the fibers and the matrix. Silicon carbide (SiC) based composites in particular make use of weak interphases.

Ceramic matrix composites reinforced with SiC fibers are among the strongest available, but at a cost [29]. Silicon carbide has a tendency to create strong bonds with many different matrix materials, so to prevent such bonding the fibers are typically coated with a thin ($\sim 2\ \mu\text{m}$) layer of carbon or boron nitride. As cracks form in the matrix near fibers they deflect into the weak debond interphase, delaying failure [18,42]. CMCs that utilize a weak interphase demonstrate a stress-strain curve with two distinct portions associated with matrix cracking and fiber failure [23:9].

The use of weak fiber-matrix interphases involves complicated and expensive processing [29]. An additional drawback to this type of CMC is the tendency of the interphase to break down in an oxidizing environment [29:212]. As the interphase decays under environmental attack, the strength of the fiber/matrix interface increases and material performance decreases below tolerable minimums. Applications where materials may be exposed to reactive combustion products are not suitable for CMCs that

suffer from increased brittleness in the presence of oxidizing gases. Oxide/oxide CMCs rely on crack deflection mechanisms that are less susceptible to environmental attack.

2.1.3 Oxide/oxide ceramic matrix composites

First introduced in the late 1980s, oxide/oxide CMCs with a porous matrix do not have a fiber-matrix interphase [47]. An optimal level of porosity, introduced into the matrix during processing, allows for crack deflection while maintaining structural integrity [40]. When matrix cracks form and propagate in these oxide/oxide CMCs, the crack front tends to deviate into the weaker portions of the porous matrix instead of propagating through the load-bearing fibers [29]. This mode of damage tolerance is unaffected by the presence of a strong fiber/matrix bond, making an interphase unnecessary. Stress-strain curves for oxide/oxide CMCs with porous matrices do not have the two distinct sections typical of CMCs with weak interfaces due to decreased effects of matrix cracking. A porous matrix is effectively cracked during processing, before the material is subjected to loads.

The advantages of oxide/oxide CMCs over CMCs with a weak interphase are twofold in oxidizing environments. First, oxide compounds are more resistant to oxidation than other ceramic compounds [25:379]. Secondly, crack deflection mechanisms in oxide/oxide CMCs are independent of an interphase that might be susceptible to environmental attack. Decreased cost and increased oxidation resistance applies to oxide/oxide CMCs as a group, but both the extent of inertness and the mechanical properties of a composite depend largely on the choice of matrix and reinforcement fibers.

An ideal CFCC would have high strength, exhibit high creep resistance, perform well at high temperatures and in oxidizing environments, and do so at minimal cost. Real-world composites may have some but not all of these properties. Thus, reinforcement and matrix materials should be chosen based on the application in question. Nextel™720/Alumina is an oxide/oxide CMC that offers a compromise between the competing aspects of composite behavior and is the subject of the current research.

2.1.4 Nextel™ 720/Alumina CMC

The CFCC studied in this work consists of Nextel™ 720 (N720) fibers contained within a porous alumina (Al_2O_3) matrix. The N720 fiber is made by the Minnesota Mining and Manufacturing Company (3M™). N720 is a diphasic fiber, and contains both alumina and mullite ($2Al_2O_3 \cdot 3SiO_2$) [17]. The alumina phase is $\alpha-Al_2O_3$ and makes up 40-45% of the fiber by volume [46]. Processing of N720 involves a proprietary sol-gel process, which consists of precipitating dilute particles out of a sol to create a gel, which is then dried and sintered to form a ceramic [4].

The addition of the mullite phase improves the high temperature creep resistance of N720 compared to pure alumina fibers such as Nextel™ 610 [46,47]. Alumina has a high theoretical tensile modulus of 400 GPa, but its creep resistance is poor due to small grain size, which is on the order of 0.1 μm [46]. The addition of Mullite boosts creep performance of the fiber, but also reduces strength and stiffness [29:213].

The Nextel™ 720/Alumina studied in this work was produced by Composite Optics Inc. Experiments were conducted using specimens cut from two separate 12 in square panels, # 4569-5 and # 4569-6. Relevant data pertaining to the panels was provided by COI [5] and is presented in Table 1.

Table 1. Physical Properties of the Nextel™ 720/Alumina Panels [5]

Panel #	Thickness (mm)	Fabric (% Volume)	Matrix (% Volume)	Porosity (%)	Density (g/cc)
4569-5	2.6518	46.3	29.4	24.3	2.78
4569-6	2.7661	45.3	30.5	24.1	2.76

The fabric pattern used was an eight harness satin weave, with a denier of 1500. 12 plies of 400-fiber tows were arranged in a 0°/90° orientation with a thread count of 27.5 threads per inch [5]. Matrix infiltration was accomplished using a sol-gel process. The material was dried through a low temperature and low pressure *vacuum bag* technique before undergoing a pressureless sintering [23:15].

When properly designed, matrix porosity provides damage tolerance mechanisms that overcome the strong bonds at the interface and allows the material to maintain sufficient strength under matrix-dominated loadings such as compression and through-thickness tension [47]. Scanning electron micrographs of as-received N720/A show excellent matrix infiltration within fiber bundles (see Figure 2). Matrix porosity is visible, as well as matrix microcracking due to sintering.

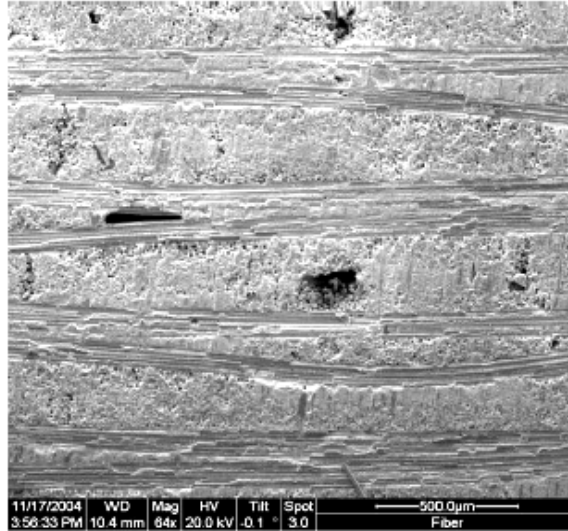


Figure 2. Surface of as-received Nextel 720/A specimen showing matrix cracking and matrix infiltration within fiber bundles. From reference [11;27].

Figure 3 contains an SEM micrograph of an N720/A fracture surface after a fatigue failure in steam environment. Matrix porosity is evident. Also visible is an example of where a matrix crack propagating in the 0° direction stopped short of causing failure of a 90°-oriented fiber. Note the granular appearance of the matrix surface.

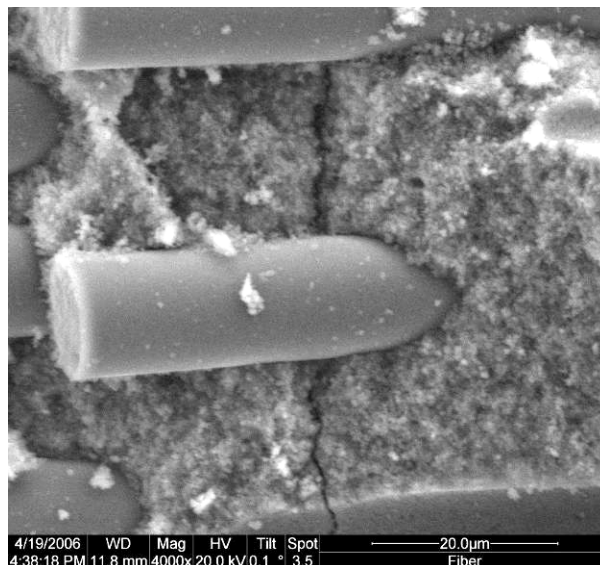


Figure 3. Fracture surface of a Nextel 720/A specimen tested in fatigue at 1200°C in steam environment with the frequency of 0.1 Hz and maximum stress of 170 MPa showing crack deflection around 90° fibers.

2.1.5 Fatigue Performance of CMCs

The exact mechanisms by which CMCs fail under fatigue loading are not completely understood [3]. Some materials, like aluminum, continue to accumulate damage at high cycle numbers, while others, like steel, exhibit a clear endurance limit below which damage does not occur regardless of cycle number. It is unclear which of the two categories CMCs fall into, if either [15]. A fatigue limit can be defined as survival of a certain number of cycles, typically between 10^5 and 10^8 depending on the application in question. However, damage can still increase in CMCs after 10^8 cycles [15,41].

The effects of fatigue on CMCs vary with material composition and damage mechanisms. Reynaud et al. [33] observed an increase in elastic modulus of a carbon/carbon composite at high cycle numbers at temperatures between 600 and 1000°C in air. However, N720/A shows a decrease in stiffness after fatigue at 1200°C in air at the frequency of 1.0 Hz, with more pronounced reductions in modulus occurring at higher stress levels [8:26].

Holmes et al. [14] investigated the effect of frequency on fatigue performance on a SiC/Calcium Aluminosilicate CMC for frequencies ranging from 25 to 350 Hz. Fatigue life decreased at the highest frequencies, and it was concluded that the material was weakened due to increased temperature from the heat dissipated by the friction of interfacial sliding.

Fatigue of N720/A in both air and steam environments was studied by Eber [8] in 2005. Performance at 1.0 Hz was considered to be outstanding in air, with specimens

achieving a run-out of 10^5 cycles at maximum stress levels up to 89% of UTS, but fatigue life in steam was significantly reduced for stress levels above 65% of UTS [8:24].

Decreased fatigue life of alumina-based CMCs in a steam environment may be caused by stress corrosion cracking (SCC) [20,39]. The reaction of water vapor with strained Si-O and Al-O bonds at crack tips could promote crack growth at higher rates than in air [39]. If these reactions are time-dependent, a critical factor in determining the decrease in fatigue life in steam for a given temperature and stress level would be the time spent at high tensile loads. Cycling at a lower frequency increases the time spent above a given stress level in each cycle (see Figure 4). If a threshold stress for initiation of time-dependent steam corrosion of N720/A exists, then lower frequency cycling above the threshold stress would lead to earlier failures, while cycling at higher frequencies would result in improved fatigue life. The aim of the current research is to evaluate the effects of frequency on fatigue behavior of N720/A both in air and in steam environments.

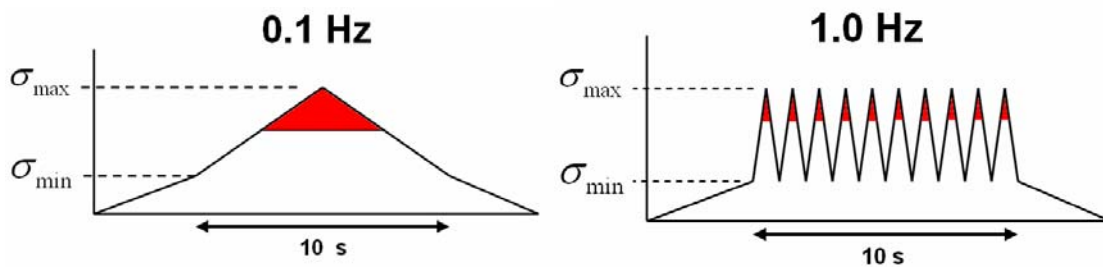


Figure 4. Diagram highlighting time spent above a given stress level at different frequencies.

2.2 Ceramic Matrix Composites in Aerospace Applications

Current aircraft engine design is limited in part by the maximum operating temperature of the construction materials [32:383]. One engine performance parameter of importance is the turbine inlet temperature, or TIT. For a given engine, an increase in TIT would allow for more thrust and greater efficiency. The specific thrust of an ideal turbojet can be found by the following equation:

$$\frac{F}{\dot{m}} = a_0 \left\{ \left[\frac{2}{\gamma - 1} \frac{\tau_\lambda}{\tau_r \tau_c} (\tau_r \tau_c \tau_t - 1) \right]^{1/2} - M_0 \right\} \quad (1)$$

Where τ_λ is the ratio of the total turbine inlet temperature to the total freestream temperature [26:143]. While this is an ideal equation, real-world powerplants can be modeled using similar formulas that take efficiency into account. Increasing TIT results in improved specific thrust and leads to better fuel efficiency, which makes improving TIT a priority in turbine engineering.

Many turbine designs achieve high TIT by using an active air cooling system to keep the turbine blades within a specified operational temperature range. Use of a material such as CMCs that could operate at or above current use temperatures without an active cooling system would decrease engine weight and complexity in addition to providing the benefits discussed above.

Weight is a major factor in aeronautical design - lighter aircraft have lower fly-away costs and improved performance [32:87]. Ceramic matrix composites are less dense than high-temperature metal superalloys [38:410]. Therefore, incorporating CMCs into aircraft engines would decrease weight directly, as well as possibly eliminate active

turbine blade cooling. In addition to increasing performance and efficiency, use of CMCs could possibly reduce harmful emissions [13].

Current temperature limitations in land-based turbines require use of an extra-lean fuel-air mixture to prevent complete combustion from taking place. In addition to decreasing fuel efficiency, this leads to emission of polluting hydrocarbons and carbon monoxide (see Figure 5 [29]).

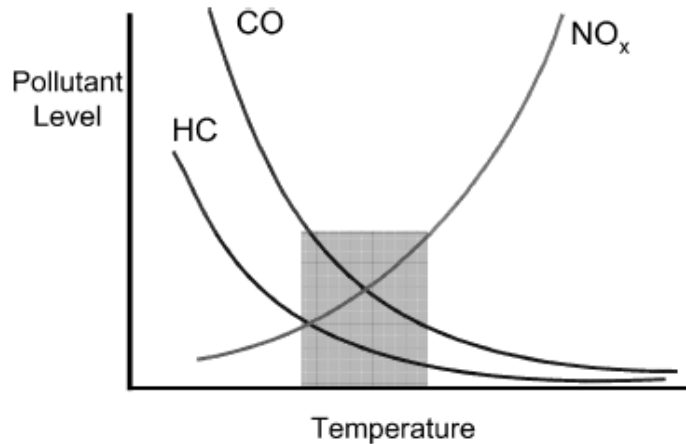


Figure 5. Pollutant emission as a function of combustion temperature. From reference [29].

Given the numerous incentives for engineers to increase efficiency, lighten aircraft, and decrease emissions, a class of materials that could accomplish one or many of these objectives would be of great interest. This makes CMCs attractive candidate materials for combustor walls [28], turbine inlet blades, and other engine components such as those shown in Figure 5 [27].

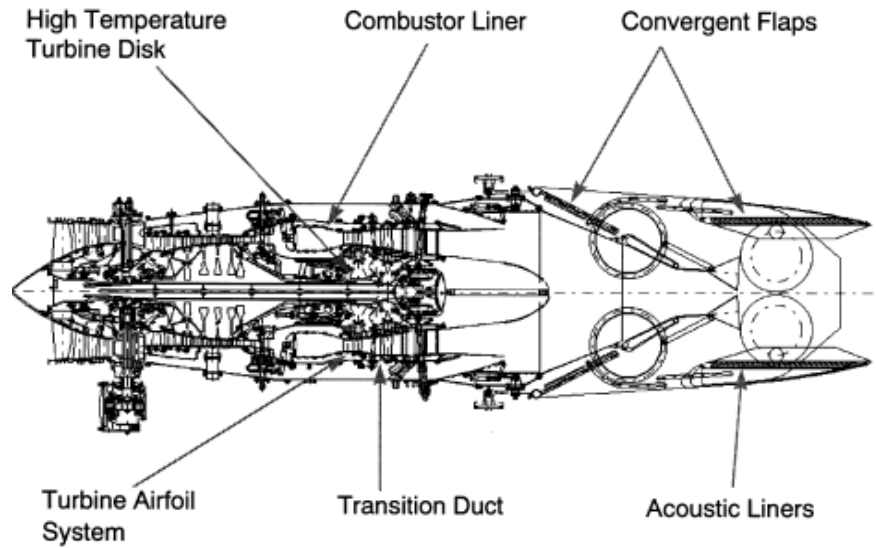


Figure 6. Turbine components with potential for CMC applications. From reference [27].

The ability of composites to increase turbofan efficiency has already been demonstrated. General Electric's new GENx high-bypass ratio turbofan, currently planned to power Boeing's new 787 transport, makes extensive use of composites, most notably in the fan blades and fan housing. The GENx is reported to have a 15.4% reduction in specific fuel consumption compared to the GE CF6 engine, which powers the Boeing 767-300ER jetliner [22].

In order to be suitable for applications such as combustion chambers, a material must have good retained strength and stiffness at high temperature and in corrosive environments [21]. Many CMCs are based on silicon carbide fibers, which have excellent mechanical properties but are also expensive and require an interphase between the fibers and matrix to provide for damage tolerance. Fiber/matrix interphases in SiC-based CMCs are subject to environmental attack [46], which can lead to poor performance in oxidizing environments.

Recent advances in CMC design have led to the creation of oxide/oxide materials that have higher oxidation resistance, simpler manufacturing processes, and lower production costs than earlier CMCs [12,16,19,30]. Many possible applications of oxide/oxide CMCs, such as turbine blades, are likely to involve cyclic loading. Accurate predictions of material behavior under operating conditions require knowledge of mechanical response at various frequencies, which is the subject of the current research.

3 Experimental Setup

3.1 Specimen Preparation

Nextel™720/Alumina specimens used in this research were cut using an abrasive waterjet by Kerf Waterjet, based in Dayton, OH. The ceramic panels were cut with an aluminum sheet set on top of the CMC in order to produce smoother cut surfaces. A dogbone specimen design is shown in Figure 7. This specimen design, which is similar to the ASTM standard D 3552 shape, places maximum stress in the gauge section of the specimen during tension testing.

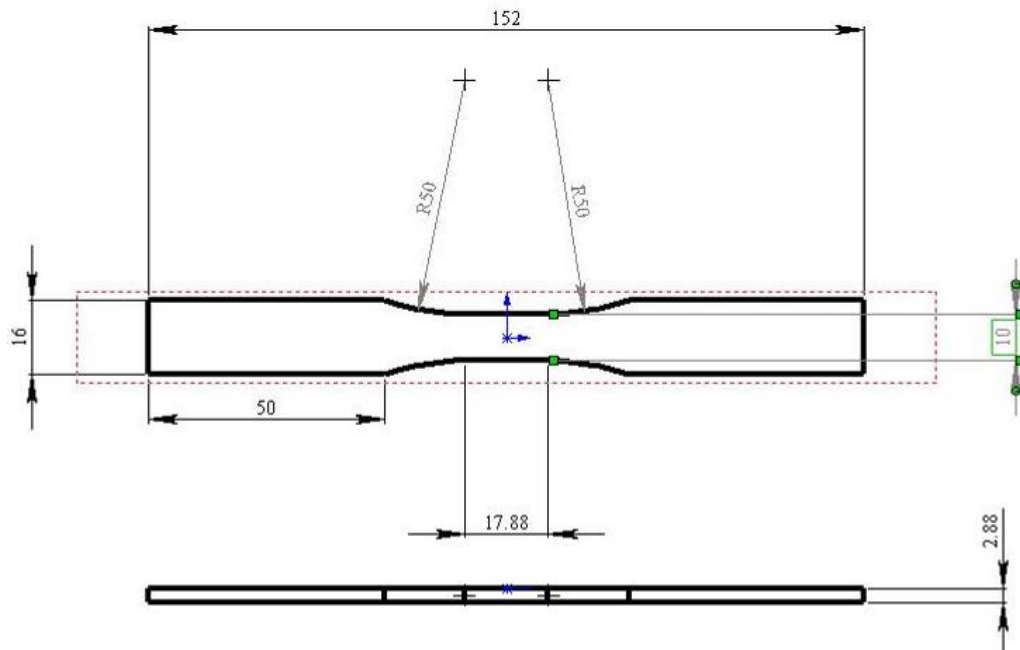


Figure 7. Test specimen, dimensions in mm.

Dimensions of the gauge section of each specimen were recorded using a Mitutoyo Corporation Digital Micrometer prior to testing. Minor perturbations in the waterjet during cutting introduced a small amount of variation in the gauge section dimensions (~ 0.01 mm).

Residue on the specimens contained small amounts of garnet which were removed before testing. The material was cleaned using an ultrasonic bath for 15 minutes, then patted dry with a clean cloth and soaked in isopropyl alcohol for 20 minutes and finally dried in an OMEGALUX LMF 3550 oven at 250°C for one hour.

Before testing, each specimen was fitted with fiberglass tabs to guard against damage from the grips used on the test equipment. The 1/16" thick tabs were attached to the test specimen using M-Bond 200 adhesive. These tabs prevented the grips from causing local surface cracks in the ceramic that could have affected test results. A specimen with fiberglass tabs attached is shown in Figure 8.

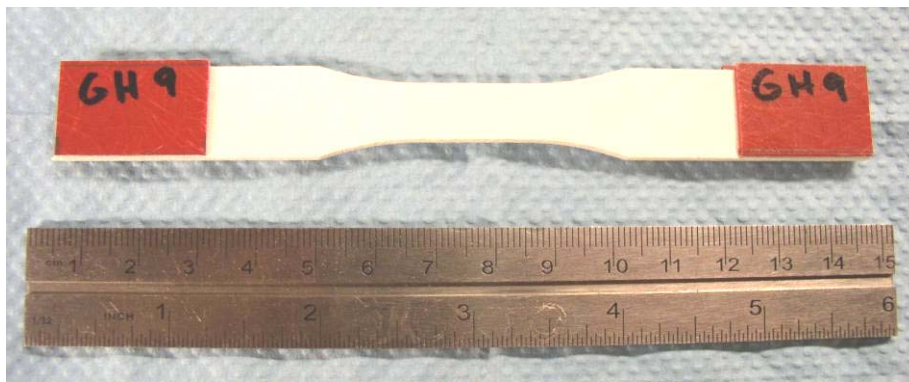


Figure 8. Tabbed N720/A CMC specimen.

3.2 Test Equipment

An MTS Systems Corporation model 810 Material Test System servo-hydraulic machine was used for all mechanical testing (see Figure 9). The maximum force available on this unit was 5 kip (approximately 25 kN). MTS Series 647 hydraulic wedge grips transferred load from the hydraulics to the test specimen, with a Surfalloy grip texture used to prevent slipping. The grips were cooled with 14°C water supplied by a Neslab model HX-75 chiller. MTS Station Manager software and Multi-Purpose Testware (MPT) were used to create and implement the experimental programs, with a Testar II controller acting as interface between the computer and the MTS 810.

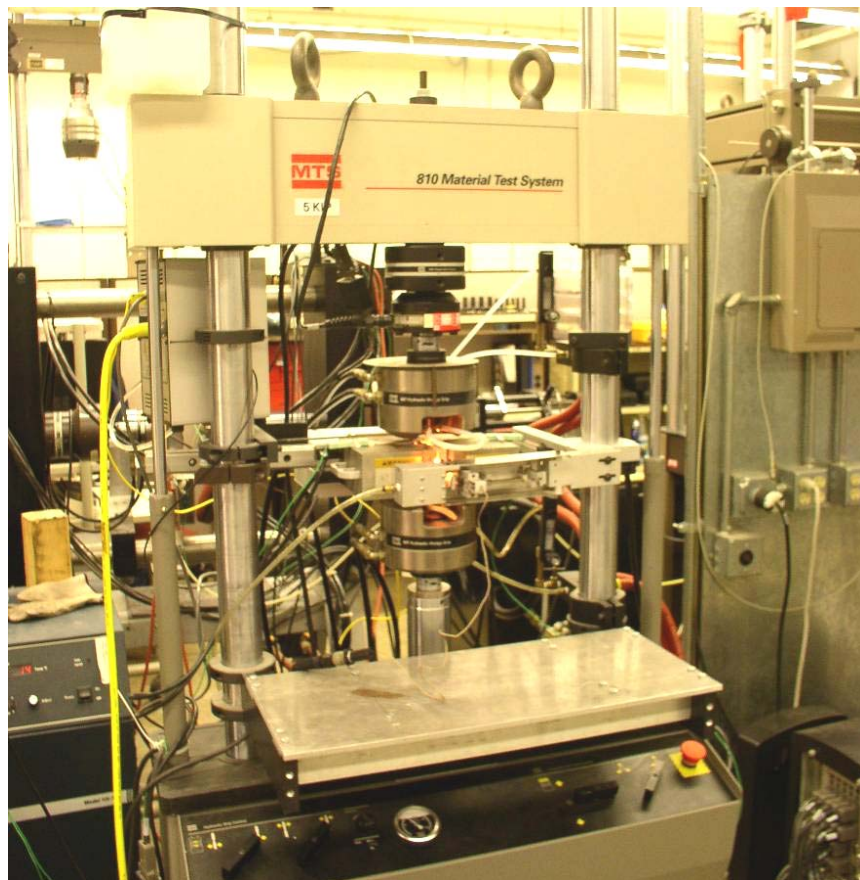


Figure 9. MTS equipment setup.

Experimental programs were implemented on a PC which communicated with the Testar II controller. Strain was recorded using an MTS high-temperature low contact force extensometer (Model 632.53E-14). Two 6" alumina extensometer rods were used to obtain accurate strain measurements at high temperatures. Strain readings from the extensometer were considered to be accurate within 0.005%. The zero offset in the extensometer strain measurements was re-set before each test, with a total offset of less than 1% for all procedures. Figure 10 shows a close-up view of the extensometer arrangement during high-temperature testing.

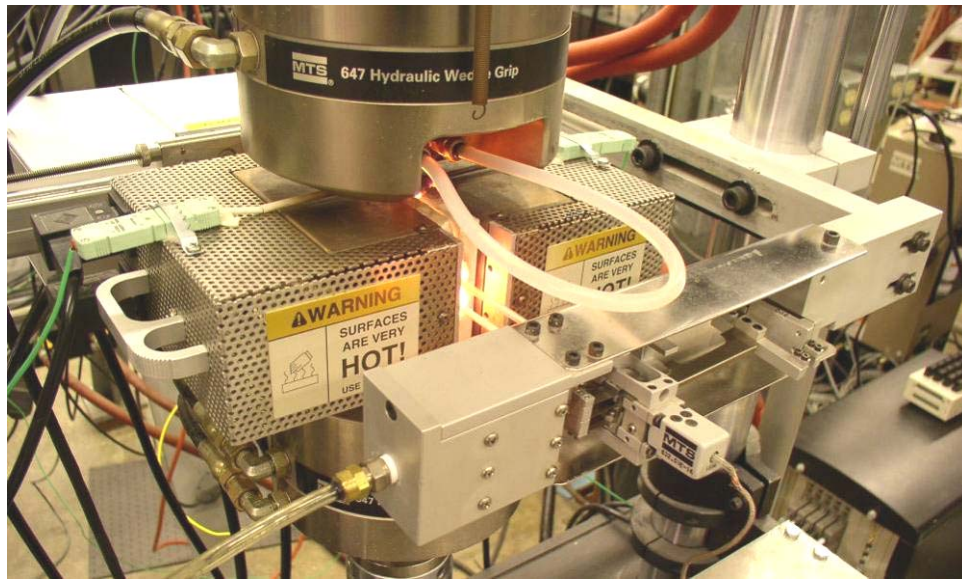


Figure 10. Close-up view of extensometer during high-temperature testing.

Gripping pressure was set at 8 MPa, which was sufficient to prevent the specimen tabs from slipping in the grips during testing, but not enough to crush the specimen. All tension-tension cyclic tests were conducted with an R ratio of 0.05, where R is the ratio of maximum stress to minimum stress. Test data was saved on the local hard drive of the computer and was later processed using Microsoft Excel.

3.3 Environmental Controls

High temperature tests utilized an AMTECO Hot-Rail Furnace System with temperature feedback provided by two S-type non-contacting thermocouples (see Figure 11). The oven was controlled by an MTS Model 409.83B Temperature Controller, with the furnace controls segregated into left and right zones. Command to the temperature controller was issued through the Testar II controller. Likewise, feedback from the furnace thermocouples was routed through the Testar II and recorded in the test data file.

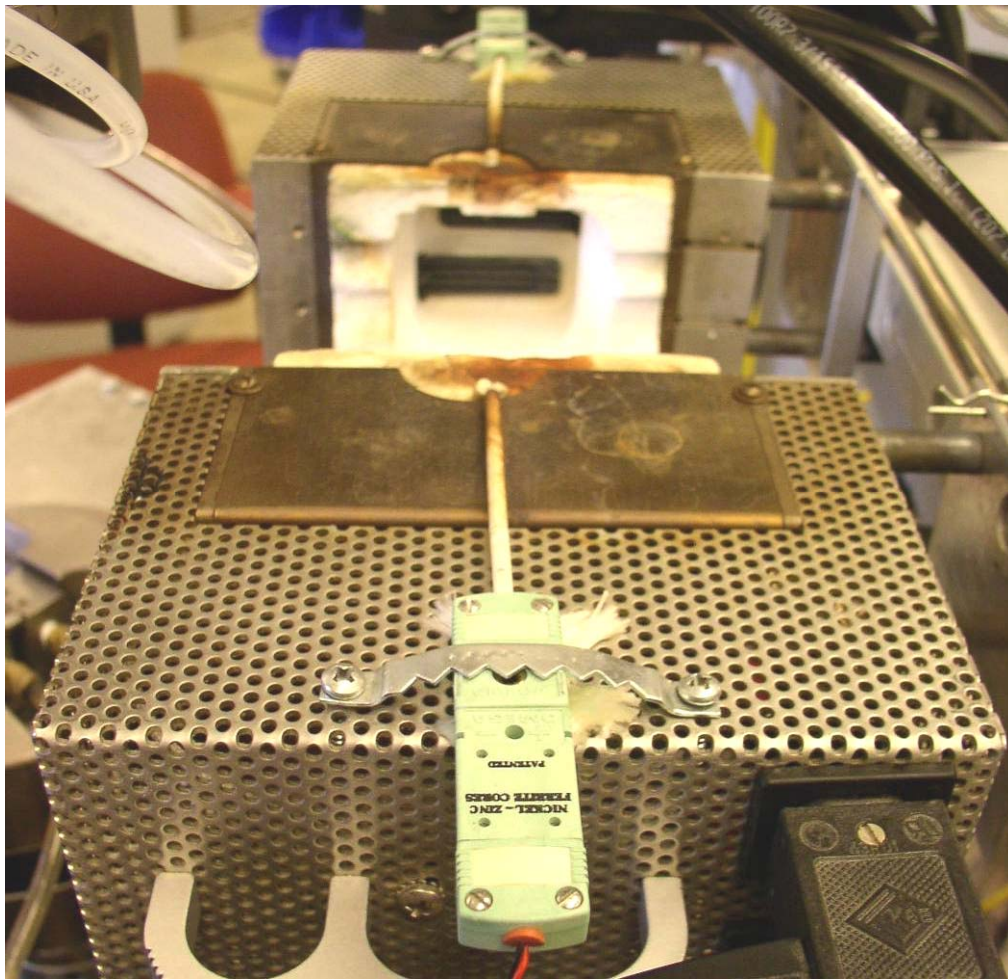


Figure 11. AMTECO furnace with control thermocouples.

All tests were conducted at 1200°C, with the oven calibrated separately for air and steam environments. Temperature calibration was conducted using a N720/A specimen with two S-type thermocouples attached to the specimen gauge section using Omega CC high temperature cement. Specimen temperature readings from the thermocouples were displayed on two separate handheld Omega HH202A thermometers and recorded manually. To determine the oven set points necessary to achieve a specimen temperature of 1200°C, the furnace temperature was raised to 900°C over a period of 30 minutes, then temperature was manually raised a few degrees at a time until the feedback from the thermocouples attached to the specimen stabilized at 1200°C. The set points were considered to be accurate if the specimen temperature remained $1200 \pm 5^\circ\text{C}$ for 8 hours.

Testing in a steam environment was accomplished by isolating the gauge section of the specimen inside an alumina susceptor and pumping in steam at a slight positive pressure. As shown in Figure 12, the cylindrical susceptor consisted of two separate semi-cylindrical halves, two ceramic hoops used to secure the assembly during testing, and two circular endplates, one with holes for the extensometer rods and the other with a hole for insertion of the feed tube for steam.

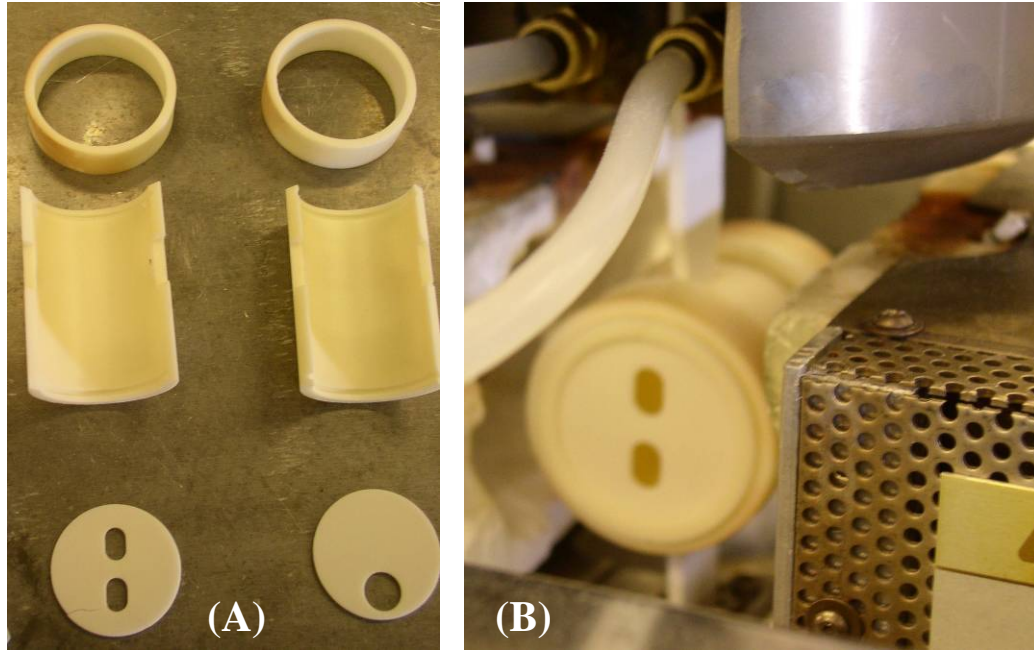


Figure 12. Photographs of alumina susceptor showing: (A) susceptor assembly and (B) susceptor with test specimen and furnace.

De-ionized water was converted into steam by an AMTECO HRFS-STMGEN Steam Generation System and then fed into the susceptor at a temperature of 266°C. The steam was pumped into the susceptor at slight positive pressure, expelling the hot air from the susceptor during testing.

3.4 Microstructural Characterization

After mechanical testing, the specimen fracture surfaces were examined with both optical and scanning electron microscopes (SEM). The resulting images were used to characterize the dominant damage mechanisms and microstructural changes. Fracture surfaces were observed using a Zeiss Discovery V12 optical microscope and

photographed using the associated Zeiss AxioCam HRc digital camera and Axiovision version 4.4 software.

Scanning Electron Microscopes (SEMs) are able to resolve much higher powers of magnification than those based on reflected light. Scanning electron microscopes operate by bombarding the specimen with a beam of electrons focused through a series of magnetic fields that act as lenses. A scintillator-photomultiplier detects the secondary and backscattered electrons emitted by the surface of the bombarded material, and the corresponding data are converted into images that can be viewed on a computer [10:147]. The SEM used in this work was an FEI Quanta 200 HV capable of operating in both high vacuum and ESEM modes (see Figure 13).



Figure 13. SEM and EDAX equipment.

Use of the SEM involved additional preparation of the fracture surfaces. Fracture surfaces were cut to within 1/4" of the damage zone using a Sherline Model 5410 diamond saw, and then mounted on lathe-finished SEM mounts using conductive SPI carbon paint. Observing poorly conducting materials such as ceramics in high vacuum mode requires coating the surface of the material with a thin layer of conductive material in order to dissipate the charge built up by the electron beam. Selected specimens were coated with carbon using a SPI Supplies SPI-Module Control and Carbon Coater. Specimens possibly experienced a small amount of additional damage during handling. Additionally, use of the carbon coating may have disturbed the fracture surfaces slightly, which could affect the results of the microstructural investigation.

Uncoated specimens (see Figure 14) can also be observed using Environmental Scanning Electron Microscope (ESEM) mode. In the ESEM mode, poor conductivity is overcome through the introduction of a small amount of water vapor into the vacuum chamber of the SEM. Secondary electrons from the surface of the specimen ionize nearby water molecules, which in turn neutralize the charge built up by the specimen. Use of ESEM decreases image quality compared to high vacuum micrographs, but allows for expeditious and convenient evaluation of fracture surfaces.



Figure 14. Uncoated N720/A specimens prepared for SEM observation.

The SEM was also equipped with an EDAX Genesis 4000 Energy Dispersive X-Ray Spectroscopy (EDS) system, which was used to survey the species of elements present in different portions of the samples. Analysis using EDS involves processing signals from photons emitted by the portions of the material that absorb the energy of the electron beam through the use of a Sapphire Si(Li) detector [45]. Liquid nitrogen (LN) was used to cool the detector crystal in order to improve the spectrometer signal to noise ratio [45:262].

3.5 Test Procedures

All tests were conducted at 1200°C. The specimens were first heated from room temperature (23°C) to 900°C at a rate of 1°C/s, and then from 900 to 1200°C at a rate of 0.5°C/s, and finally held at temperature for an additional 15 minutes prior to mechanical testing. Tests conducted in steam environment used heating procedures identical to the

test conducted in air, with steam pumped into the susceptor at a slight positive pressure beginning at the onset of heating and continuing throughout the duration of testing.

Fatigue tests were conducted in load control. Load was raised initially to minimum fatigue stress (5% of maximum stress) over 20 seconds. A ramp shape was used for all fatigue cycles. Load as a function of time varied depending on the fatigue frequency (see Figure 15). If a specimen survived to the run-out condition, the load was lowered from the minimum stress to zero over a span of 20 seconds.

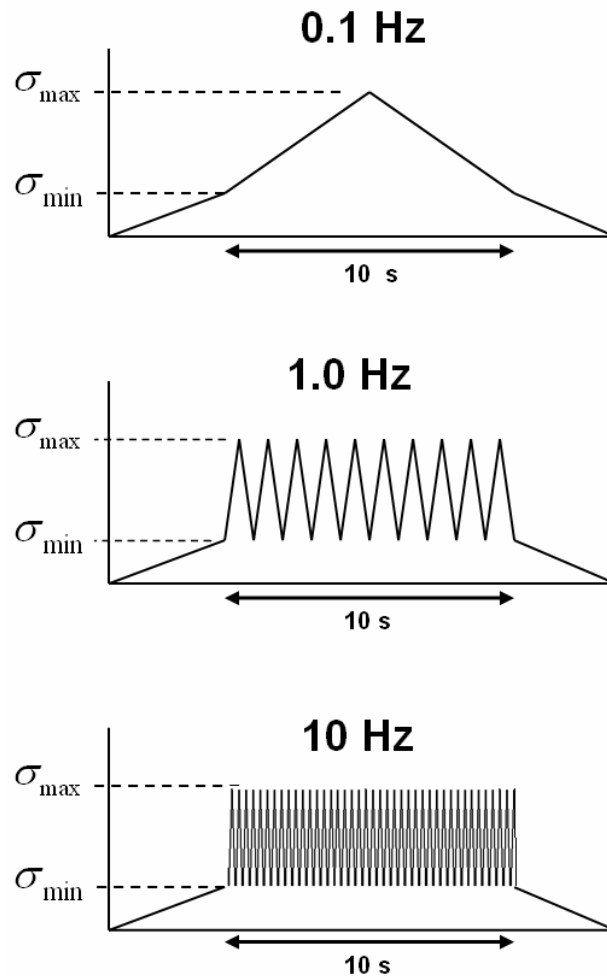
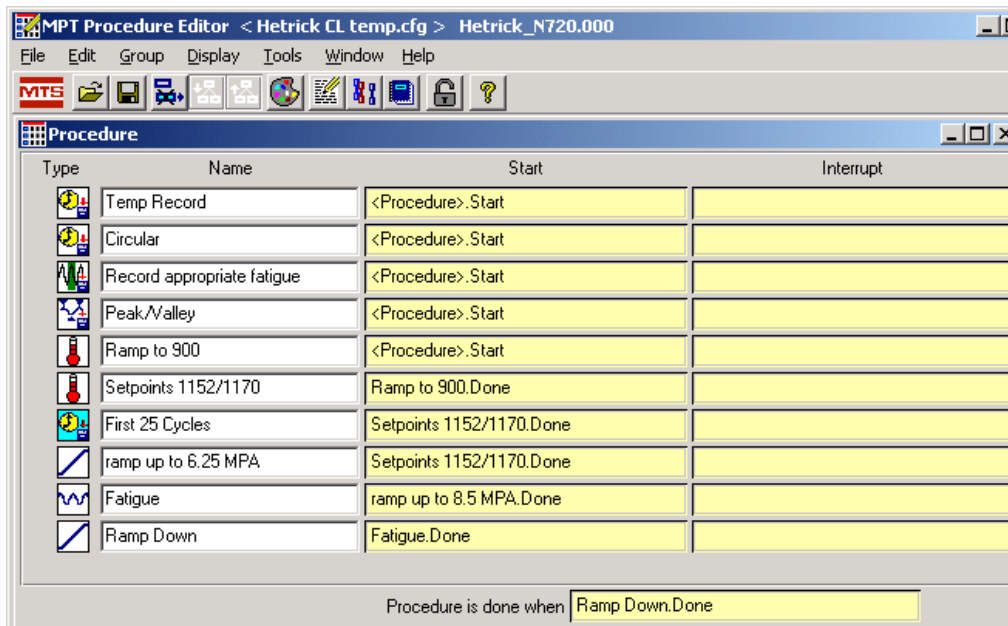


Figure 15. Diagram of load as a function of time over a span of 10 seconds for the frequencies of 0.1, 1.0, and 10 Hz. Figure is not to scale.

Specimens that achieved run-out were held at 1200°C and zero load from the conclusion of cyclic loading until tensile testing. Tensile tests were conducted in stroke command with a constant displacement rate of 0.05mm/s.

Time, cycle number, strain, displacement, load, command, and temperature were measured and recorded during each test. A *Temp Ramp* file recorded the system behavior during heating. A *circular* data file used a circular buffer to record the last five minutes of test data in case of malfunction. The initial mechanical loadings as well as the first 25 fatigue cycles were recorded in the *First 25 Cycles* file, with the sampling frequency set according to the loading rate. To prevent data saturation, later portions of fatigue testing were separated into two different files - the *Peak/Valley* file contained data taken at the maximum and minimum stress levels of each cycle, while the *Record Appropriate Fatigue* file recorded complete cycles spaced out in a logarithmic manner. A typical test procedure for cyclic loading in steam is reproduced in Figure 16.



The screenshot shows the 'MPT Procedure Editor' window with the file 'Hetrick CL temp.cfg' and 'Hetrick_N720.000'. The 'Procedure' tab is active, displaying a table of test steps. The table has four columns: 'Type', 'Name', 'Start', and 'Interrupt'. The steps are as follows:

Type	Name	Start	Interrupt
Temp Record		<Procedure>.Start	
Circular		<Procedure>.Start	
Record appropriate fatigue		<Procedure>.Start	
Peak/Valley		<Procedure>.Start	
Ramp to 900		<Procedure>.Start	
Setpoints 1152/1170		Ramp to 900.Done	
First 25 Cycles		Setpoints 1152/1170.Done	
ramp up to 6.25 MPA		Setpoints 1152/1170.Done	
Fatigue		ramp up to 8.5 MPA.Done	
Ramp Down		Fatigue.Done	

At the bottom of the window, it states 'Procedure is done when' followed by a text box containing 'Ramp Down.Done'.

Figure 16. Typical test procedure.

4 Results and Discussion

4.1 Section Summary

The organization of this section is based on the order in which experiments were conducted. Each combination of frequency and environment is examined, followed by a concluding section in which observations and overall trends are discussed.

Table 2 summarizes the results of fatigue tests conducted in the current research. Fatigue run-out was defined as 10^5 cycles at the frequency of 0.1 Hz and 10^6 cycles at the frequency of 10 Hz. Specimens GH1 and GH9 achieved run-out, therefore the failure strains listed for these tests represent those obtained in subsequent tensile tests.

Table 2. Summary of N720/A specimen data. All fatigue tests conducted at 1200°C.

Specimen name	Fatigue Rate (Hz)	Environment	Max Stress (MPa)	Initial Modulus (GPa)	Cycles to Failure (N)	Time to Failure (hours)	Failure Strain (%)	Thermal Strain (%)
GH1*	0.1	Air	170	52.3	>100,017*	>277.8	0.38*	0.85
GH2	0.1	Steam	170	49.8	12	0.0323	0.53	0.88
GH3	0.1	Steam	125	47.8	1,850	5.14	1.15	0.92
GH4	0.1	Steam	150	52.9	75	0.215	0.63	0.93
GH5	0.1	Steam	100	49.5	17,498	48.61	2.67	0.88
GH6	0.1	Steam	75	59.2	56,093	155.82	3.35	No Data
GH7	10	Steam	170	49.9	11,387	0.322	0.96	0.91
GH9*	10	Steam	150	58.7	>1,000,010*	>27.78	0.48*	0.87
Average				52.5				

* indicates a run-out

The specimen tested in air at the frequency of 0.1 Hz with the maximum stress of 170 MPa achieved a run-out, therefore the fatigue limit in air at 0.1 Hz was established to be at least 170 MPa and testing at lower stress levels was not conducted. The stress level of

170 MPa corresponds to 89% of the UTS of N720/A at 1200°C (192 MPa). Note that 170 MPa is also the fatigue limit previously established for this material in air at 1200°C at the frequency of 1.0 Hz [8].

One specimen was tested for each combination of environment, load, and frequency. This represents a small data set, therefore these results should be considered to be representative of overall trends in behavior of this material rather than absolute. Testing additional specimens under the same conditions may improve understanding.

4.2 Thermal Expansion

As stated earlier, all tests were conducted at 1200°C. In addition to the initial calibration discussed in Section 3.3, test temperatures were verified by comparing thermal strains of the samples to those measured in previous investigations of N720/A conducted at the same temperature. Thermal strains obtained for all specimens are listed in Table 2 and Table 3 compares thermal strain mean values and standard deviations produced in prior studies of N720/A at 1200 °C.

Table 3. Thermal strains produced by N720/A CMC due to temperature expansions from 23 to 1200 °C. Results from prior studies are also included [11,23]

Author	Specimens	Mean Thermal Strain (%)	Thermal Strain Standard Deviation (%)	Coefficient of Linear Thermal Expansion ($10^{-6} K^{-1}$)
Harlan [11]	12	0.867	0.174	7.43
Mehrman [23]	16	0.902	0.0717	7.66
Current Research	7	0.891	0.0294	7.57

Results in table 3 show good agreement with previous measurements of thermal strain of the same material. The coefficient of linear thermal expansion (α) for monolithic alumina ($\sim 9 \cdot 10^{-6} K^{-1}$) is slightly higher than the values of α obtained for the N720/A composite in the studies listed in Table 3 [9]. In all tests mechanical strain was calculated by subtracting thermal strain from the total strain.

4.3 Fatigue in laboratory air at the frequency of 0.1 Hz

4.3.1 Strain and stiffness data

In prior work investigating fatigue behavior of N720/A in air and in steam at 1200°C, the CMC was subjected to cyclic loading in air at a frequency of 1.0 Hz and maximum stress levels of 170, 150, 125, and 100 MPa [8]. All of the aforementioned tests achieved a run-out, defined as 10^5 cycles.

Specimen GH1 was subjected to cyclic loading at 1200°C in laboratory air at a maximum stress of 170 MPa and the frequency of 0.1 Hz. The reduction in frequency by an order of magnitude compared to the tests conducted in reference [8] did not cause failure, despite the longer test duration required to achieve a run-out of 10^5 cycles. Due to an error in the test procedure, specimen GH1 was held at zero-load at 1200°C for 8 hours after completing the first 200 fatigue cycles. This additional time at temperature was a small portion of the overall test time of 285 hours, and it is not believed to have had any significant effects on the experimental results.

Specimen GH1 accumulated less mechanical strain than the specimen in the 170 MPa fatigue test at 1.0 Hz [8]. Figure 17 presents maximum and minimum strain as a function of cycle number. The difference between maximum and minimum strain remains unchanged as cycling progresses, which indicates that the material did not undergo significant softening or hardening. This is typical of all specimens, and other charts of strain versus cycle number will only display maximum strain for each test.

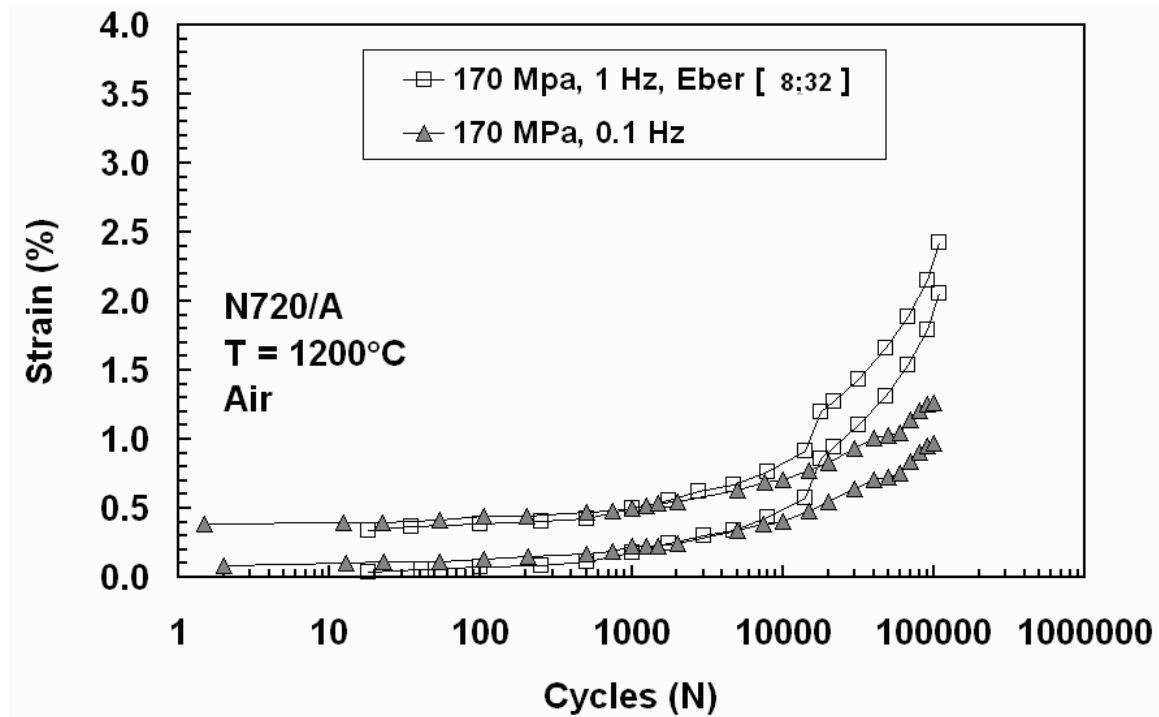


Figure 17. Maximum and minimum strain versus cycle number for fatigue of N720/A in air at 1200°C with maximum stress level of 170 MPa. Data from reference [8:32] is also included.

Strain for both tests is nearly identical up to approximately 1000 cycles, where the 1.0 Hz test exhibits accelerated ratcheting compared to the 0.1 Hz test. Maximum strain at 10^5 cycles was 2.42 % for the 1.0 Hz test and only 1.26 % for the 0.1 Hz test.

Stiffness was calculated by taking the slope of a linear best-fit curve for the upload portion of the stress versus strain curve. Stress versus strain curves for the initial cycles of specimens examined in the current research did not exhibit linear elastic behavior, thus the value of initial modulus was taken to be the stiffness calculated for the second load cycle. The stiffness of the specimen tested with the frequency of 0.1 Hz remained within 5% of the initial value after 10^5 cycles (see Figure 18). It is also seen that modulus does not vary significantly with cycle number for the test conducted at 1.0 Hz [8]. Note that for both frequencies stiffness as a function of cycle number remains steady in the presence of strain accumulation. Therefore ratcheting has little effect on modulus of N720/A in air at 1200°C.

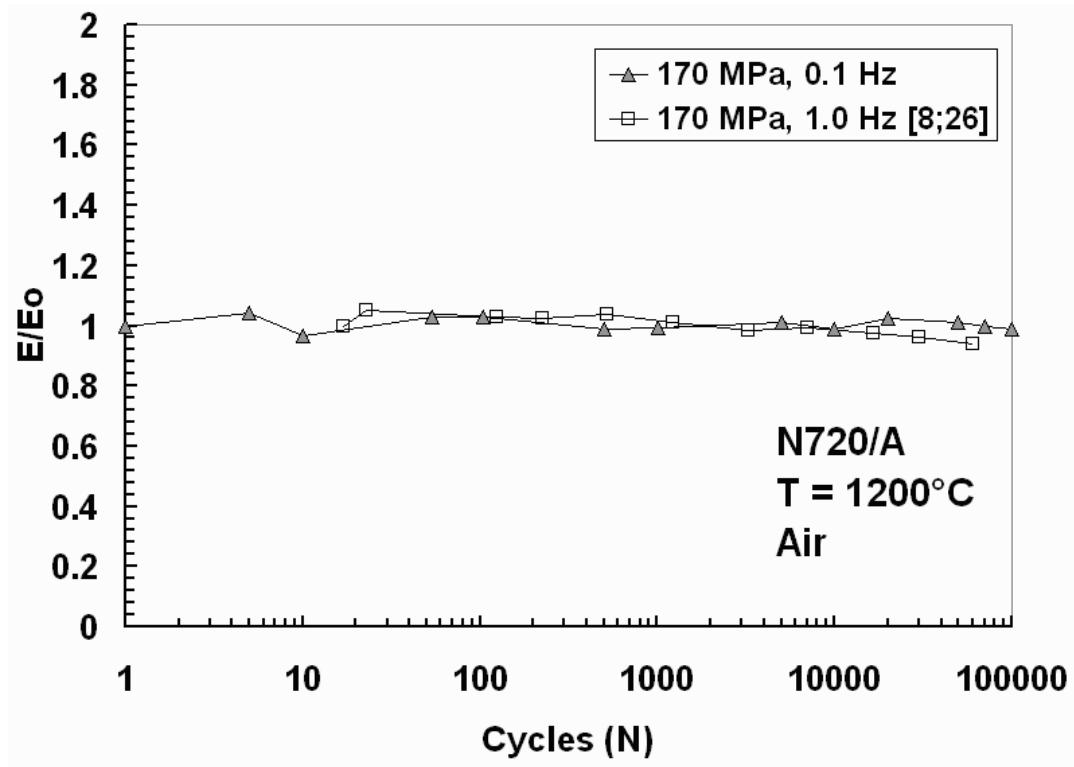


Figure 18. Normalized stiffness as a function of cycle number for the specimen tested at 1200°C in air with the frequency of 0.1 Hz. Data from reference [8;26] is also included.

4.3.2 Residual Strength and Stiffness

After surviving 10^5 cycles of tension-tension fatigue in air at 0.1 Hz, specimen GH1 was tested for residual mechanical properties. The specimen was maintained at 1200°C at zero load for six hours between completion of the fatigue test and the beginning of the tensile test, results of which are presented in Table 4.

Table 4. Results of tensile test for N720/A specimen at 1200°C following survival of 10^5 cycles with the frequency of 0.1 Hz and maximum stress 170 MPa

Specimen #	Initial Modulus (GPa)	Final Modulus (GPa)	% Change in E	Residual UTS (MPa)	Failure Strain (%)
GH1	52.3	51.7	-1.1%	194.4	0.384

The residual UTS of 194.4 MPa is close to the residual strength of 192 MPa observed by Eber for the higher frequency specimen subjected to the same stress level and environment [8:34]. This result suggests that UTS is not affected by a reduction in stiffness due to fatigue.

Testing at 0.1 Hz in air was discontinued after a run-out was achieved at 170 MPa. Further testing at lower stress levels would be likely to result in a run-out as well.

4.4 Fatigue in steam environment at the frequency of 0.1 Hz

4.4.1 Strain and Stiffness Data

Fatigue performance of N720/A at 1200°C in air was excellent at both 1.0 Hz and 0.1 Hz (see Section 4.3). Proper evaluation of the properties of N720/A CMC requires investigation of mechanical performance in oxidizing environments similar to those the composite may be exposed to in proposed applications. In the current research, five tests were carried out in steam at the frequency of 0.1 Hz. Maximum stress levels were 170, 150, 125, 100, and 75 MPa. All tests were conducted at a temperature of 1200°C with an R ratio of minimum to maximum stress of 0.05. Data presented earlier in Table 2 pertaining to the specimens tested in steam at the frequency of 0.1 Hz are repeated in Table 5 for convenience.

Table 5. Results of fatigue testing of N720 CMC at 1200°C in steam with the frequency of 0.1 Hz.

Specimen #	Maximum Stress (MPa)	E _o (GPa)	Cycles to Failure (N)	Time to failure (h)	Failure Strain (%)
GH2	170	49.8	12	0.0323	0.53
GH4	150	52.9	75	0.215	0.63
GH3	125	47.8	1850	5.14	1.15
GH5	100	49.5	17498	48.61	2.67
GH6	75	59.2	56093	155.82	3.35

Fatigue response in steam was highly degraded compared to that in air. The specimen tested in air at 170 MPa at 0.1 Hz survived over 10⁵ cycles, while the specimen tested at the same stress level and frequency in steam failed after only 12 cycles. Run-out was not achieved even at the low stress level of 75 MPa. One of the primary reasons for

development of oxide/oxide composites was to increase resistance to the effects of oxidizing environments, but it is seen that the effects of steam on mechanical performance of N720/A are significant. The presence of steam dramatically decreases fatigue life for the frequency of 0.1 Hz.

Strain accumulated under cyclic loading depends on both maximum load and test environment (see Figure 19). Specimens tested at lower stress levels exhibit both longer cyclic lives and higher accumulated strain. The failure strain at a maximum stress of 75 MPa was 3.35%, more than six times the failure strain of 0.53% accumulated in the 170 MPa test. The N720/A CMC exhibits non-catastrophic delayed failure accompanied with significant strain accumulation at low load levels. The effect of frequency on failure strain is discussed in Section 4.6.

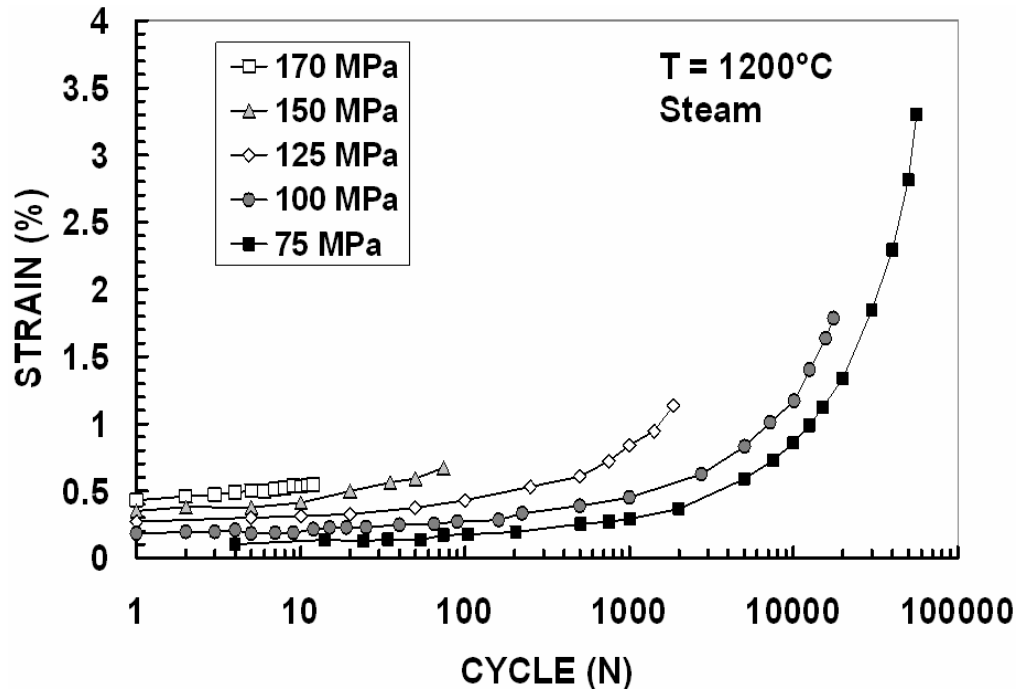


Figure 19. Maximum strain as a function of cycle number for N720/A specimens subjected to fatigue testing in steam at 1200°C with the frequency of 0.1 Hz and maximum stresses of 170, 150, 125, 100, and 75 MPa.

Figure 20 contains plots of normalized stiffness as a function of cycle number for specimens tested at stress levels of 170, 150, 125, 100, and 75 MPa at the frequency of 0.1 Hz in steam. Behavior of normalized Young's modulus versus cycle number for specimens tested with the frequency of 0.1 Hz in steam varied slightly more than that of specimens tested with the same frequency in air. The specimen tested at a maximum stress of 75 MPa exhibited a 15% decrease in stiffness at cycle numbers greater than 10^4 . Other specimens tested at 0.1 Hz in steam retained full stiffness until failure.

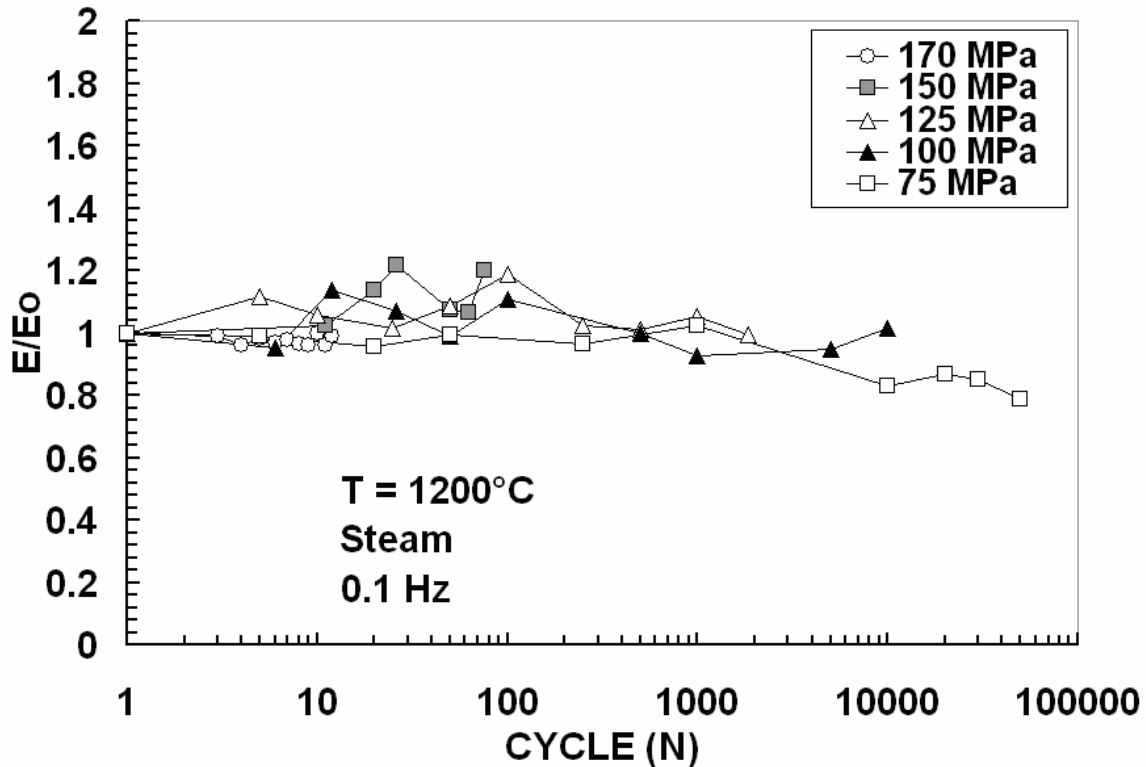


Figure 20. Normalized stiffness as a function of cycle number for N720/A specimens subjected to fatigue testing in steam at 1200°C with the frequency of 0.1 Hz and maximum stresses of 170, 150, 125, 100, and 75 MPa.

4.4.2 Energy Dissipation

Eber [8] observed energy dissipation in fatigue loading of N720/A at 1 Hz at high temperatures through the narrowing of hysteresis loops. Typical results for both air and steam environments revealed an initial decrease in hysteresis energy density (HED) during the first few cycles, followed by a stabilization of HED at higher cycle numbers [8:32]. The hysteresis energy density for a single cycle is equal to the area enclosed by the hysteresis loop. Eber calculated HED using a quadrilateral method which approximated the upload and download portions of the stress-strain curves as straight lines. In the current work, HED was approximated by summing the areas of quadrilaterals comprising the entirety of the curve, as shown in Figure 21.

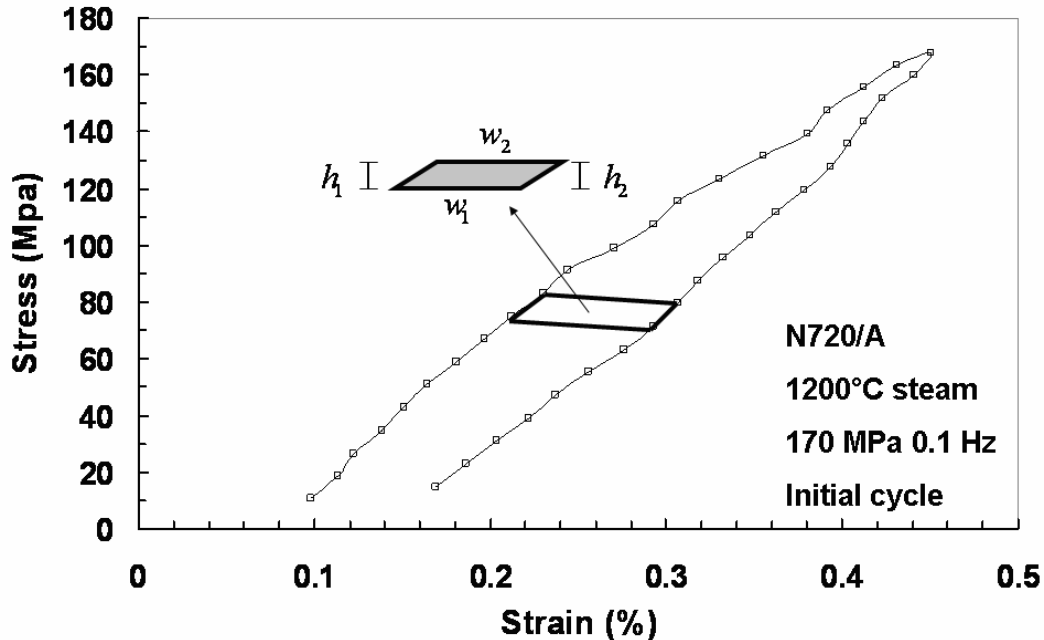


Figure 21. Illustration of typical quadrilateral used in hysteresis energy density calculations, including hysteresis loop for the initial cycle of the specimen tested in steam at 1200°C with the frequency of 0.1 Hz and maximum stress of 170 MPa.

The area of each hysteresis loop was approximated as the sum of the areas of the constituent quadrilaterals formed by sets of four adjacent data points. All quadrilaterals were approximated as parallelograms.

Approximate area of a parallelogram as shown in Figure 20:

$$A \approx \frac{h_1 + h_2}{2} \cdot \frac{w_1 + w_2}{2} \quad (2)$$

For a hysteresis loop comprised of n quadrilaterals, the HED is then

$$HED = \sum_{i=1}^n \left[\frac{h_i + h_{i+1}}{2} \cdot \frac{w_i + w_{i+1}}{2} \right] \quad (3)$$

The accuracy of this method of HED calculation increases as the rate of data sampling increases. The HED was recorded as zero in cases where similarity in strain between the upload and download portions of a cycle resulted in a negative HED value. The accuracy of the quadrilateral summation technique could be increased by averaging the HED results of several cycles in sequence. Doing so would tend to cancel out any random errors introduced into the measurement.

The HED versus cycle number is plotted in Figure 22 for specimens tested with the frequency of 0.1 Hz at 1200°C in steam at maximum stresses of 170,150,125,100, and 75 MPa. It is seen that the majority of energy dissipation occurs in the first 10 cycles. The HED values remain fairly stable for subsequent cycles even as strain continues to accumulate (see Figure 19). Hysteresis energy densities for specimens tested at lower maximum stress levels stabilize at lower values than those obtained for specimens tested at higher stress levels.

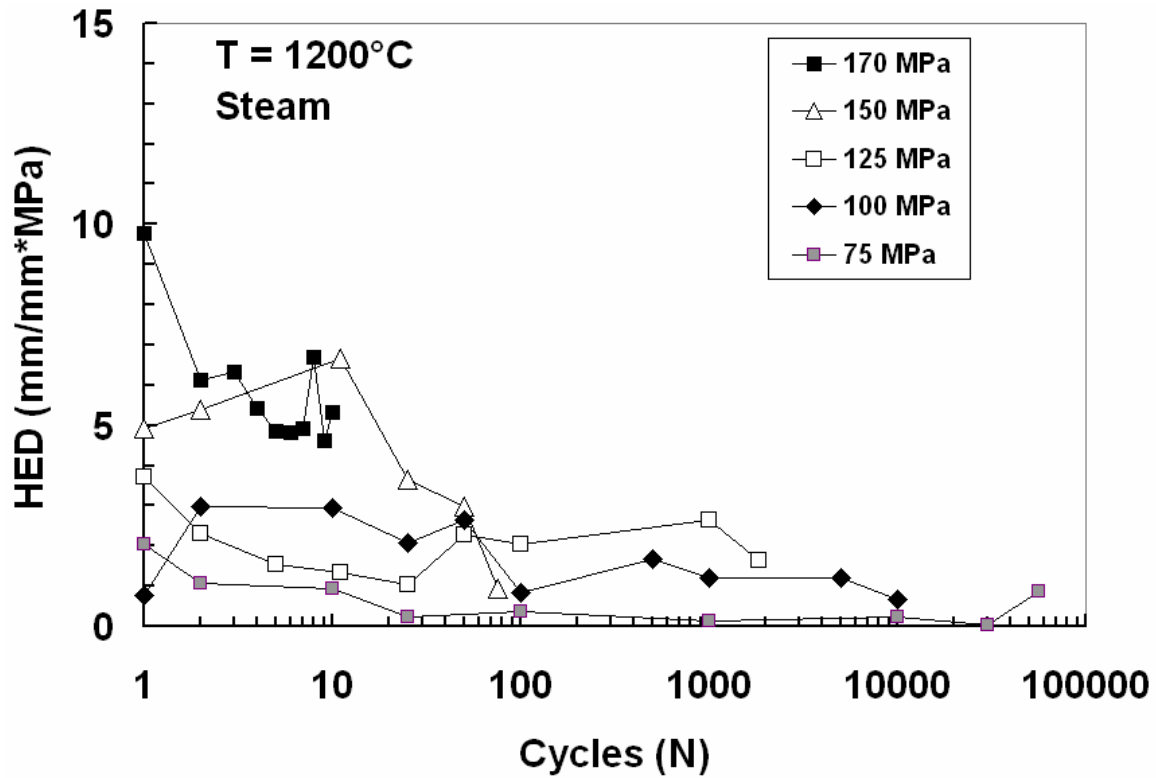


Figure 22. Hysteresis energy density as a function of cycle number for N720/A specimens subjected to fatigue testing in steam at 1200°C with the frequency of 0.1 Hz and maximum stresses of 170, 150, 125, 100, and 75 MPa.

Specimens tested at lower maximum loads exhibit significantly lower values of HED for the first cycle compared to specimens tested at higher loads (see Figure 22). The small HED values obtained for the 75 MPa case are likely due to the stresses remaining within the elastic range of the material. Note that all specimens failed in fatigue despite the lack of significant energy dissipation in later cycles.

4.5 Cyclic loading at the frequency of 10 Hz in steam at 1200 °C

Two additional fatigue tests were conducted in steam with the frequency of 10 Hz, two orders of magnitude higher than the frequency of 0.1 Hz used in the tests described in Section 4.3. Maximum stress levels investigated were 170 and 150 MPa. For the 10 Hz tests, run-out was defined as survival of 10^6 cycles. It was possible to implement this more rigorous run-out definition because the shorter test times associated with the frequency of 10 Hz allowed for completion of a million cycles in 27.78 hours. Results are summarized in Table 6. Note that at 10 Hz run-out was achieved for the relatively high stress level of 150 MPa (78% UTS).

Table 6. Results of fatigue tests of N720/A CMC at 1200°C in steam, 10 Hz.

Specimen #	Maximum Stress (MPa)	E_0 (GPa)	Cycles to Failure (N)	Time to Failure (h)	Failure Strain (%)
GH7	170	49.9	11387	0.322	0.96
GH9*	150	58.7	>1,000,032*	>27.78*	N/A

* indicates a run-out

It is seen that increasing test frequency by two orders of magnitude for the specimens tested at a maximum stress of 170 MPa results in increasing fatigue life by nearly three orders of magnitude. The specimen tested at a maximum stress of 170 MPa with the frequency of 0.1 Hz failed after only 12 cycles, while the specimen tested at the same load with the frequency of 10 Hz survived 11,387 cycles. By comparison, the N720/A specimen tested by Eber [8] at 1.0 Hz at a maximum stress of 170 MPa in steam failed at the intermediate value of 202 cycles.

Results reveal that increasing the frequency of cyclic loading in steam environment improves fatigue performance of the N720/A CMC. As the frequency

increases from 1.0 to 10 Hz, the fatigue limit in steam increases from 125 to 150 MPa. Fatigue life of N720/A at 10 Hz in steam is similar to that obtained at 1.0 Hz in air at all but the highest load level of 170 MPa [8:24]. Thus accurate predictions of time to failure require knowledge of both test environment and loading rate.

Strain accumulated in the 10 Hz tests is approximately twice that accumulated in 0.1 Hz tests for a given maximum stress (see Figures 19 and 23). Damage mechanisms in N720/A appear to be affected by the loading rate. At 10 Hz, strain accumulation in the 170 MPa test is not significant until 100 cycles. Reducing the maximum stress to 150 MPa delays the onset of strain ratcheting until 10^4 cycles.

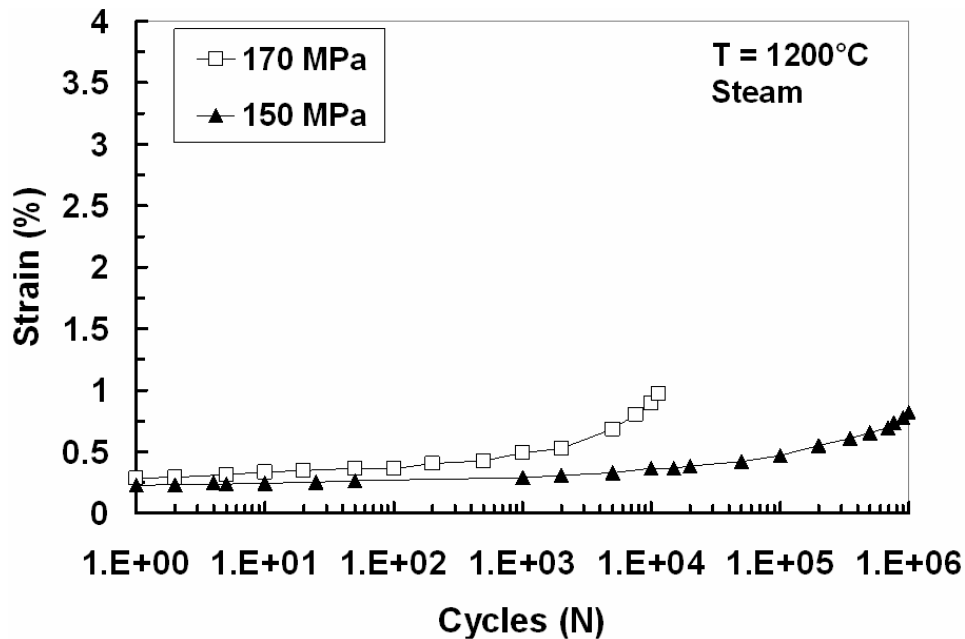


Figure 23. Maximum strain as a function of cycle number for N720/A specimens subjected to fatigue testing in steam at 1200°C with the frequency of 10 Hz and maximum stresses of 170 and 150 MPa.

Failure strain produced in the 170 MPa test conducted at 10 Hz was 0.96%, nearly twice the value of the failure strain produced in the 170 MPa test conducted at 0.1 Hz (0.53%).

Stiffness as a function of cycle number exhibits greater stability for specimens tested with the frequency of 10 Hz than those tested with the frequency of 0.1 Hz (see Figures 20 and 24).

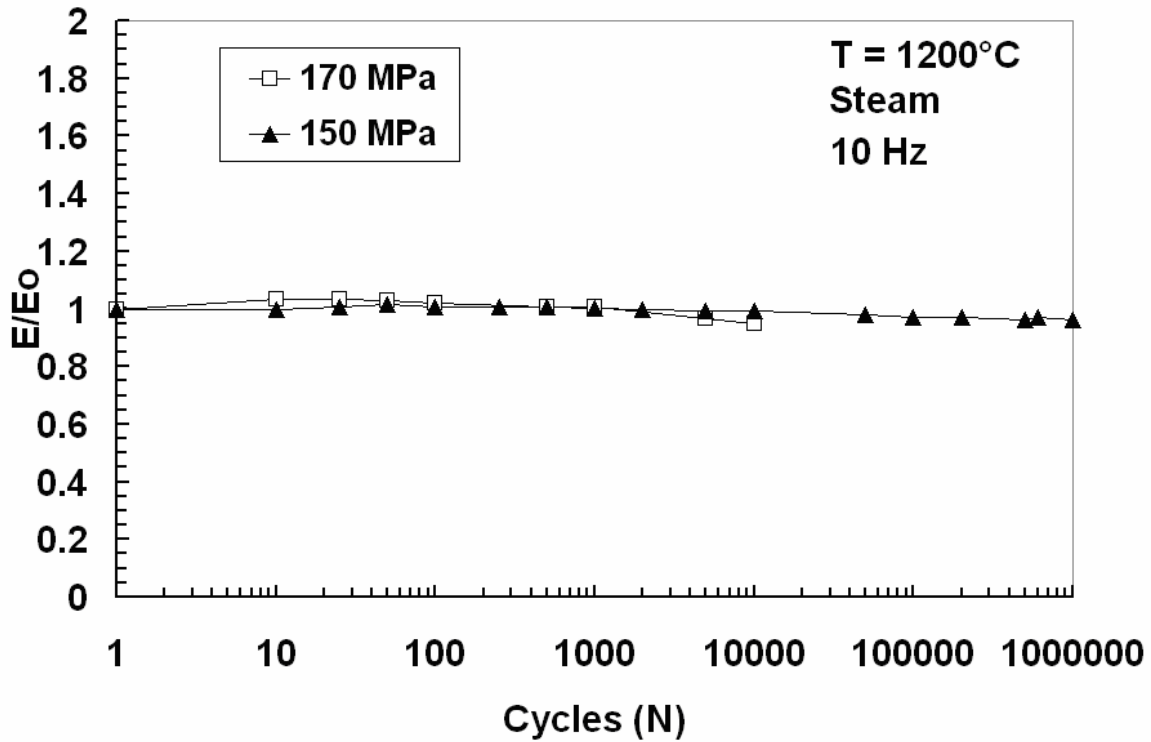


Figure 24. Normalized stiffness as a function of cycle number for N720/A specimens subjected to fatigue testing in steam at 1200°C with the frequency of 10 Hz and maximum stresses of 170 and 150 MPa.

Hysteresis energy density was not calculated for the specimens tested at the frequency of 10 Hz because minimal hysteresis was observed and the HED values quickly became negligibly small.

4.6 Conclusions on the effects of frequency on fatigue in steam

It is seen that the loading rate has a dramatic effect on fatigue performance in steam. For a given maximum stress level, lower frequency tests produce lower times to failure. Note that longer cyclic lives were accompanied by larger strain accumulations. Figure 25 shows a plot of the maximum applied stress versus time to failure. Specimens that achieved a run-out are represented by data points denoting the time when testing was halted. The arrows indicate fatigue life in excess of the recorded data (a run-out).

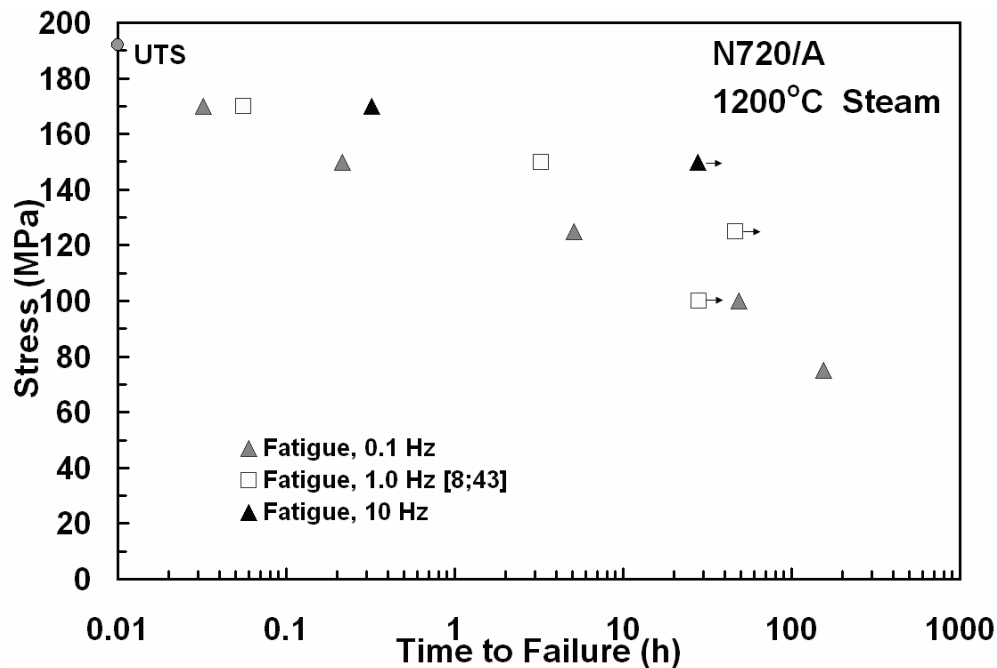


Figure 25. Times to failure for N720/A specimens subjected to fatigue in steam at 1200°C. Data from reference [8:43] is also included.

Strain accumulated in fatigue in steam at 1200°C depends on both maximum stress level and the loading rate. Higher loading rates lead to higher failure strains at the same stress level (see Figure 26). This suggests that increasing the frequency of cyclic loading improves the ability of the material to behave in a less brittle manner. Specimens

that achieved a run-out are indicated in Figure 26 by an arrow. Points for run-out specimens represent the maximum strain after survival of 10^5 or 10^6 cycles, depending on the test frequency.

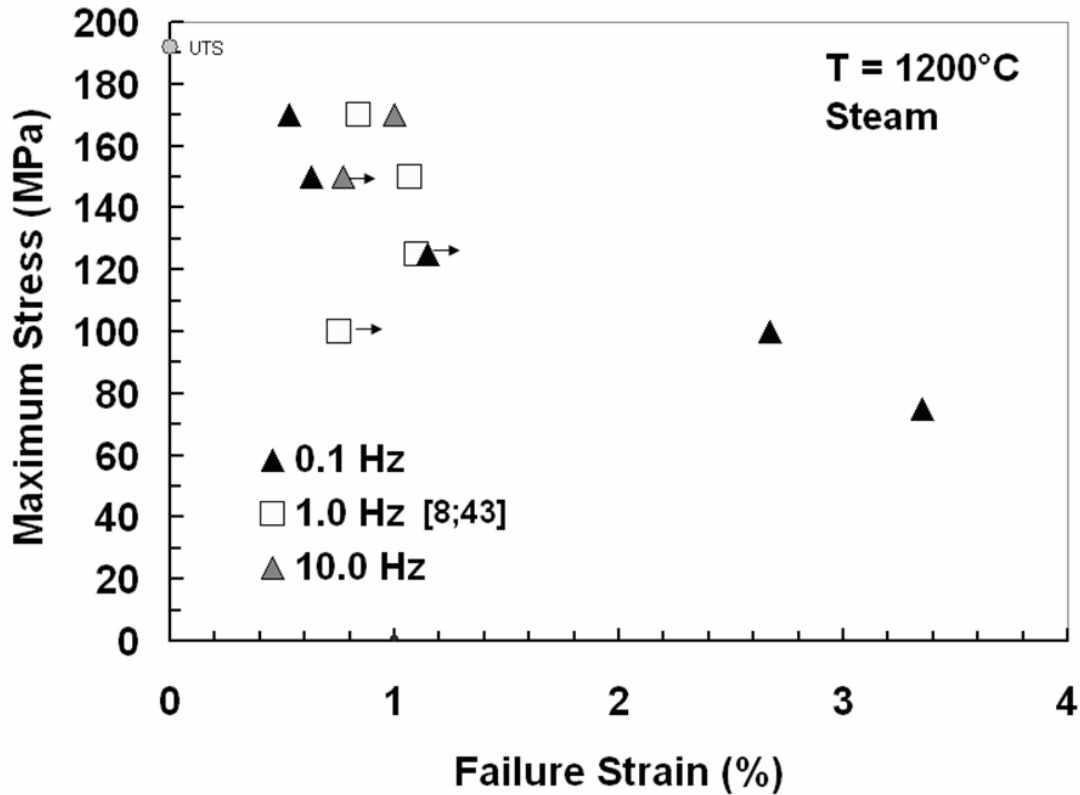


Figure 26. Maximum stress versus failure strain for N720/A specimens tested in fatigue at 1200°C in steam environment. Strains for specimens that achieved run-out are denoted by an arrow. Run-out strains are equivalent to the maximum strain at run-out. Note that no run-outs were achieved for the frequency of 0.1 Hz. Data from reference [8:43] is included.

Fatigue response of N720/A at elevated temperature in steam depends on the frequency. Applying faster cycling rates improves performance, as manifested by longer times to failure and increased failure strain. Deformation in alumina-based ceramics is known to be time dependent [2,23]. Further understanding of damage mechanisms present at different loads and frequencies requires microstructural characterization of the specimen fracture surfaces, which is the topic of Section 5.

5 Fracture Surface Investigation

A qualitative investigation of the fracture surfaces of all specimens was carried out using both an optical microscope and an SEM.

5.1 Optical Microscopy

5.1.1 Tensile failure in air

Specimens that achieved run-out were subjected to a tensile test in displacement control at 1200°C to measure residual strength and stiffness. While the fracture surfaces obtained in tensile tests conducted on fatigue run-out specimens should not be compared directly to the fracture surfaces of specimens that failed in fatigue, these images serve well as baseline examples of the appearance of tensile fracture surfaces for N720/A. Both specimens shown in Figure 27 were subjected to tensile tests to failure after surviving 10^5 cycles at 1200°C in air with a maximum stress of 170 MPa. The specimen shown in Figure 27 (a) was tested with the frequency of 0.1 Hz and that shown in Figure 27 (b) was tested with the frequency of 1.0 Hz [8].

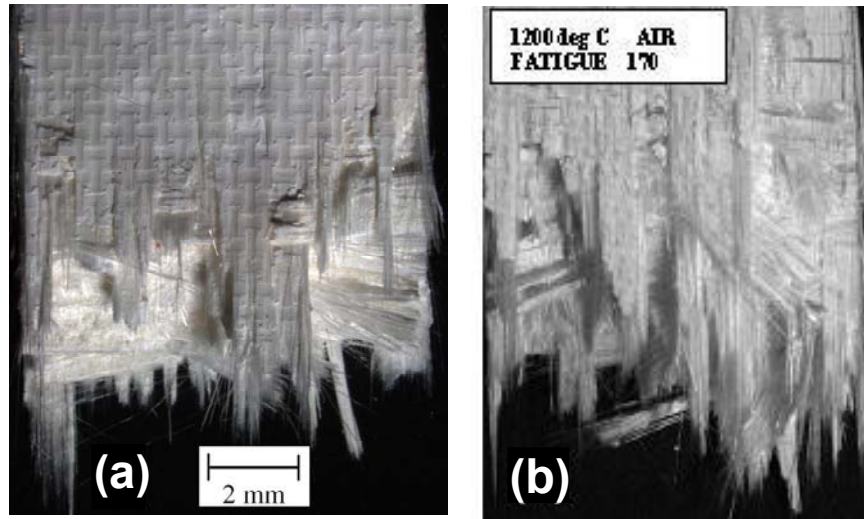


Figure 27. Fracture surfaces of Nextel 720/A specimens tested in tension following survival of 10^5 cycles at 1200°C in air environment (maximum stress = 170 MPa) at frequencies of: (a) 0.1 Hz, and (b) 1.0 Hz. Micrograph of specimen tested at 1.0 Hz is from reference [8].

Both specimens produced similar residual strength values (194 MPa and 192 MPa). Micrographs in Figure 27 (a) and (b) reveal that the specimen tested at 1.0 Hz had a somewhat larger damage zone and a higher degree of fiber pull-out.

5.1.2 Fatigue failure in steam at the frequency of 0.1 Hz

Figure 28 shows optical micrographs of three specimens tested at 0.1 Hz and three specimens tested at 1.0 Hz [8]. The images are arranged so that the lower left hand corner corresponds to the lowest maximum stress and the lower frequency of cyclic loading, while the image in the upper right hand corner represents the highest load and the higher frequency. Note that for each frequency, specimens tested with the fatigue stresses of 100, 125, and 150 MPa are shown.

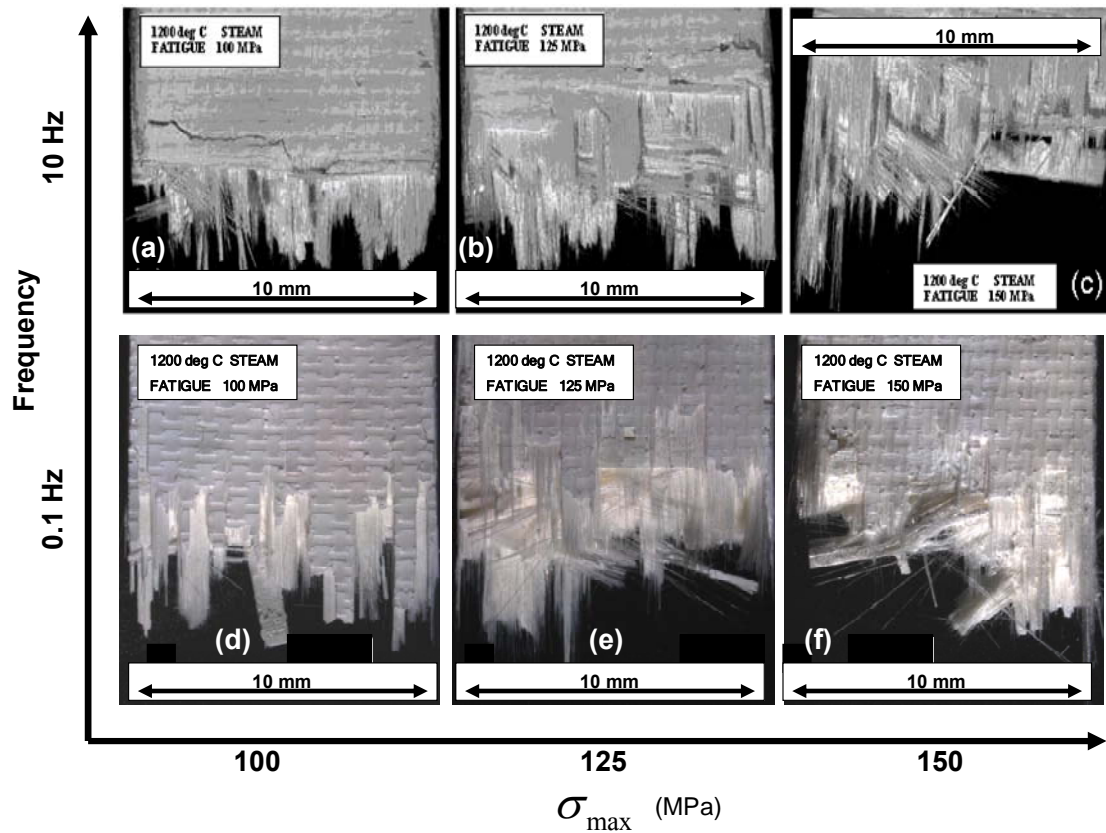


Figure 28. Fracture surfaces of Nextel 720/A specimens tested in fatigue at 1200°C in steam environment at maximum stresses of: (a,d) 100 MPa, (b,e) 125 MPa, and (c,f) 150 MPa, and frequencies of: (a,b,c) 10 Hz, and (d,e,f) 0.1 Hz. Specimens tested at 1.0 Hz exhibit higher degrees of fiber pull-out than those tested at the frequency of 0.1 Hz. Micrographs (a,b,c) are from reference [8].

Fracture mechanisms appear to vary based on both maximum stress and frequency. The specimen subjected to a 100 MPa test at 0.1 Hz exhibits variation in the fracture location of the 0° fiber tows woven into the composite, but little pull-out of individual fibers within each tow (see Figure 28 (d)). All fracture surfaces shown in Figure 28 are dominated by coordinated failure of fiber bundles with limited areas of fiber pull-out. The shapes of the fracture surfaces and the sizes of the damage zones are

similar for two specimens tested at different frequencies at a given stress level in Figure 28. The specimens tested at 1.0 Hz exhibit more fiber pull-out than those tested at 0.1 Hz.

Side views of the fracture surfaces produced in 0.1 Hz tests at the maximum stress levels of 150, 125, 100, and 75 MPa are shown in Figures 29 (a), (b), (c), and (d), respectively. Note that no significant delamination is seen in Figures 29 (a)-(d). Conversely, all four specimens shown in Figures 29 (a)-(d) exhibit both fiber pullout and variation in fiber tow lengths at the fracture surface.

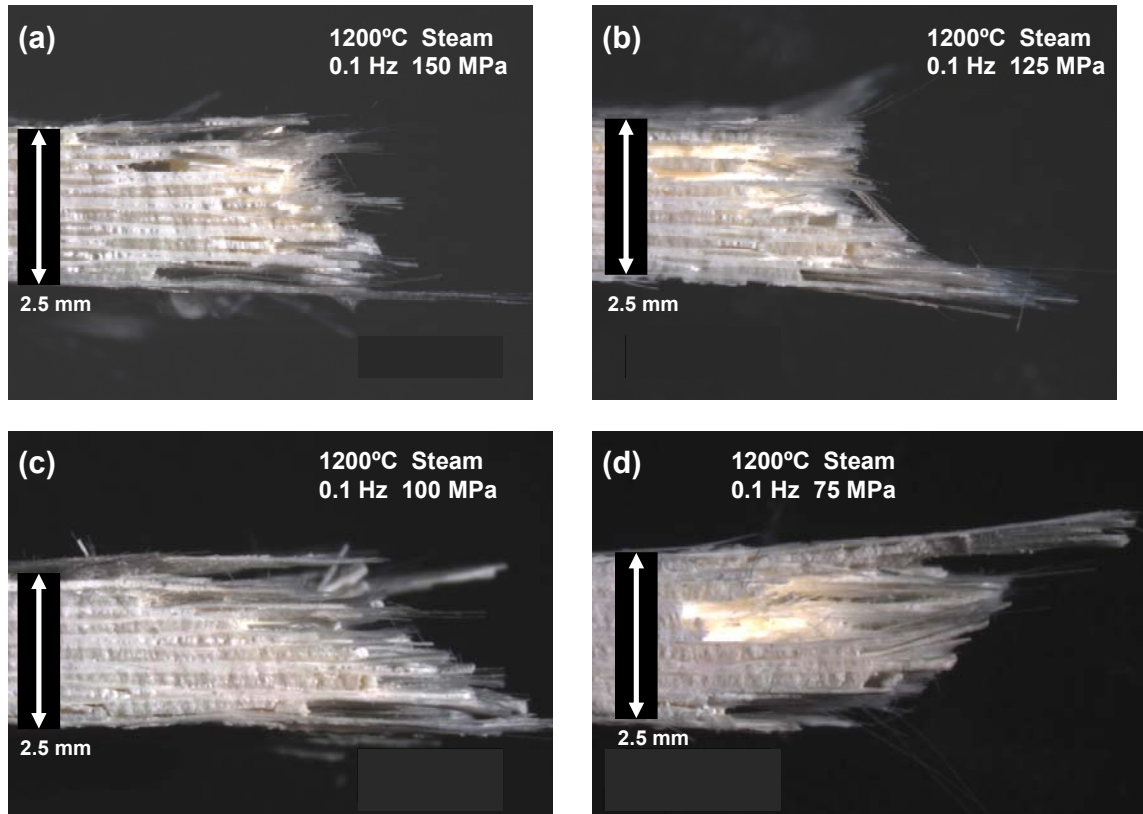


Figure 29. Fracture surfaces of Nextel 720/A specimens tested in fatigue at 1200°C in steam environment (frequency = 0.1 Hz) at maximum stresses of: (a) 150 MPa, (b) 125 MPa, (c) 100 MPa, and (d) 75 MPa.

5.1.3 Effect of frequency on fracture surface characteristics

As discussed in Section 4, fatigue frequency has a profound effect on the number of cycles to failure and failure strain. Figures 30 (a), (b), and (c) show specimens subjected to fatigue tests at the maximum stress of 170 MPa with frequencies of 0.1, 1.0, and 10 Hz, respectively. The damage zone produced at 0.1 Hz is small, on the order of 2mm (see Figure 30 (a)). Semi-planar failure dominates, but small areas of fiber pull-out can be seen. The specimen tested at 1.0 Hz, shown in Figure 30 (b), produced a longer damage zone and an increased level of fiber pullout. A significant change in the appearance of the fracture surface of the specimen tested at 10 Hz shown in Figure 30 (c). The length of the damage zone has increased to nearly 10 mm. Fiber pullout is considerable, with significant variation in pull-out length, both between separate fiber tows and individual adjacent filaments.

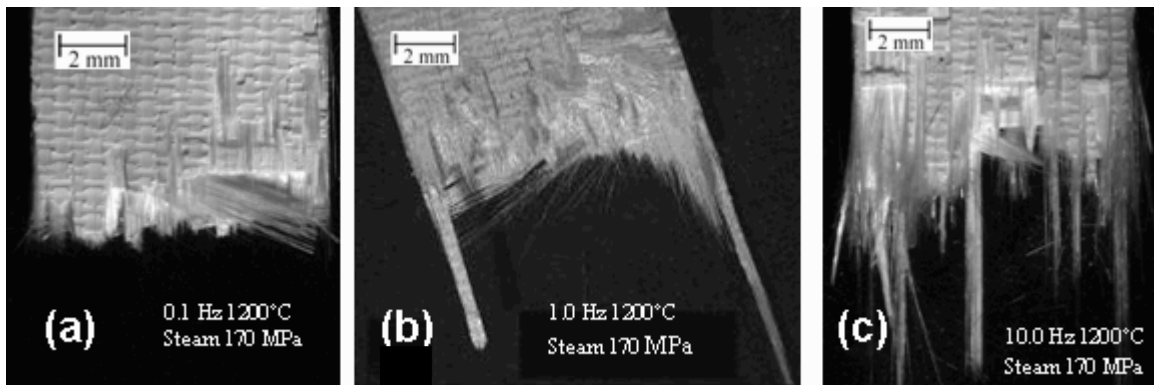


Figure 30. Fracture surfaces of Nextel 720/A specimens tested in fatigue at 1200°C in steam environment (maximum stress = 170 MPa) at frequencies of: (a) 0.1 Hz, (b) 1.0 Hz, and (c) 10 Hz. Damage zone size and fiber pullout increase with frequency. Micrograph (b) is from reference [8].

When N720 fibers are tested in tension, they tend to fail due to microcracks initiated during processing [7,46]. The distribution of these inherent stress concentrations varies between individual fibers, causing them to fail at different locations along the fiber axis. The extent of variation in failure locations amongst the fibers seen in Figure 30 (c) suggests weakening of the fiber/matrix interface. This is also seen in Figures 31 (a) and (b), which show side views of specimens subjected to fatigue tests at the maximum stress of 170 MPa with the frequencies of 0.1 and 10 Hz, respectively.

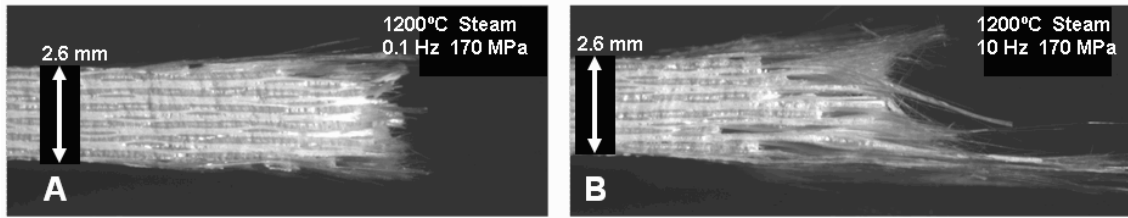


Figure 31. Fracture surfaces of Nextel 720/A specimens tested in fatigue at 1200°C in steam environment (maximum stress = 170 MPa) at frequencies of: (A) 0.1 Hz, and (B) 10 Hz. The specimen tested with the frequency of 10 Hz exhibits greater variation in fiber failure location.

Micrographs in Figures 30 and 31 give insight as to why increasing frequency at the same stress level tends to increase fatigue life. The increased amounts of fiber pull-out and variation in fiber failure location seen in fracture surfaces of specimens tested at 10 Hz may indicate that the fibers are failing more independently than in tests conducted at lower frequencies. This is likely due to a weakening of the fiber-matrix interface. Weakening of the fiber-matrix bond enhances existing crack deflection mechanisms, which in turn improves composite toughness, delays failure, and prolongs fatigue life.

5.2 Scanning Electron Microscopy

5.2.1 General SEM observations

Fracture surfaces of N720/A specimens observed in the current research rarely display a uniform appearance. Several different fracture surface topographies are present in each specimen, and the dominant characteristics vary depending on load and frequency. Tensile response in N720/A with 0°/90° fiber orientation is fiber-dominated. The porous matrix allows for cracks to propagate around the load-bearing fibers and delay failure. This phenomenon can be observed directly at magnifications above 500x, as shown in Figure 32.

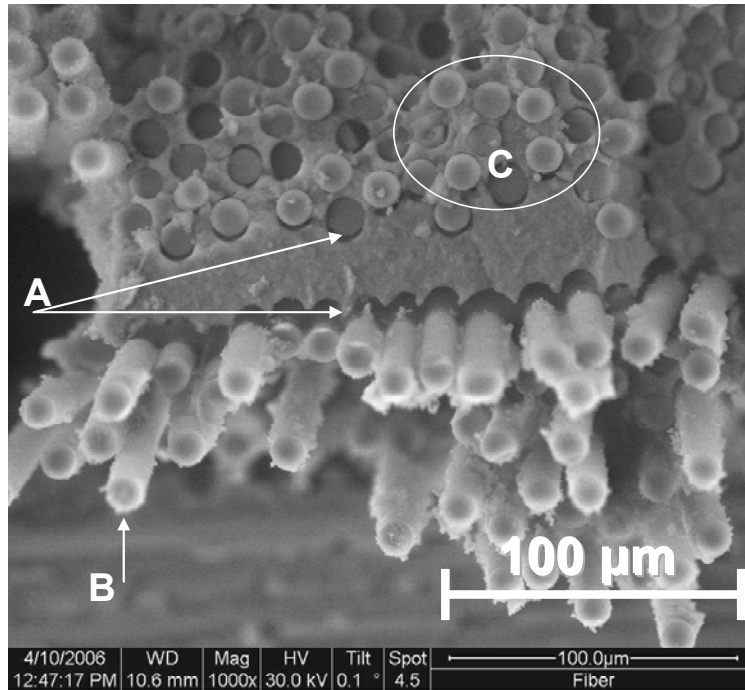


Figure 32. Fracture surface of a Nextel 720/A specimen tested in fatigue at 1200°C in steam environment (maximum stress = 75 MPa, frequency = 0.1 Hz) with emphasis placed on areas of: (A) crack deflection around fibers, (B) fiber pull-out, and (C) coordinated failure.

5.2.2 ESEM micrographs and discussion

Specimens were observed at magnifications of 50x, 100x, 500x, and 1000x using the ESEM mode. These observations served to reinforce observations made with the optical microscope. Fracture surfaces obtained at 0.1 Hz at maximum stresses of 170 and 150 MPa are shown in Figures 33 (a,b), and (c,d), respectively. Failures produced at higher stress levels consistently display larger regions of planar fracture, though fiber pullout is still seen in all specimens. The specimen tested at 0.1 Hz with a maximum stress of 170 MPa shown in Figure 33 (a,b), exhibits the least amount of fiber pull-out and the smallest damage zone of the four specimens shown in Figures 33 and 34.

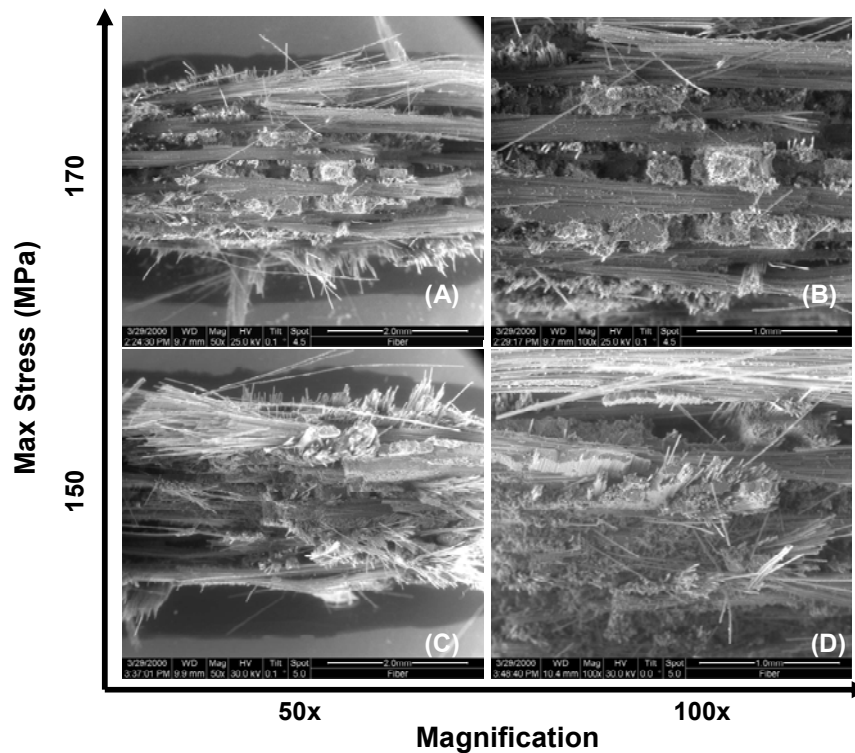


Figure 33. Fracture surfaces of Nextel 720/A specimens tested in fatigue at 1200°C in steam environment (frequency = 0.1 Hz) at maximum stresses of: (a,b) 170 MPa, and (c,d) 150 MPa. All micrographs exhibit both areas of coordinated fracture and fiber pull-out.

Different damage mechanisms can be observed within a single 0° fiber tow, as seen in Figure 34 (b). A rectangular, matrix-rich area in the middle of the tow is surrounded by a large number of individual pulled out fibers. This demonstrates one of the advantages of CMCs over monolithic ceramics – the existence of a single stress concentration in a CMC is unlikely to cause the entire specimen to fail. Note that the multiple regions of planar failure were initiated by different local microcracks. The irregularity of the damage zone also indicates that the fiber tows failed at different times during the fatigue test.

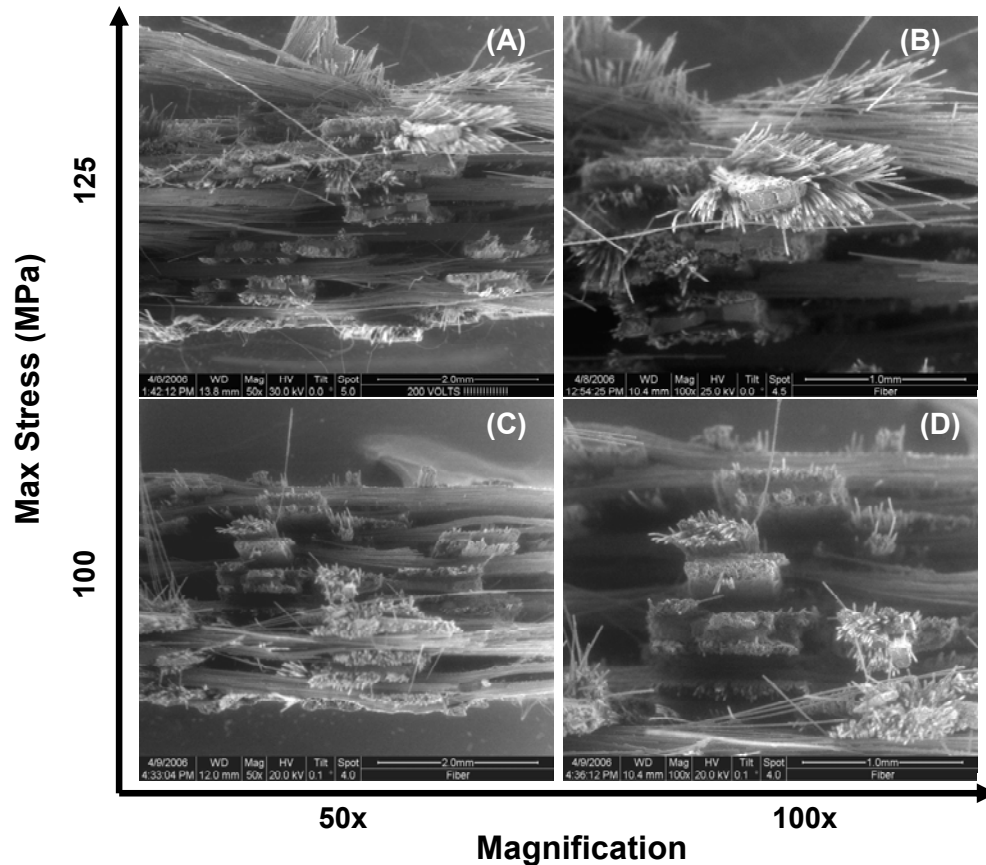


Figure 34. Fracture surfaces of Nextel 720/A specimens tested in fatigue at 1200°C in steam environment (frequency = 0.1 Hz) at maximum stresses of: (a,b) 125 MPa, (c,d) 100 MPa. All micrographs exhibit both areas of coordinated fracture and fiber pull-out.

Magnifications higher than 100x were used to study trends in the characteristics of fibers, matrix, and interfacial regions in ESEM mode. More regions of fiber pull-out were observed in specimens tested at lower maximum stress. Figure 35 (a) shows an area of fiber pull-out from the fracture surface produced in the 170 MPa test at 0.1 Hz. Note that there is little variation in the lengths of the pulled out fibers. It is also seen that these fibers did not fail due to a single crack front. Regions of fiber pullout produced at 0.1 Hz and maximum stresses of 150, 125, and 75 MPa are shown in Figure 35 (b), (c), and (d), respectively. As discussed in Section 4, longer fatigue lives are produced at lower stress levels. The higher levels of fiber pull-out observed for cases of longer cyclic life are consistent with larger failure strains.

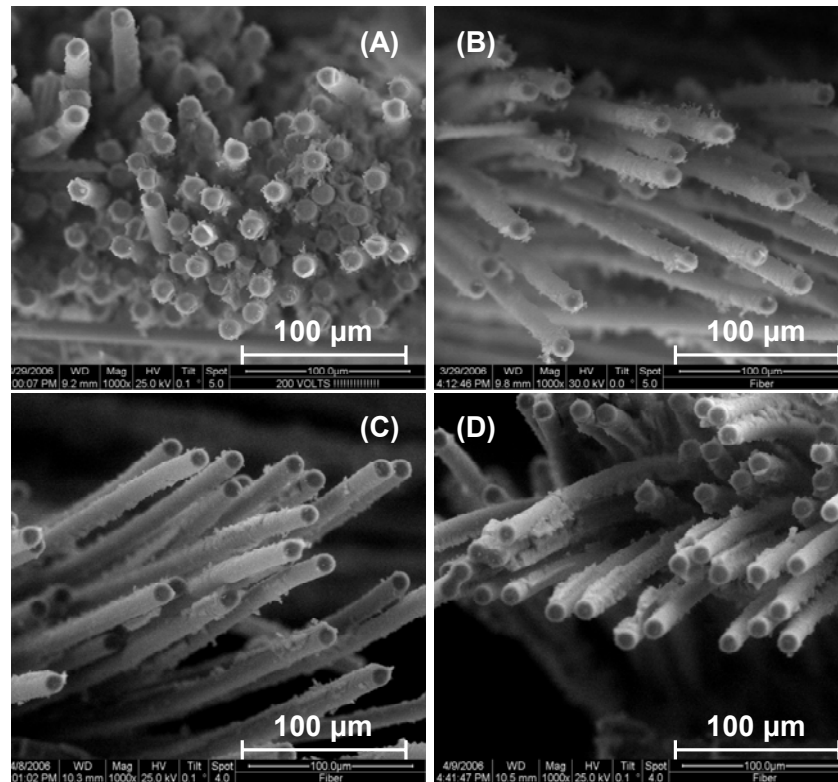


Figure 35. Fracture surfaces of Nextel 720/A specimens tested in fatigue at 1200°C in steam environment (frequency = 0.1 Hz) at maximum stresses of: (a) 170 MPa, (b) 150 MPa, (c) 125 MPa, and (d) 100 MPa. Micrographs show: (a) coordinated fiber failure, (b,c,d) fiber pull-out.

The correlation between a higher number of cycles to failure and longer fiber pull-out lengths is highly evident in the case of the specimen tested at 10 Hz and maximum stress of 170 MPa (see Figure 36). The fracture surface of this specimen is dominated by regions of fiber pull-out with only limited areas of coordinated failure. Only a few 90° tows are visible and matrix-rich areas are difficult to observe. If fibers and matrix fail in a coordinated fashion, only small amounts of matrix crumble away as the specimen fails, leaving ample matrix-rich areas to observe, as in the case of the specimen tested at 0.1 Hz and maximum stress of 170 MPa in steam. In the case of the specimen tested at 10 Hz and 170 MPa in steam, no significant amounts of matrix are seen on the fracture surface, suggesting that matrix cracks have essentially caused matrix to disintegrate in the failure region.

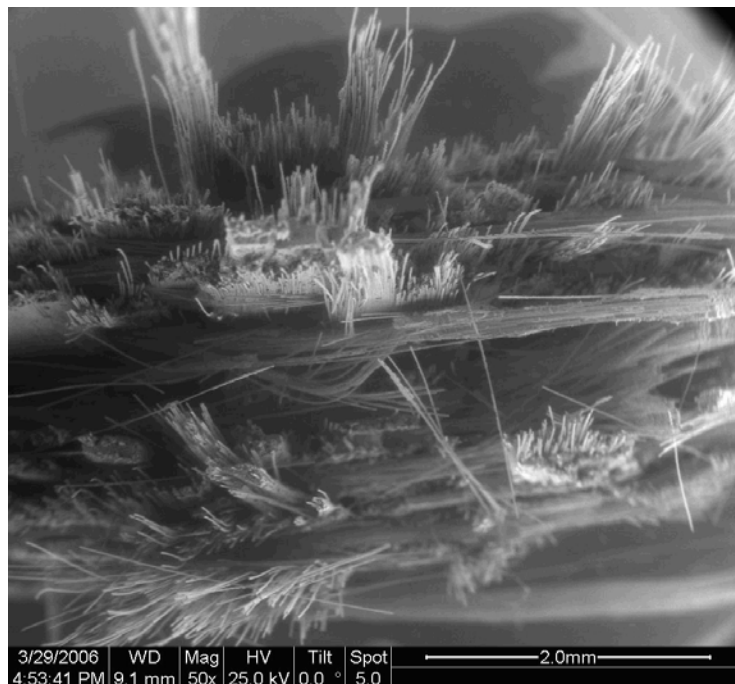


Figure 36. Fracture surface of a Nextel 720/A specimen tested in fatigue at 1200°C in steam environment (maximum stress = 170 MPa, frequency = 10 Hz) showing extensive fiber pull-out. Damage zone is seen in Figures 30 (c) and 31 (B).

The fracture surface produced at 10 Hz and 170 MPa showed variation in the fracture locations of adjacent fibers within individual tows. Typical variation in length of fiber pullout in this specimen is shown in Figure 37. Another distinguishing feature of this specimen that was not observed in other samples was that fairly large pieces of matrix material (up to two fiber diameters or $\sim 20\text{ }\mu\text{m}$ in width) remained attached to fibers.

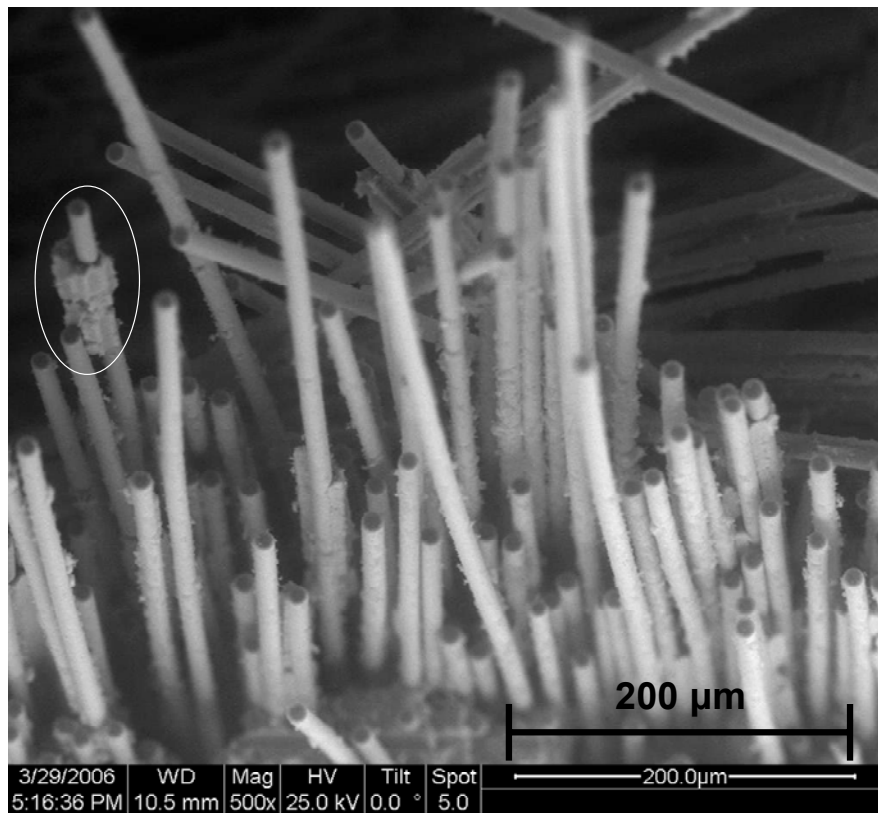


Figure 37. Fracture surface of a Nextel 720/A specimen tested in fatigue at 1200°C in steam environment (maximum stress = 170 MPa, frequency = 10 Hz) showing pulled-out fibers of varying lengths. Note the large pieces of matrix material attached to some fibers (circled).

The fibers set at odd angles in the background of Figure 37 are likely from the upper portion of a 90° bundle.

5.2.3 Fracture surface observation in high vacuum SEM mode

Specimens tested in steam at 170 MPa and frequencies of 0.1 and 10 Hz were coated with carbon and studied using high vacuum (HV) SEM mode. Despite identical environments and stress levels, the fracture surfaces of these two samples exhibit strikingly different topography. Figures 38 (a,b) and (c,d) show fracture surfaces produced in 170 MPa fatigue test conducted at frequencies of 10 and 0.1 Hz, respectively.

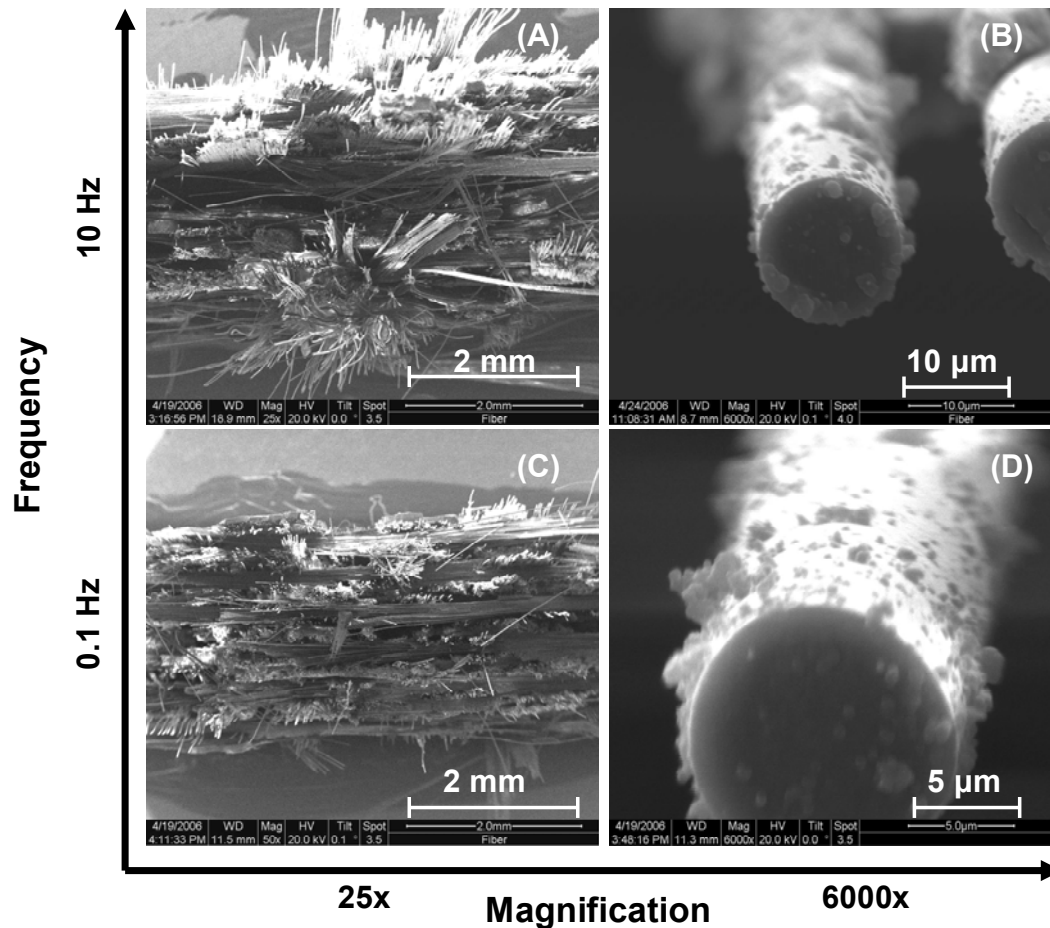


Figure 38. Fracture surfaces of Nextel 720/A specimens tested in fatigue at 1200°C in steam environment (maximum stress = 170 MPa) at frequencies of: (a,b) 10 Hz, and (c,d) 0.1 Hz. Micrographs (b) and (d) exhibit small pieces of matrix attached to the exposed fibers.

Regions of planar failure dominate the fracture surface produced at 0.1 Hz, while extensive fiber pullout is produced at 10 Hz. Conversely, the appearance of the pulled out fibers is similar for both cases. Micrographs in Figures 38 (b) and (d) both show particles of matrix still attached to the fiber, with the particle size varying from near a single grain to pieces larger than 1 μm . To a very small extent this wooly appearance of the fiber surface may be attributed to the tiny pieces of carbon attached to the surface during coating, but images of fibers located deeper within the material where carbon coating hardly penetrated reveal that the attached shapes are indeed pieces of matrix material.

The specimen tested at 10 Hz continued to accumulate charge during HV observation (see Figure 39). The long sections of fiber pull-out shielded inner parts of the specimen tested at the frequency of 10 Hz from being properly coated with carbon. Fibers from these interior portions such as those shown in Figure 39 should be free from any excessive carbon buildup that the longer pullout sections might be subject to. The brightness of the fiber in the lower-right corner of Figure 39 is indicative of charging, which results from a combination of specimen shape and coating thickness. If the particles attached to the fibers that create the wooly appearance contained significant amounts of carbon, then such charging would not be observed. This, together with the granular appearance of the wooly particles, suggests the conclusion that this surface topography was produced because the fiber did not detach completely from the matrix during fiber pull-out.

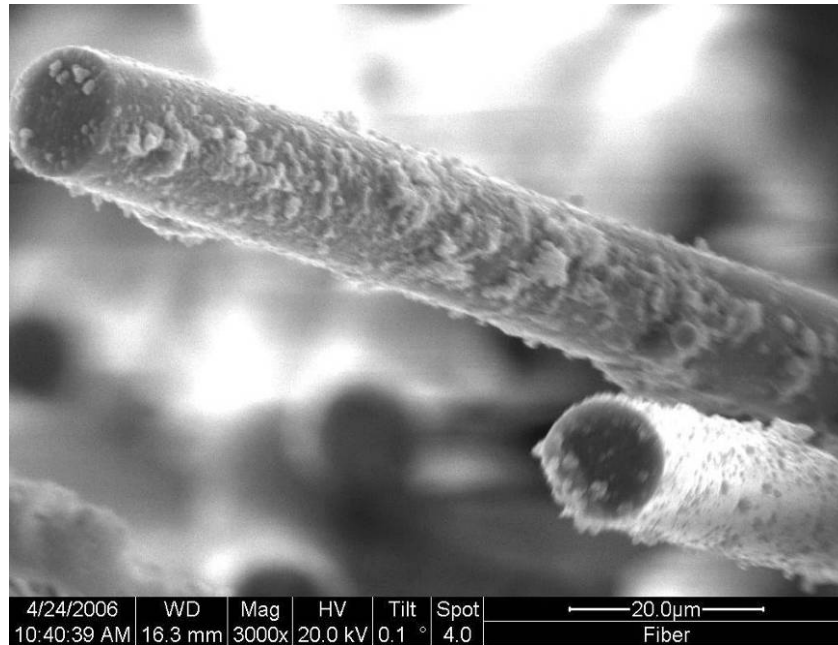


Figure 39. Fracture surface of a Nextel 720/A specimen tested in fatigue at 1200°C in steam environment (maximum stress = 170 MPa, frequency = 10 Hz) showing wooly fibers located deep within the specimen fracture surface.

The wooliness of the fiber surface can also be viewed as a manifestation of the crack deflection mechanism present in N720/A. It makes sense intuitively that as cracks are deflected around fibers into the matrix, parts of the matrix remain attached to the fiber. This can be seen in Figure 40 (b), where details of the fracture surface produced in the 170 MPa fatigue test at 10 Hz are presented.

The irregular path of the crack around the fiber in Figure 40 (b) suggests the reason for the variety of particle sizes on the outer surface of the fibers. Portions of the fiber surface have separated cleanly from the matrix as is the case on the upper-left side, but the other sections are left with a jagged pattern of matrix particles that remain attached after the crack has passed through the area. It is likely that some of the larger attached matrix particles are sheared off during fiber pullout.

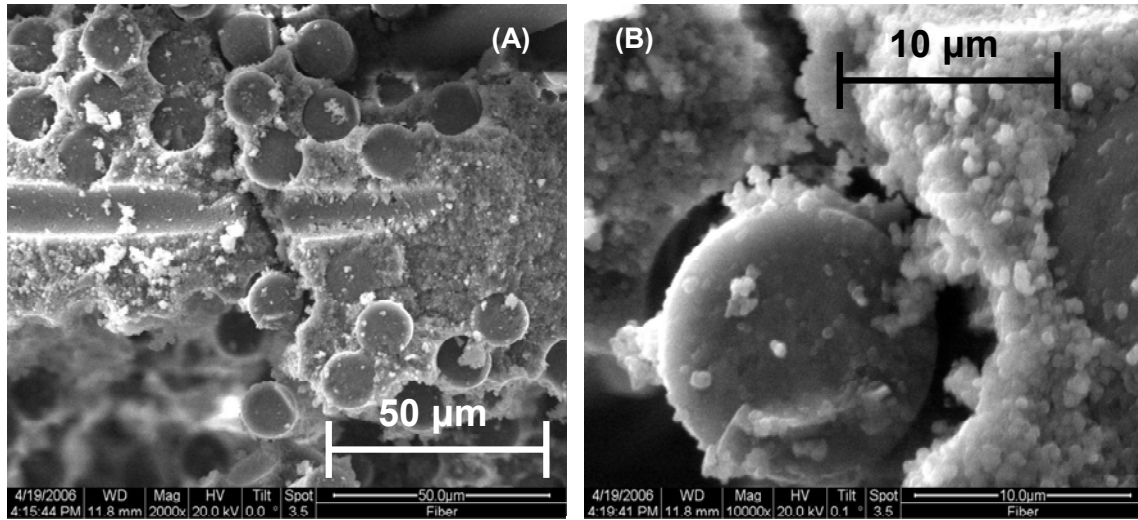


Figure 40. Fracture surface of a Nextel 720/A specimen tested in fatigue at 1200°C in steam environment (maximum stress = 170 MPa, frequency = 10 Hz) showing: (a) crack deflection around 0° fibers, and (b) a magnified view of the same area.

Images taken at magnification levels up to 25x indicate that cyclic loading at higher frequencies weakens the fiber/matrix interface, resulting in improved fatigue performance of the CMC. Higher power ESEM micrographs show the variations in fiber pull-out length with maximum stress and frequency. Detailed high-vacuum images of the fiber surfaces in Figures 38, 39, and 40 reveal that specimens fatigued at different frequencies retain similarities in crack deflection mechanisms. Further study is necessary before the reasons behind improved fatigue performance at higher frequencies can be fully understood.

5.3 Energy Dispersive X-ray Spectroscopy (EDS)

Fatigue life of N720/A is adversely affected by the presence of steam. The exact nature of the interaction between steam and the N720/A CMC is not known. Steam could possibly act as a catalyst for a chemical or physical reaction between fiber and matrix within the composite. Such a reaction in cyclic loading could be accelerated by the fatigue stress and frequency. Evidence of species migration between fiber and matrix would indicate reactivity.

Silicon is present in N720/A in the mullite phase of the fibers, but not in the alumina matrix. Wannaparhun et al. [44] observed trace amounts of silicon in the matrix of N720/A specimens using X-ray analysis, which was attributed to possible contamination during processing. If a rise in silicon in the matrix above the nominal amount were observed, this may indicate leaching of silicon from the mullite phase of the fiber into the matrix.

Prior work by Mehrman [23] analyzed N720/A specimens tested in creep at 1200°C in air and in steam environment using Energy Dispersive Spectroscopy (EDS). Greater evidence of migration of silicon species from the fibers to the matrix was observed for specimens tested in steam than those tested in air. This was presented as a possible cause of decreased creep performance of N720/A in steam environment.

Energy Dispersive Spectroscopy was used in the current work to qualitatively evaluate the effects of load and frequency on silicon species migration from fibers to matrix. Three specimens tested in steam were coated with carbon for observation in the high vacuum mode of the SEM: the specimens tested with the frequency of 0.1 Hz and

maximum stresses of 170 and 75 MPa, and the specimen tested with the frequency of 10 Hz and maximum stress of 170 MPa. The latter two specimens exhibited fiber pull-out and were subject to charging during high vacuum observation, despite the presence of the carbon coating. These fracture surfaces were analyzed using EDS in the ESEM mode, during which no charging was perceived. The electron beam was placed in spot mode during collection to improve precision. Analysis using EDS was conducted with parameters set within the manufacturer's recommendations of 10 mm working distance, 1000-2000 counts per second, and 20-40% dead time.

Figure 41 shows spectra of fiber and matrix from the specimen tested in steam with the frequency of 0.1 Hz and maximum stress of 170 MPa. Spectra of N720 fibers indicate the presence of four primary elements: carbon from the specimen coating, aluminum and oxygen from the alumina and mullite phases, and silicon from the mullite phase. Spectra of isolated matrix-rich areas exhibit slightly lower oxygen counts and only a minute amount of silicon. These spectra are typical of fibers and matrix observed in the current research. Note that the counts for each energy level are normalized with respect to the maximum aluminum content of the spectra. This normalization technique facilitates comparison of spectra with small differences in the number of total counts. All spectra presented in this section are normalized in this manner. Counts shown in the figures are unitless and should be interpreted qualitatively in terms of their relative magnitudes.

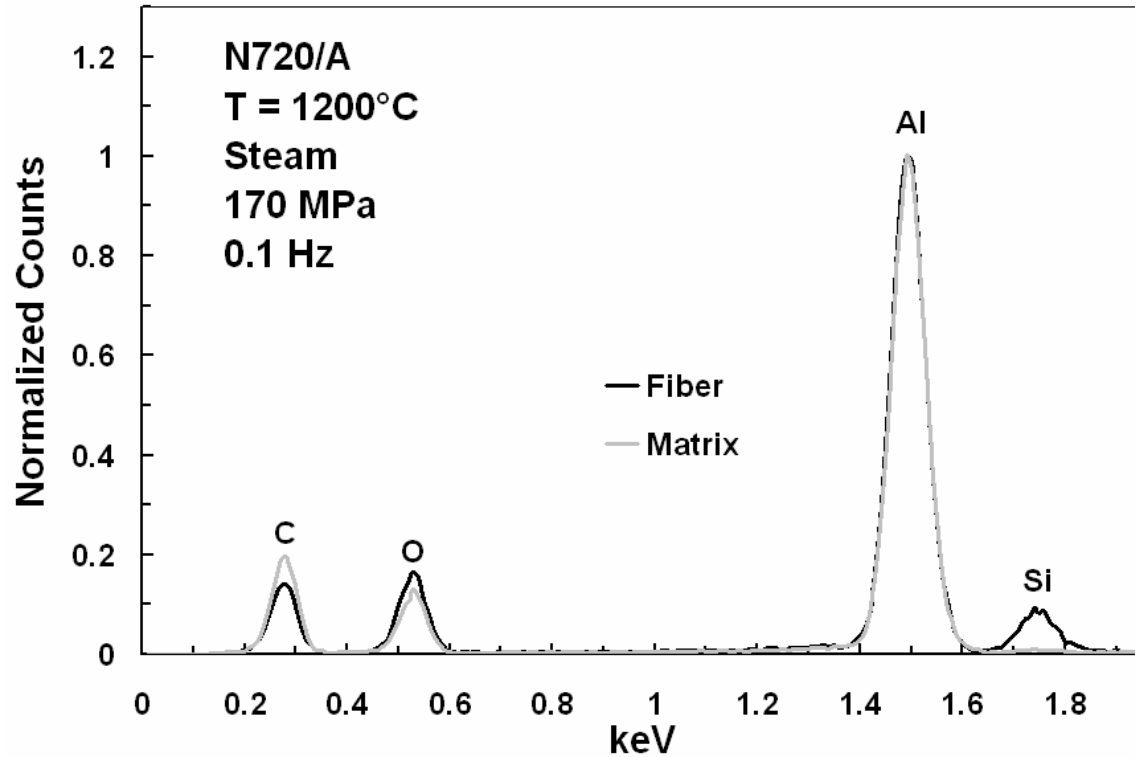


Figure 41. EDS spectra of fiber and matrix of N720/A composite tested in fatigue at 1200°C in steam environment with maximum stresses 170 MPa and frequency 0.1 Hz.

The reaction volume of the SEM beam is teardrop-shaped, which may contaminate results if the fibers and matrix are close to the area of interest. Contamination was avoided by analyzing the spectra of matrix-rich areas located in the matrix interior away from fibers, as well as the spectra of matrix located at the edge of the troughs where 0° fibers were present before failure. Figure 42 shows fracture surface locations that were analyzed using EDS. Due to uncertainties in the size and shape of the reaction volume, results in this section should be interpreted as qualitative.

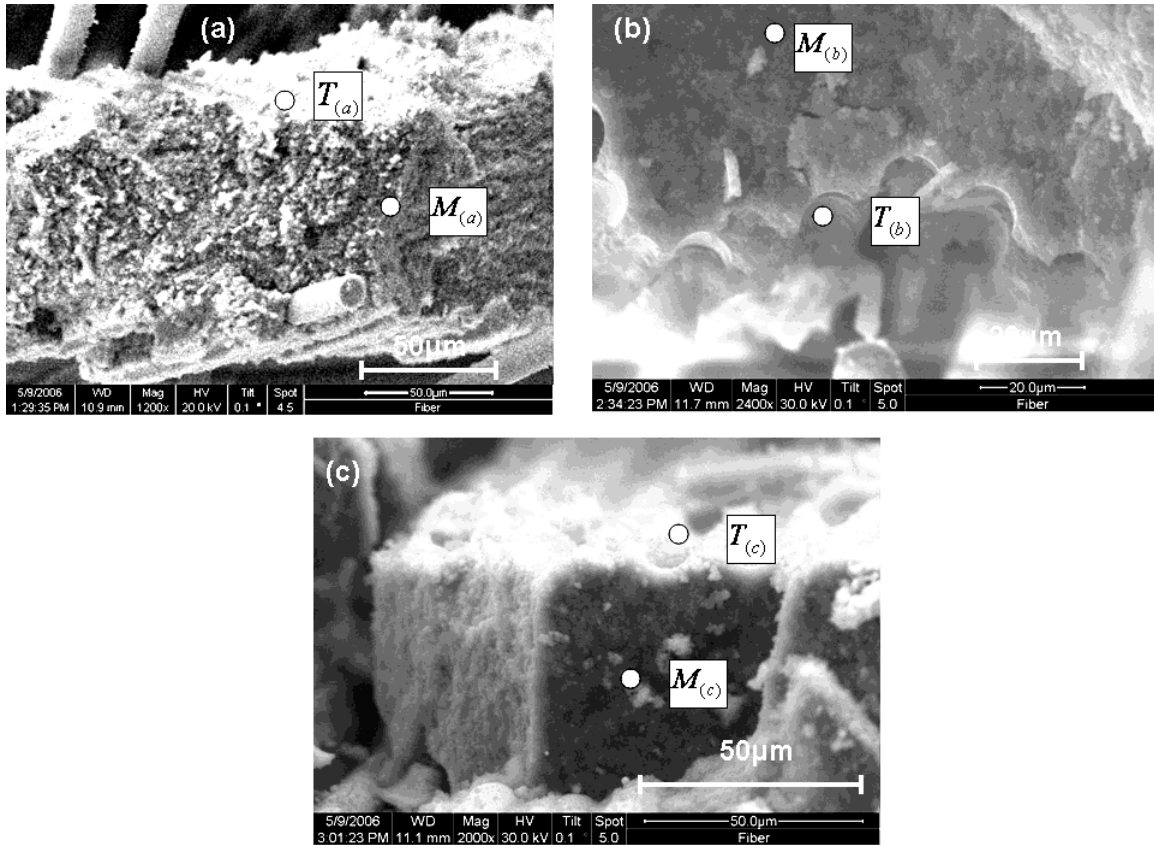


Figure 42. Fracture surfaces of Nextel 720/A specimens tested in fatigue at 1200°C in steam environment with maximum stresses and frequencies: (a) 170 MPa, 0.1 Hz, (b) 75 MPa, 0.1 Hz, (c) 170 MPa, 10 Hz. Areas analyzed with EDS are indicated on each micrograph as follows: T(a), T(b), and T(c) indicate matrix troughs left by pulled out fibers, while M(a), M(b), and M(c) indicate matrix interior.

Spectra for matrix-rich areas located away from the fiber/matrix interface reveal similar levels of silicon for all three specimens analyzed (see Figure 43). The small degree of variation in these spectra implies that if migration of silicon species depends on load and/or frequency, then the reaction between fiber and matrix is mostly limited to areas adjacent to the fiber/matrix interface.

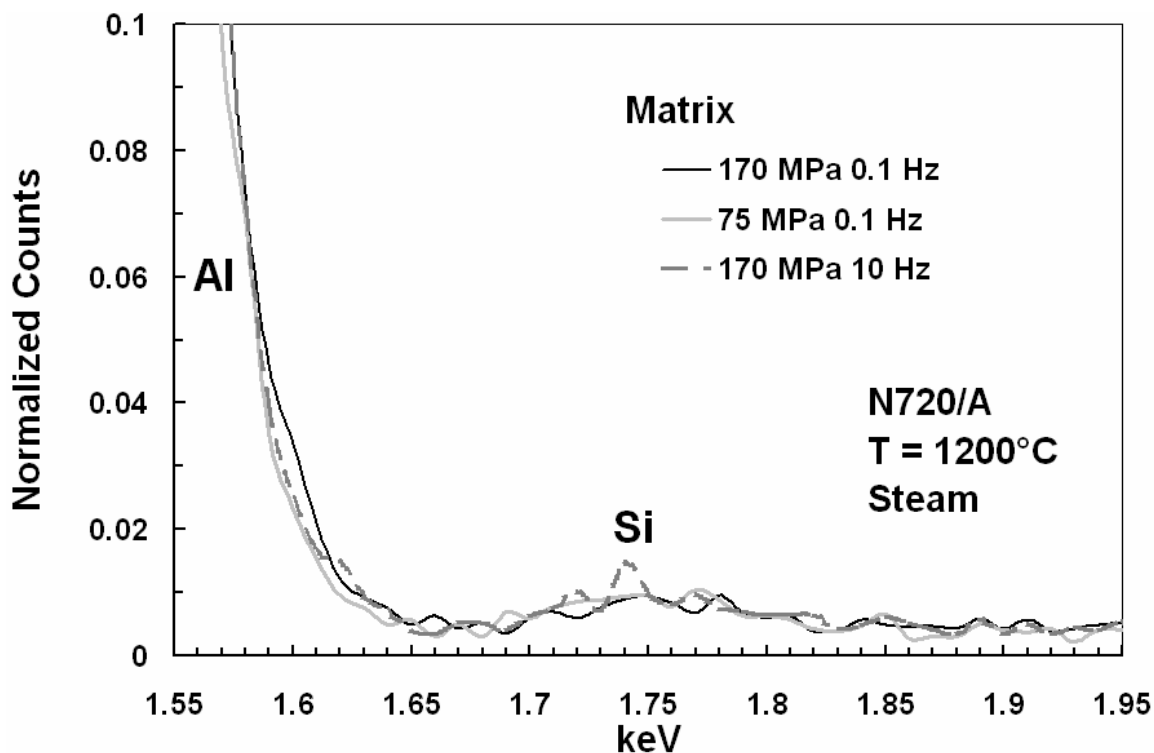


Figure 43. EDS spectra of matrix from three N720/A specimens tested in fatigue at 1200°C in steam environment with maximum stresses and frequencies of: 170 MPa and 0.1 Hz, 75 MPa and 0.1 Hz, and 170 MPa and 10 Hz.

Figure 44 compares the size of the silicon peaks for spectra of interior matrix and of matrix near the fiber/matrix interface in the specimens tested at 170 MPa with the frequencies of 0.1 Hz and 10 Hz. For both specimens, the spectra of matrix near the fiber edges exhibit noticeably larger silicon peaks than the spectra of the matrix interiors, which suggests leaching of silicon species from the mullite phase of the fibers. It is seen that the size of the silicon peak for the matrix near the interface appears higher for the specimen tested at 10 Hz than for the specimen tested at 0.1 Hz. Thus the reactivity between fiber and matrix in steam at high temperature may depend on loading rate, with the higher frequency corresponding to a increased evidence of species migration.

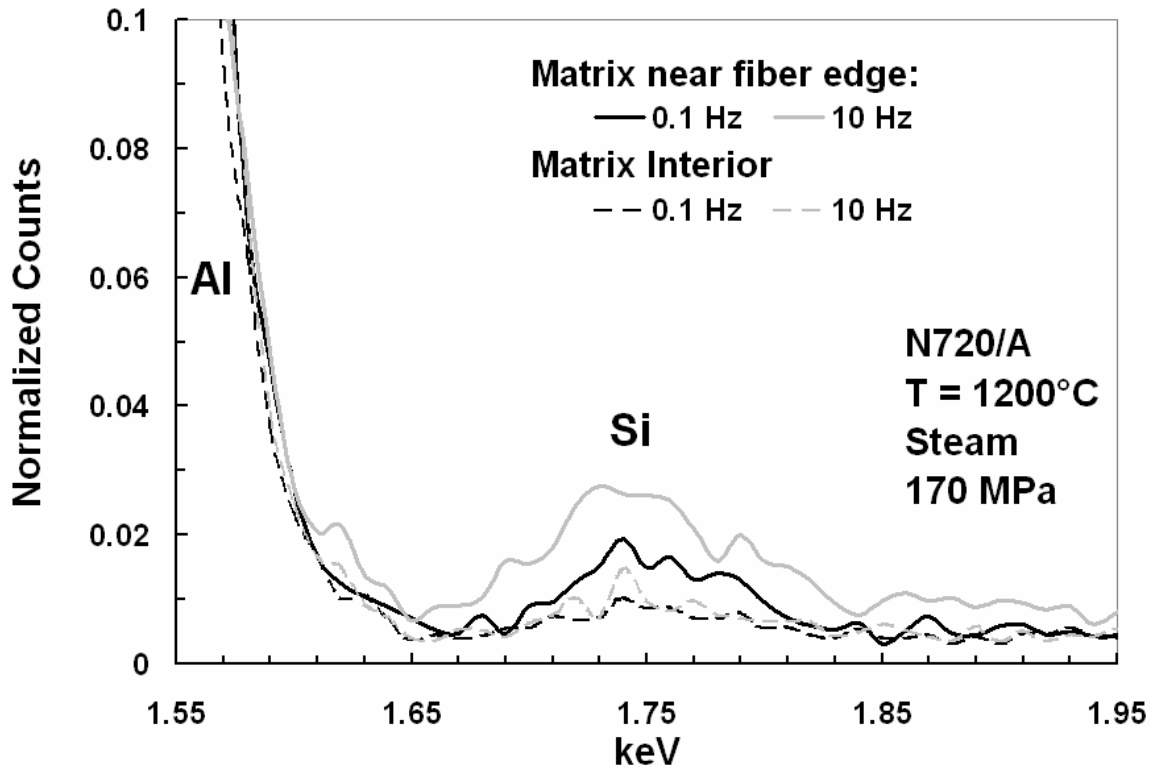


Figure 44. EDS spectra of matrix near fiber edge from two N720/A specimens tested in fatigue at 1200°C in steam environment with maximum stress 170 MPa and frequencies of 0.1 Hz and 10 Hz.

The specimen tested with the frequency of 10 Hz and maximum stress of 170 MPa showed improved fatigue performance over the specimen tested at the frequency of 0.1 Hz at the same stress level, but the former specimen also exhibits slightly more silicon species migration than the latter. If leaching of silicon species from the fibers to the matrix is a symptom of the degraded performance of N720/A in steam environment, it is possible that testing at 10 Hz may allow the composite to withstand higher levels of oxidation than is possible at lower frequencies. Conversely, the degree of silicon species accumulation in the matrix near the fiber/matrix interface may simply be a poor indicator of fatigue life.

Fatigue stress does not appear to affect the level of silicon species migration from fibers to matrix during fatigue testing of N720/A in steam. Figure 45 shows spectra of the matrix near the fiber-matrix interface for the specimens tested with the frequency of 0.1 Hz and maximum stresses of 170 MPa and 75 MPa. The silicon peaks for the two samples are of similar size.

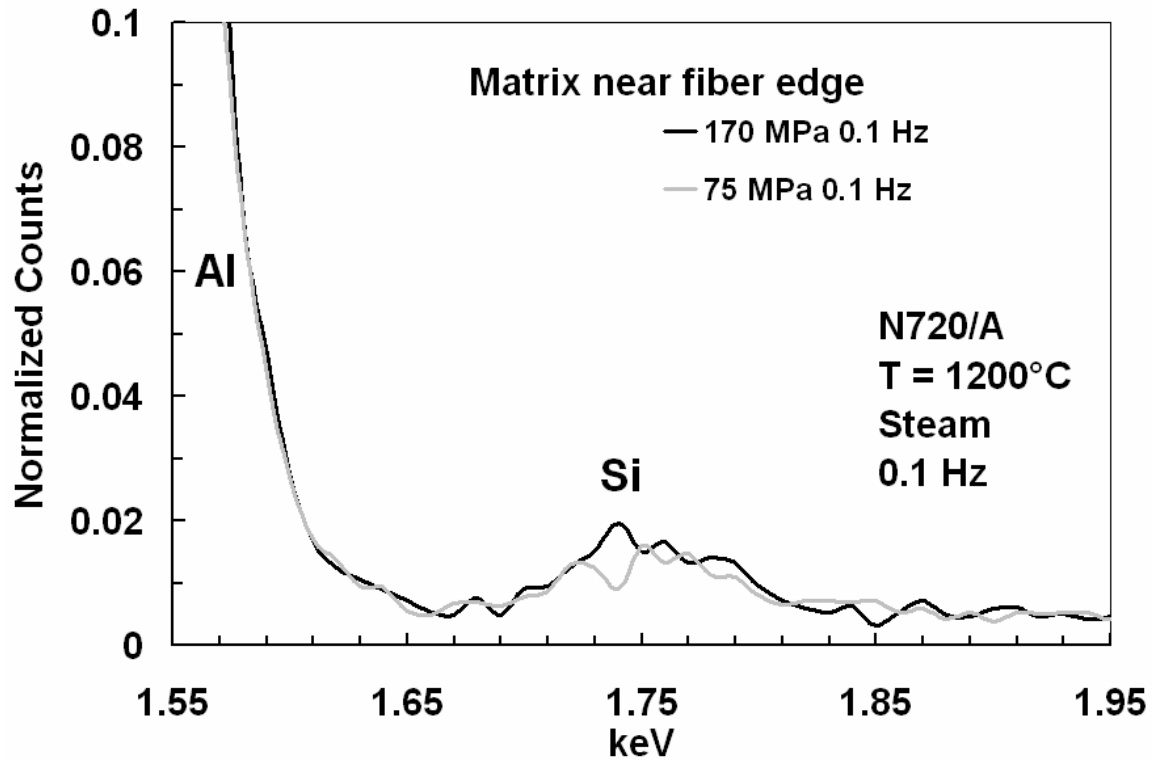


Figure 45. EDS spectra of matrix near fiber edge from two N720/A specimens tested in fatigue at 1200°C in steam environment with the frequency of 0.1 Hz and maximum stresses of 170 MPa and 75 MPa.

The specimen tested with the lower maximum stress had a much longer fatigue life (155.82 hours) than the specimen tested with the higher maximum stress (0.03 hours). The evidence that similar amounts of silicon were leached from the fiber over such disparate time periods implies that the rate of species migration may decrease with load.

A qualitative EDS-based assessment of the migration of silicon species from fiber to matrix indicates that for a given frequency the level of species migration appears to be independent of stress, but the maximum stress may accelerate such migration. It is seen that frequency has an effect on the overall accumulation of silicon within the matrix near the interface. Further analysis may yield additional insight into the underlying causes behind the trends observed in this work. A quantitative assessment is necessary before any definitive conclusions are drawn regarding the relationship between silicon species migration and decreased fatigue performance of N720/A CMC in the presence of steam.

6 Conclusions and Recommendations

6.1 Conclusions

6.1.1 Mechanical testing in air

Fatigue performance of N720/A at 1200°C in air environment at a loading rate of 0.1 Hz was comparable to that at 1.0 Hz [8]. The CMC survived 10^5 cycles at 0.1 Hz at a maximum stress equivalent to 88% of the UTS with high retained strength and stiffness. Frequency does not seem to have a significant effect on in-air fatigue performance of N720/A at 1200°C.

6.1.2 Mechanical Testing in Steam

N720/A CMC exhibits degraded mechanical performance in the presence of steam. Fatigue tests conducted in steam environment at 1200°C resulted in increased brittleness and decreased fatigue life compared to similar tests conducted in air. Specimens tested at lower maximum stress levels exhibited higher numbers of cycles to failure as well as larger failure strain levels.

Fatigue performance in steam environment showed a strong dependence on frequency, as opposed to results obtained in air. An order of magnitude decrease in frequency from 1.0 Hz to 0.1 Hz led to shorter times to failure as well as smaller failure strains. An order of magnitude increase in frequency from 1.0 Hz to 10 Hz resulted in longer fatigue life and less brittle behavior. The fatigue limit of N720/A in steam was found to be 150 MPa at 10 Hz, 125 MPa at 1.0 Hz [8], and less than 75 MPa at 0.1 Hz,

with run-out defined as survival of 10^6 cycles for the frequency of 10 Hz and survival of 10^5 cycles for the frequencies of 1.0 and 0.1 Hz. Decreased fatigue performance in steam environment compared to that in air likely depends upon uninterrupted time spent at high load levels.

Significant elastic modulus degradation was not observed within the small number of specimens tested. Specimens tested with the frequency of 10 Hz exhibited smaller variations in stiffness as a function of cycle number than specimens tested at 0.1 Hz.

Evaluation of hysteresis energy density for the frequency of 0.1 Hz showed that a majority of energy dissipation occurred during the first few cycles of each test. Hysteresis energy density was smaller at a given cycle number for tests conducted at lower maximum stress levels. The value of HED approached zero for high cycle numbers for the specimen tested with the frequency of 0.1 Hz and maximum stress of 75 MPa.

6.1.3 Microscopy

Optical micrographs revealed a high degree of fiber pullout and large damage zone size for the specimen subjected to cyclic loading in steam with the frequency of 10 Hz. High variation in fracture location between adjacent fibers in the specimen tested at the frequency of 10 Hz may indicate a weakening of the fiber/matrix interface.

Images obtained through use of a scanning electron microscope showed matrix cracks propagating around fibers through the porous matrix. All specimens showed areas

of coordinated failure as well as fiber pull-out. Fracture surfaces of specimens tested with the frequency of 0.1 Hz appeared to be dominated by coordinated failure, with the degree of pullout increasing for specimens tested at lower maximum stresses. Small pieces of matrix attached to the exposed surfaces of pulled-out fibers were observed in all specimens.

6.1.4 Spectroscopy

A qualitative EDS analysis revealed evidence of silicon species migration from the mullite phase of the fibers to the alumina matrix. Spectra normalized with respect to the maximum aluminum content for areas of isolated matrix material were similar for all test frequencies and load levels observed. The silicon peak of the matrix near the fiber/matrix interface for the specimen tested with the frequency of 10 Hz appeared more prominent than the silicon peaks obtained for the specimens tested with the frequency of 0.1 Hz. Leaching of silicon from the fibers may occur at a slower rate for specimens tested at lower maximum loads.

6.1.5 Final Conclusions

While N720/A is an excellent candidate for applications in air at temperatures up to 1200°C, care should be taken when considering its use in the presence of steam. Frequency has significant effects on the fatigue performance of the composite in steam environment, with tests conducted at higher frequencies resulting in longer fatigue lives

and increased failure strains. Factors affecting the fatigue damage mechanisms of oxide/oxide CMCs with a porous matrix in steam are not well understood currently and should be investigated further.

6.2 Recommendations for Further Work

Holmes [14] observed a correlation between decreased fatigue performance of a SiC-reinforced CMC at high frequencies and temperature increase due to frictional heating. An investigation should be made into the temperature rise of N720/A at various frequencies and maximum stress levels.

Mehrman [23] showed that a prior fatigue improves the creep performance of N720/A. If fatigue performance depends on load frequency, then creep performance of pre-fatigued material should also be rate-dependent. Mehrman conducted all fatigue tests at a frequency of 1.0 Hz, thus varying the frequency of cyclic loading prior to creep testing could help shed some light on the damage mechanisms present at different frequencies.

There likely exists an optimal frequency where fatigue performance of N720/A CMC is maximized. This frequency would conceivably be high enough to weaken the bonds between fiber and matrix substantially, yet not so high as to exacerbate damage due to frictional heating. Additional testing of N720/A at higher frequencies is necessary to determine if such an upper limit exists.

Appendix A Additional Micrographs

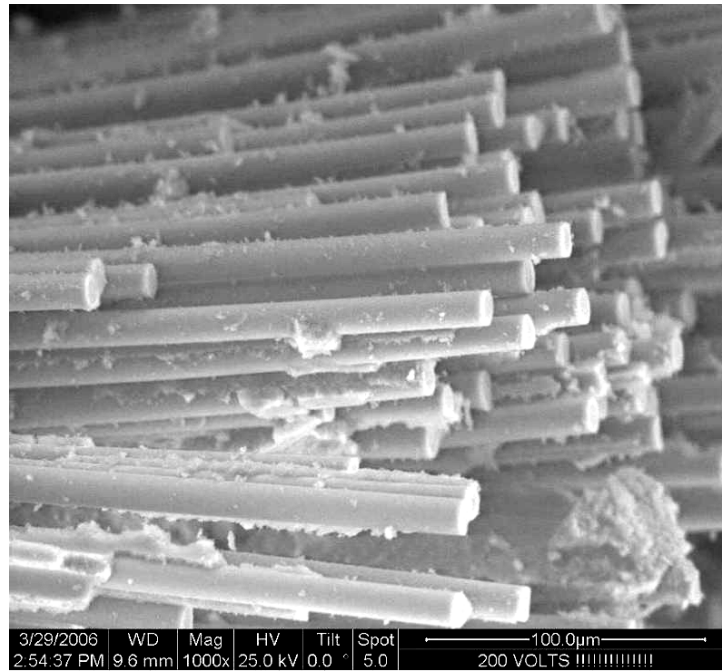


Figure 46. Fracture surface of a Nextel 720/A specimen tested in fatigue at 1200°C in steam environment (maximum stress = 170 MPa, frequency = 0.1 Hz) showing 90° fiber bundle.

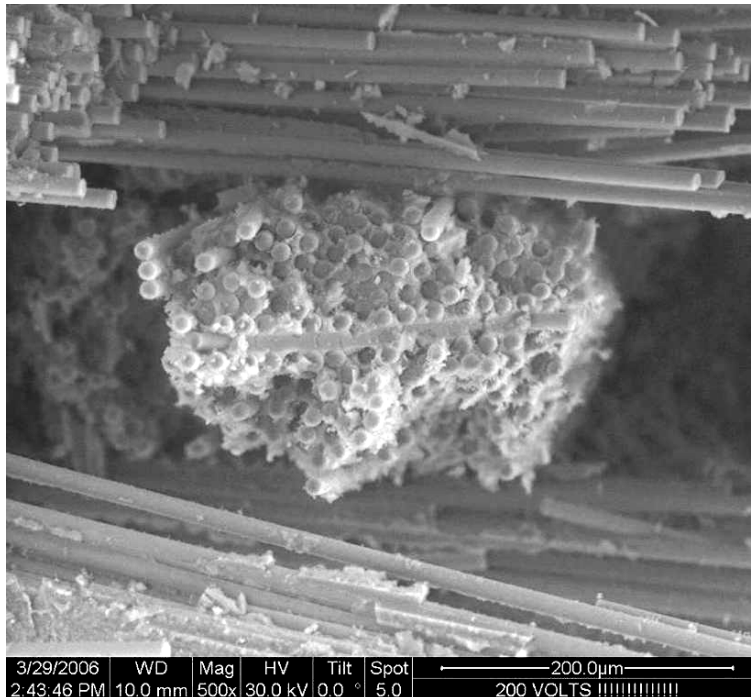


Figure 47. Fracture surface of a Nextel 720/A specimen tested in fatigue at 1200°C in steam environment (maximum stress = 170 MPa, frequency = 0.1 Hz) showing coordinated failure of a 0° fiber bundle.

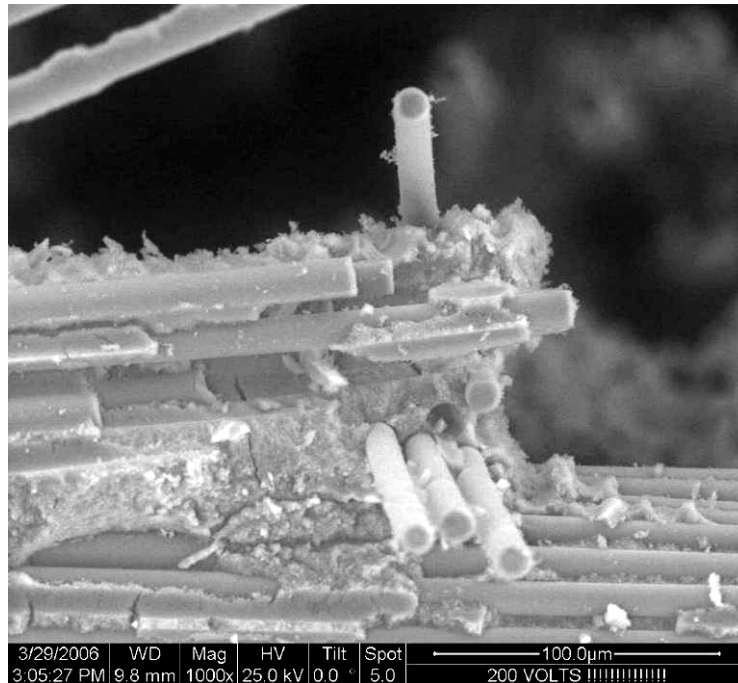


Figure 48. Fracture surface of a Nextel 720/A specimen tested in fatigue at 1200°C in steam environment (maximum stress = 170 MPa, frequency = 0.1 Hz) showing 0° fibers at the edge of a 90° bundle.

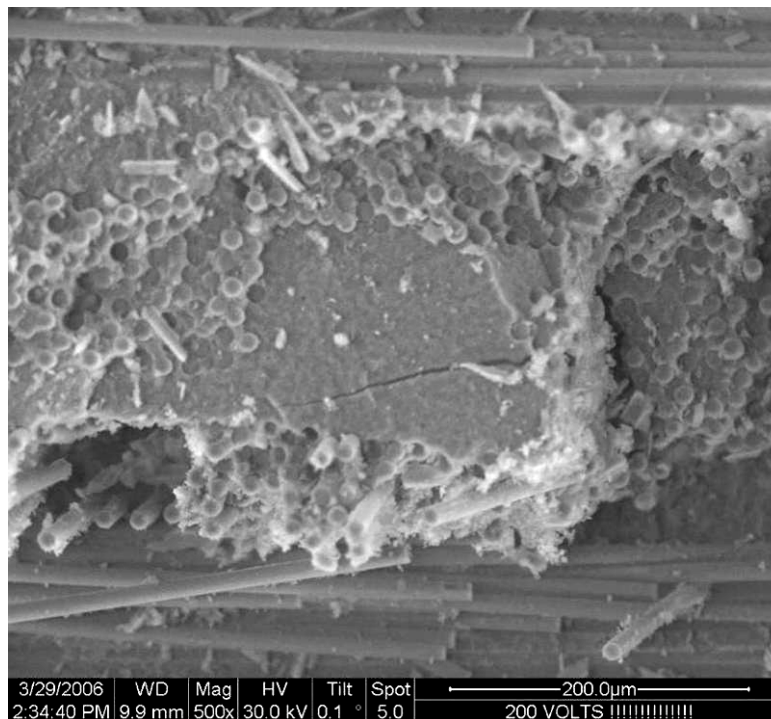


Figure 49. Fracture surface of a Nextel 720/A specimen tested in fatigue at 1200°C in steam environment (maximum stress = 170 MPa, frequency = 0.1 Hz) showing matrix rich area.

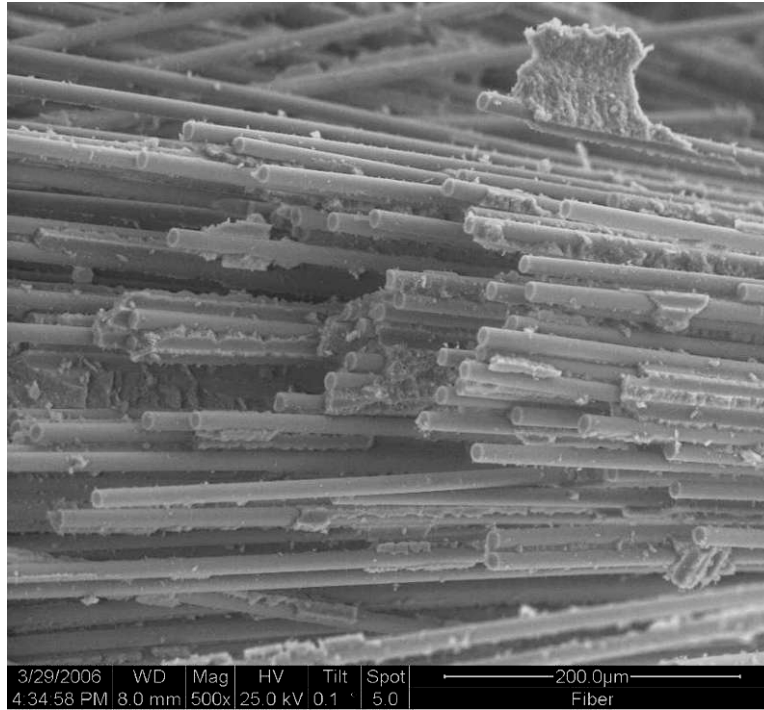


Figure 50. Fracture surface of a Nextel 720/A specimen tested in fatigue at 1200°C in steam environment (maximum stress = 150 MPa, frequency = 0.1 Hz) showing 90° fibers with variation in failure location.

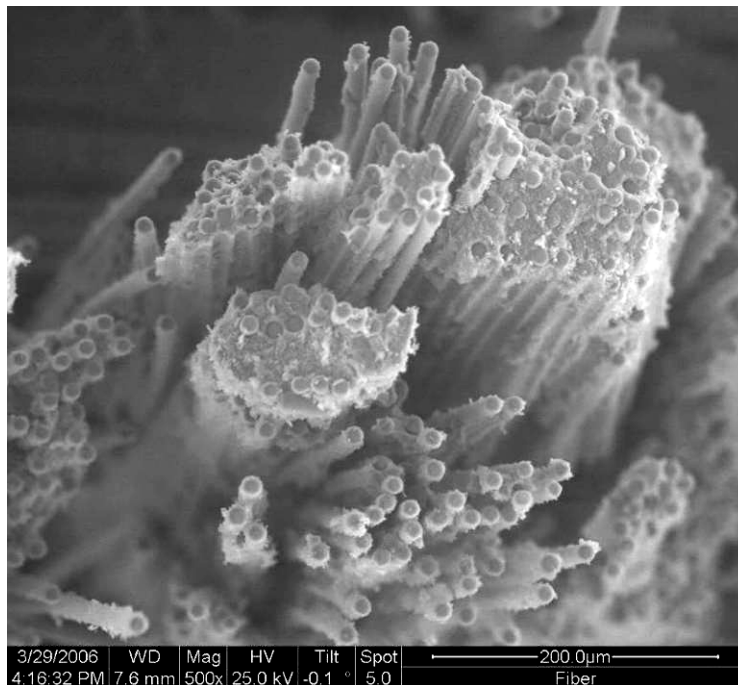


Figure 51. Fracture surface of a Nextel 720/A specimen tested in fatigue at 1200°C in steam environment (maximum stress = 150 MPa, frequency = 0.1 Hz) showing both pull-out and coordinated failure in a single tow.

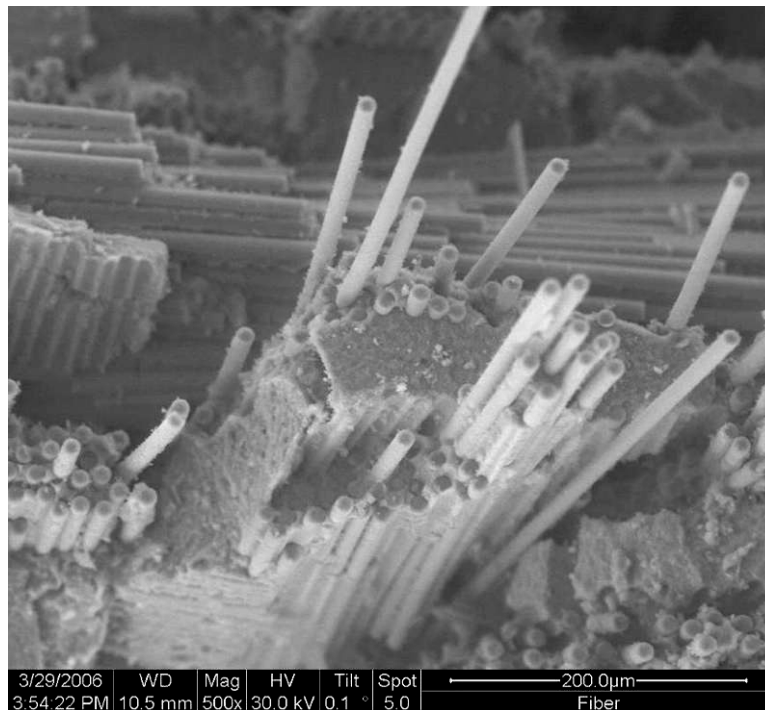


Figure 52. Fracture surface of a Nextel 720/A specimen tested in fatigue at 1200°C in steam environment (maximum stress = 150 MPa, frequency = 0.1 Hz) showing matrix rich area with isolated fiber pull-out.

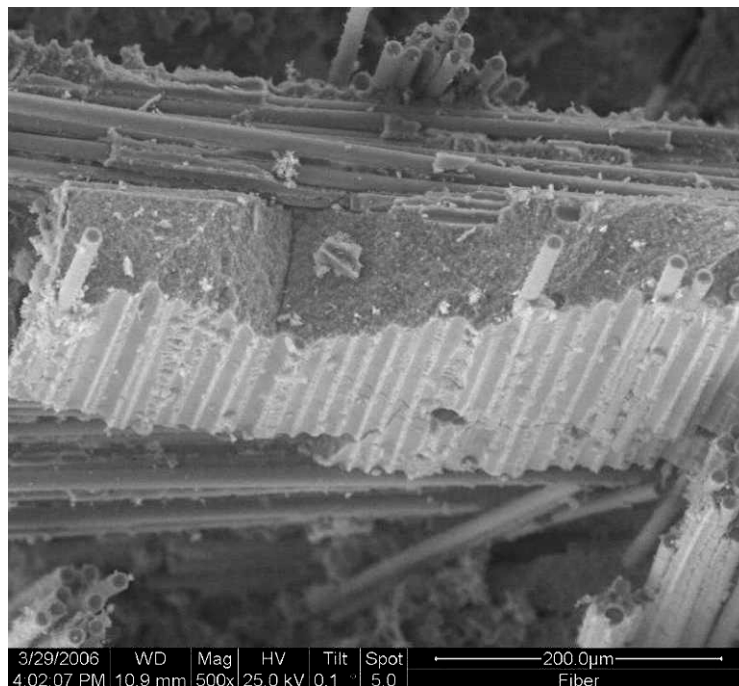


Figure 53. Fracture surface of a Nextel 720/A specimen tested in fatigue at 1200°C in steam environment (maximum stress = 150 MPa, frequency = 0.1 Hz) showing matrix rich area with matrix troughs from 0° fibers.

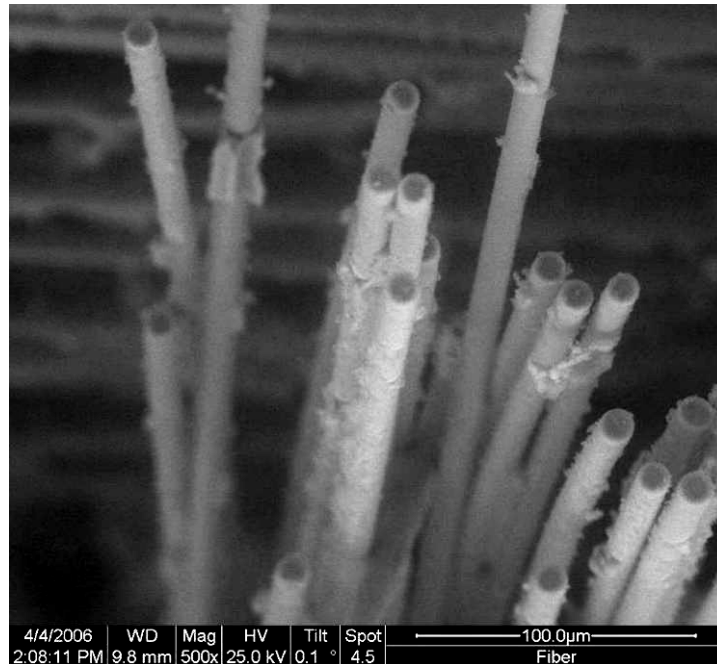


Figure 54. Fracture surface of a Nextel 720/A specimen tested in fatigue at 1200°C in steam environment (maximum stress = 125 MPa, frequency = 0.1 Hz) showing fiber pull-out.

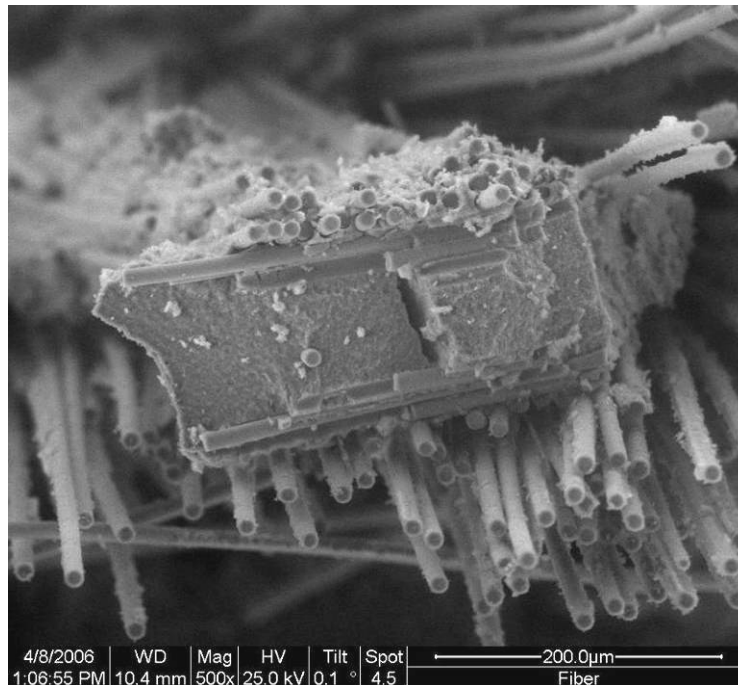


Figure 55. Fracture surface of a Nextel 720/A specimen tested in fatigue at 1200°C in steam environment (maximum stress = 125 MPa, frequency = 0.1 Hz) showing matrix rich area within 0° fiber bundle.

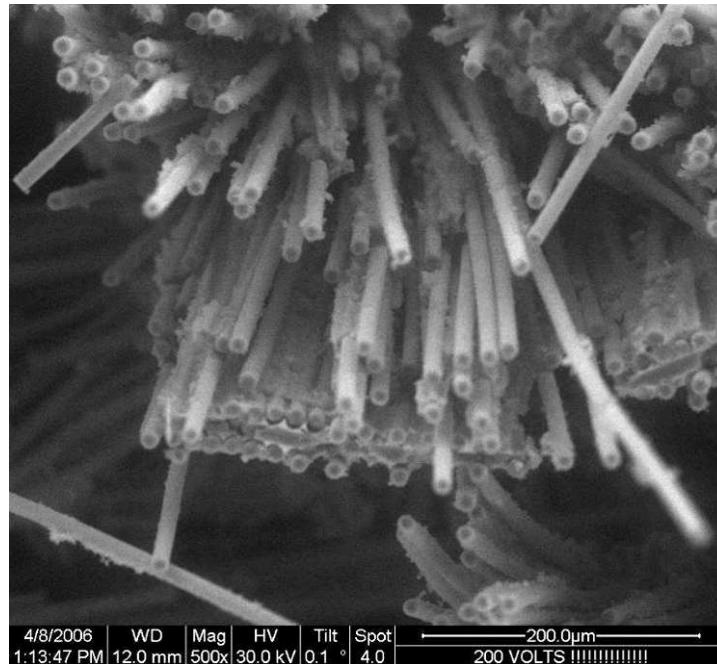


Figure 56. Fracture surface of a Nextel 720/A specimen tested in fatigue at 1200°C in steam environment (maximum stress = 125 MPa, frequency = 0.1 Hz) showing 0° fiber pull-out.

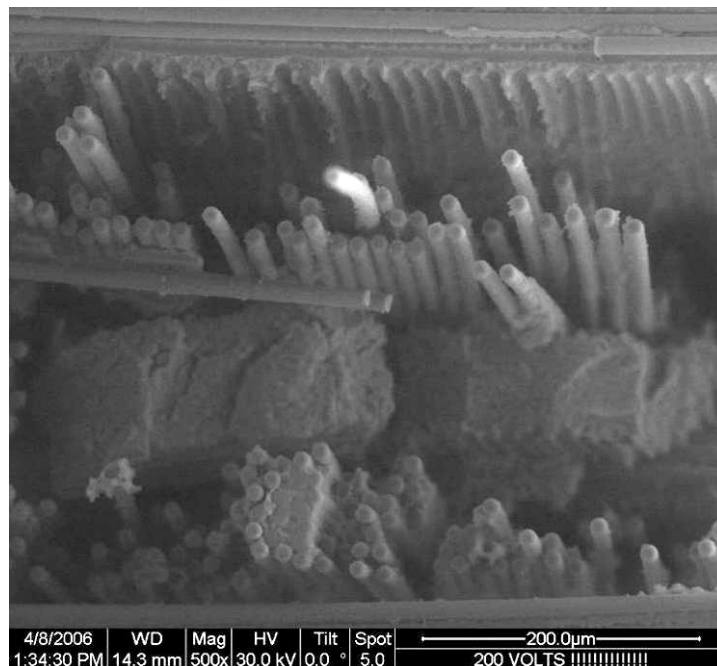


Figure 57. Fracture surface of a Nextel 720/A specimen tested in fatigue at 1200°C in steam environment (maximum stress = 125 MPa, frequency = 0.1 Hz) showing matrix rich areas with well-formed matrix troughs from 0° fibers.

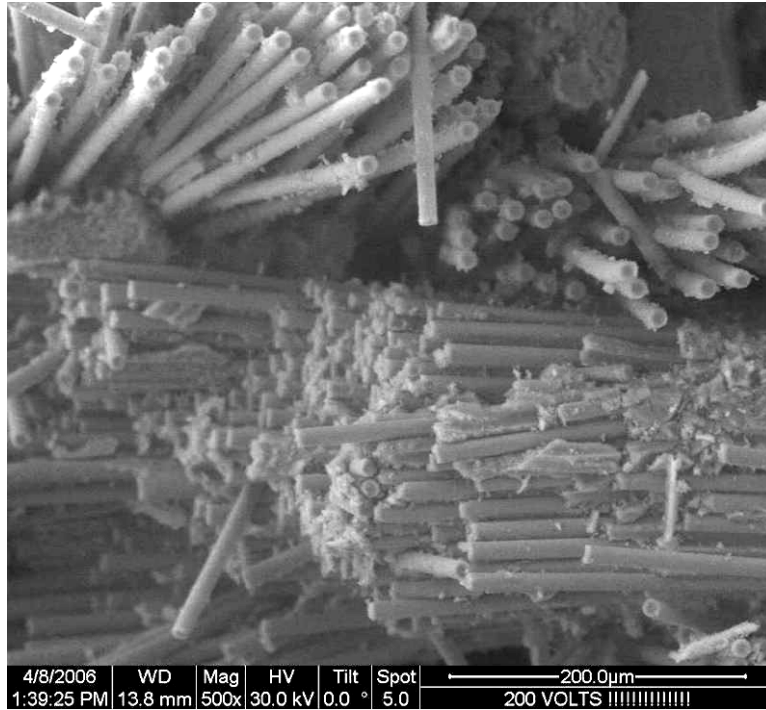


Figure 58. Fracture surface of a Nextel 720/A specimen tested in fatigue at 1200°C in steam environment (maximum stress = 125 MPa, frequency = 0.1 Hz) showing 90° fiber bundle.

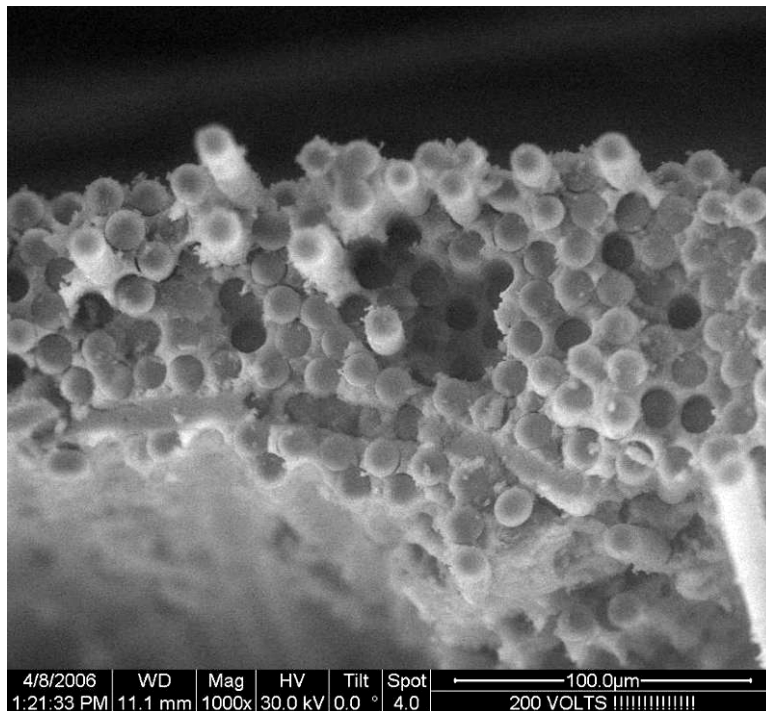


Figure 59. Fracture surface of a Nextel 720/A specimen tested in fatigue at 1200°C in steam environment (maximum stress = 125 MPa, frequency = 0.1 Hz) showing coordinated fracture.

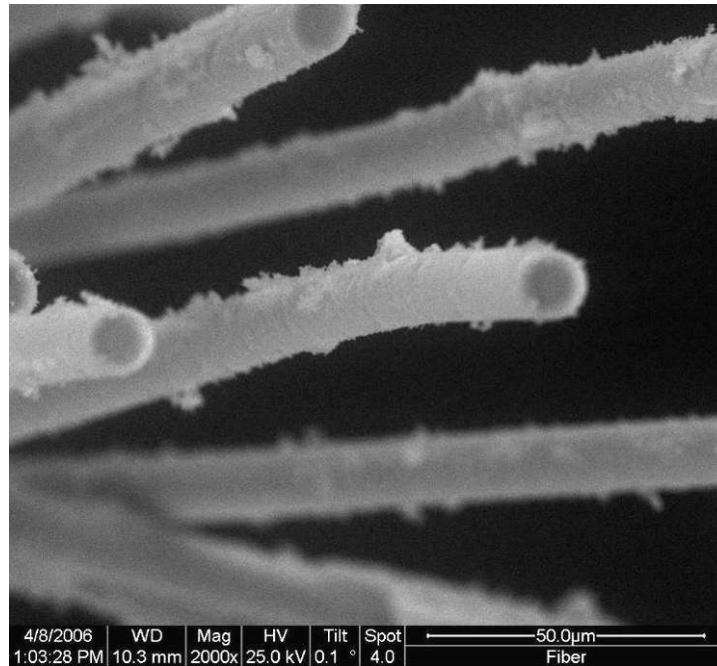


Figure 60. Fracture surface of a Nextel 720/A specimen tested in fatigue at 1200°C in steam environment (maximum stress = 125 MPa, frequency = 0.1 Hz) showing 0° fiber pull-out at high magnification.

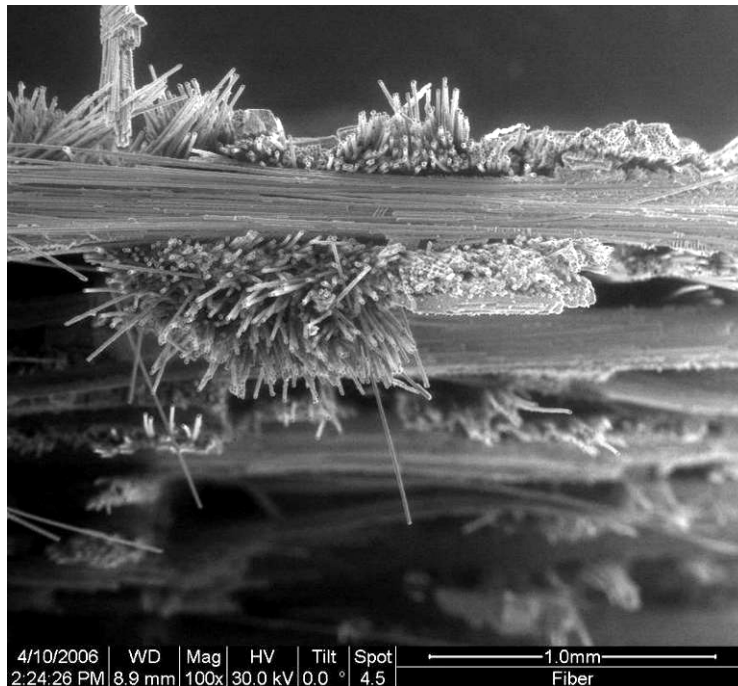


Figure 61. Fracture surface of a Nextel 720/A specimen tested in fatigue at 1200°C in steam environment (maximum stress = 100 MPa, frequency = 0.1 Hz) showing 0° and 90° fiber bundles.

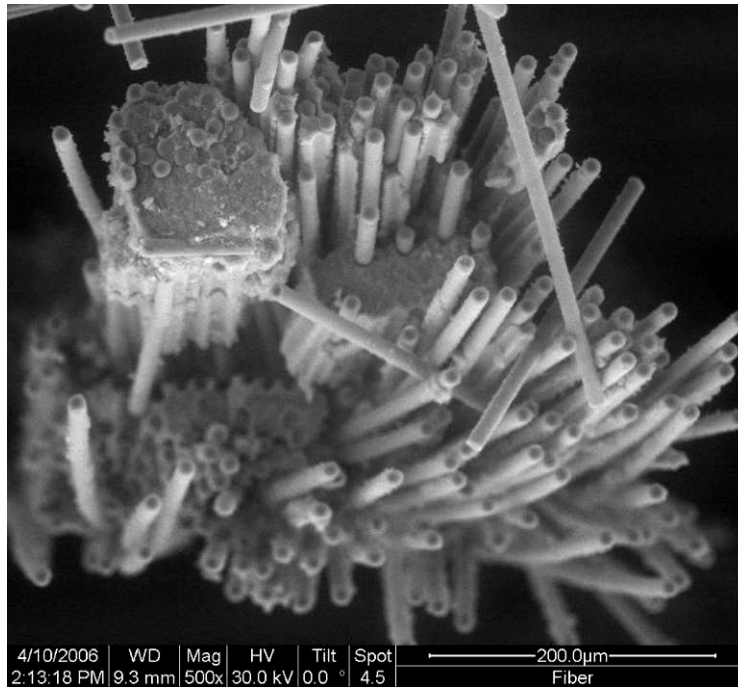


Figure 62. Fracture surface of a Nextel 720/A specimen tested in fatigue at 1200°C in steam environment (maximum stress = 100 MPa, frequency = 0.1 Hz) showing 0° fiber bundle with variation in fracture location.

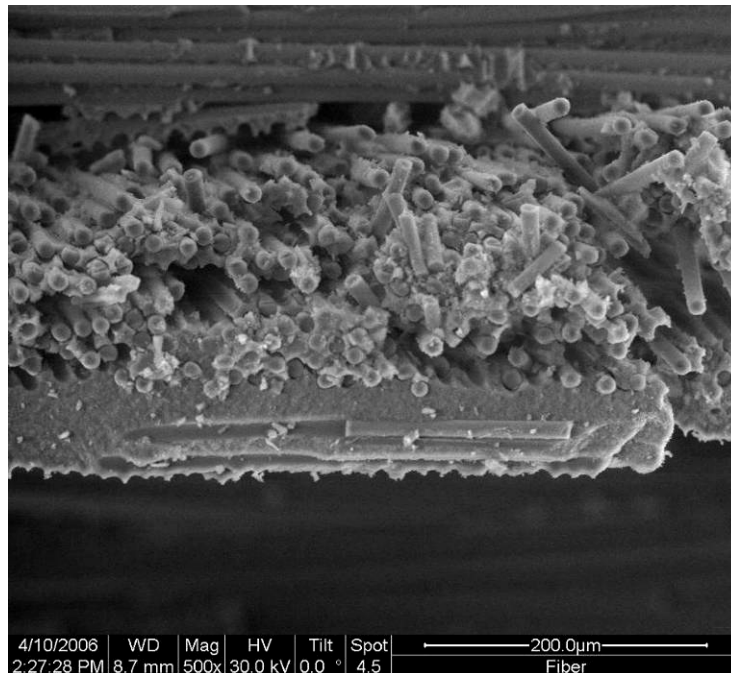


Figure 63. Fracture surface of a Nextel 720/A specimen tested in fatigue at 1200°C in steam environment (maximum stress = 100 MPa, frequency = 0.1 Hz) showing 0° fiber bundles with matrix-rich area.

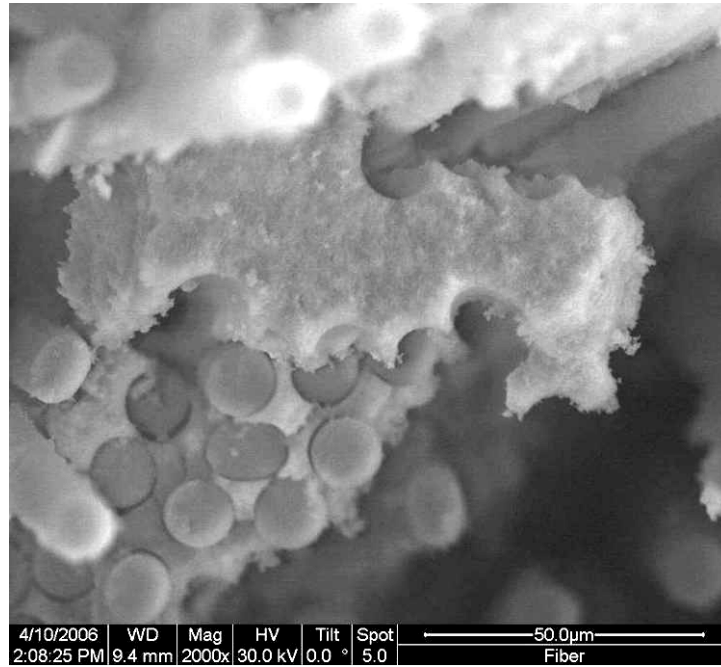


Figure 64. Fracture surface of a Nextel 720/A specimen tested in fatigue at 1200°C in steam environment (maximum stress = 100 MPa, frequency = 0.1 Hz) showing well-formed matrix shape at high magnification.

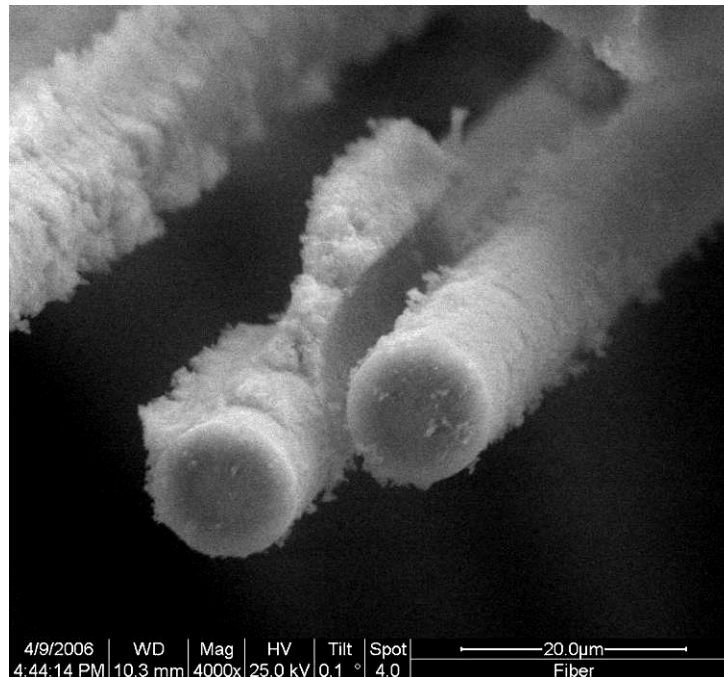


Figure 65. Fracture surface of a Nextel 720/A specimen tested in fatigue at 1200°C in steam environment (maximum stress = 100 MPa, frequency = 0.1 Hz) showing 0° pulled-out fiber surfaces.

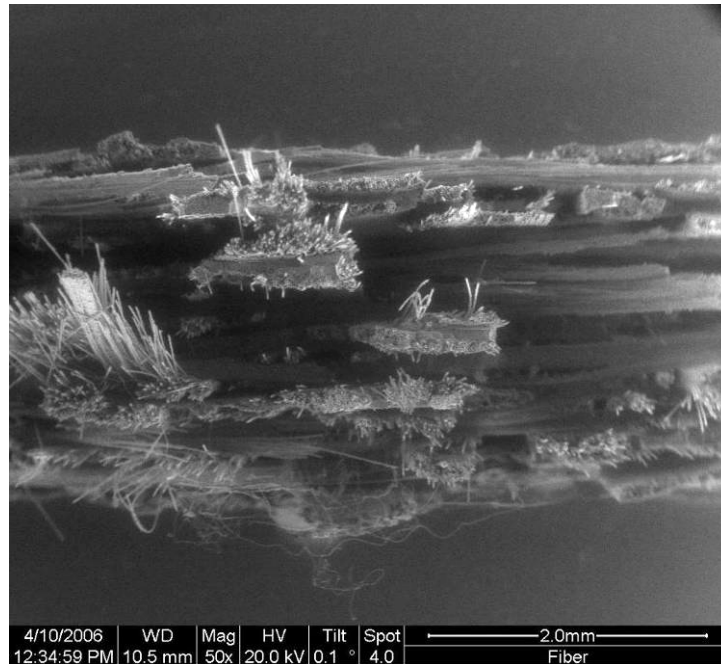


Figure 66. Fracture surface of a Nextel 720/A specimen tested in fatigue at 1200°C in steam environment (maximum stress = 75 MPa, frequency = 0.1 Hz) showing overall fracture surface.

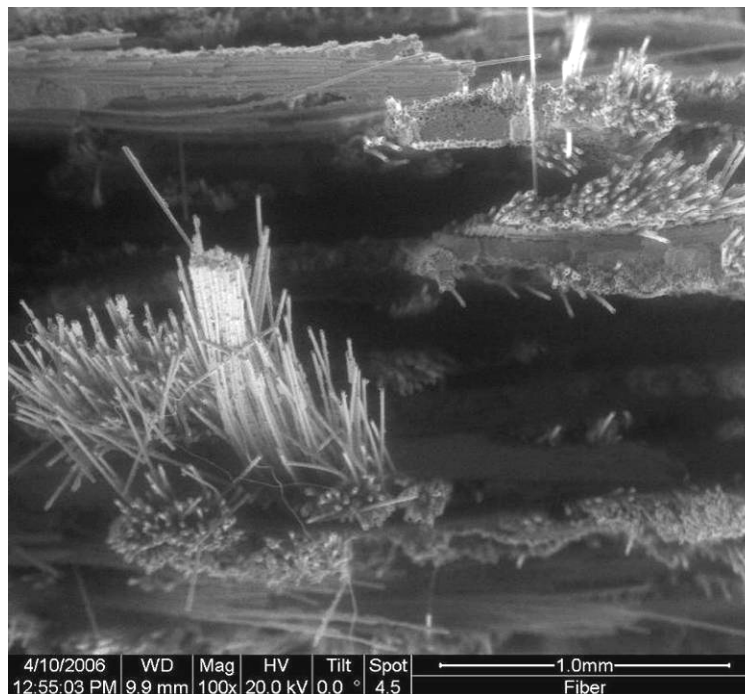


Figure 67. Fracture surface of a Nextel 720/A specimen tested in fatigue at 1200°C in steam environment (maximum stress = 75 MPa, frequency = 0.1 Hz) showing separate 0° fiber tows.

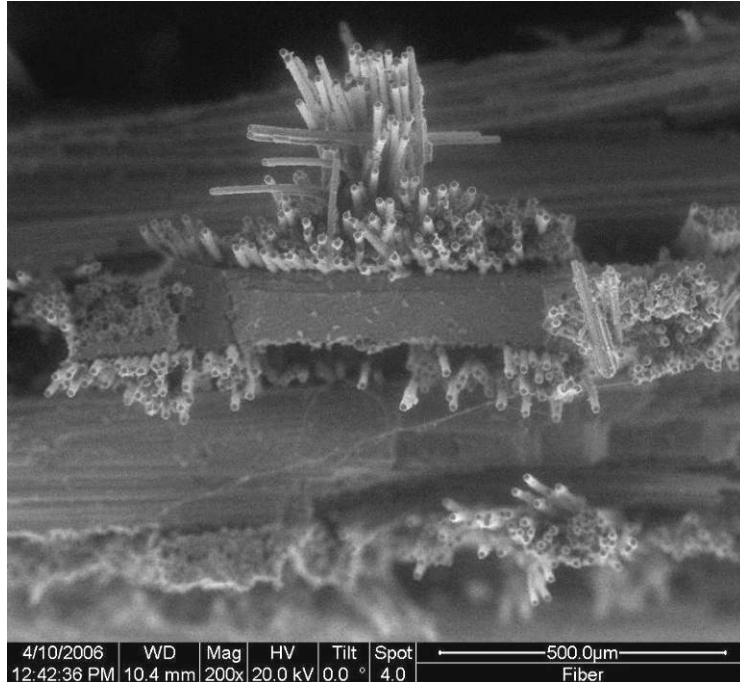


Figure 68. Fracture surface of a Nextel 720/A specimen tested in fatigue at 1200°C in steam environment (maximum stress = 75 MPa, frequency = 0.1 Hz) showing 0° fiber tow with matrix-rich areas.

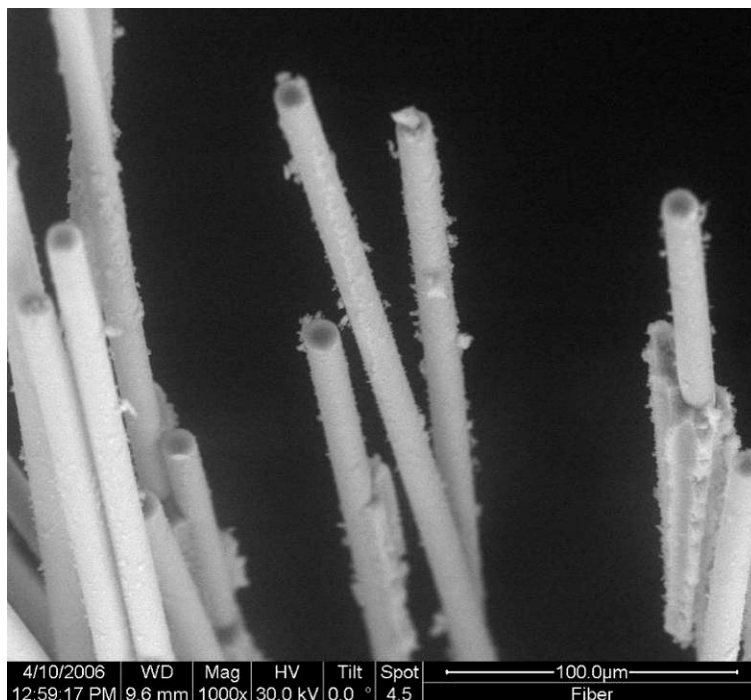


Figure 69. Fracture surface of a Nextel 720/A specimen tested in fatigue at 1200°C in steam environment (maximum stress = 75 MPa, frequency = 0.1 Hz) showing 0° pulled-out fibers.

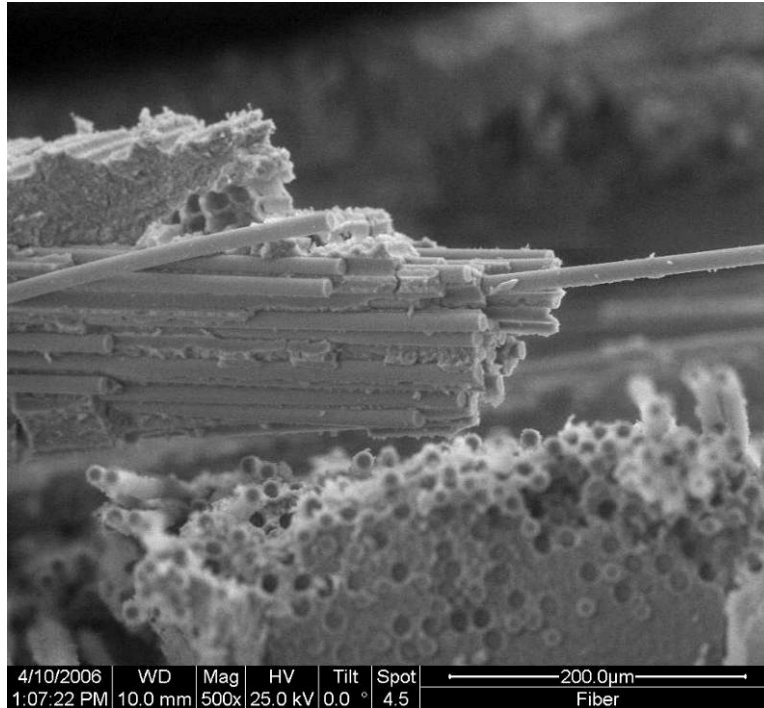


Figure 70. Fracture surface of a Nextel 720/A specimen tested in fatigue at 1200°C in steam environment (maximum stress = 75 MPa, frequency = 0.1 Hz) showing separate 90° fiber tow with matrix rich area and pull-out.

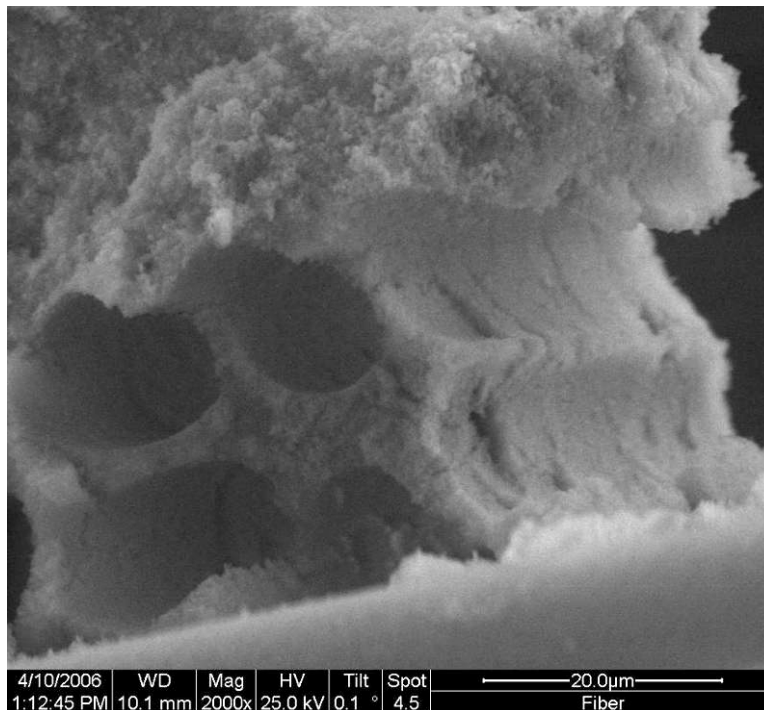


Figure 71. Fracture surface of a Nextel 720/A specimen tested in fatigue at 1200°C in steam environment (maximum stress = 75 MPa, frequency = 0.1 Hz) showing matrix cavities from 0° fibers.

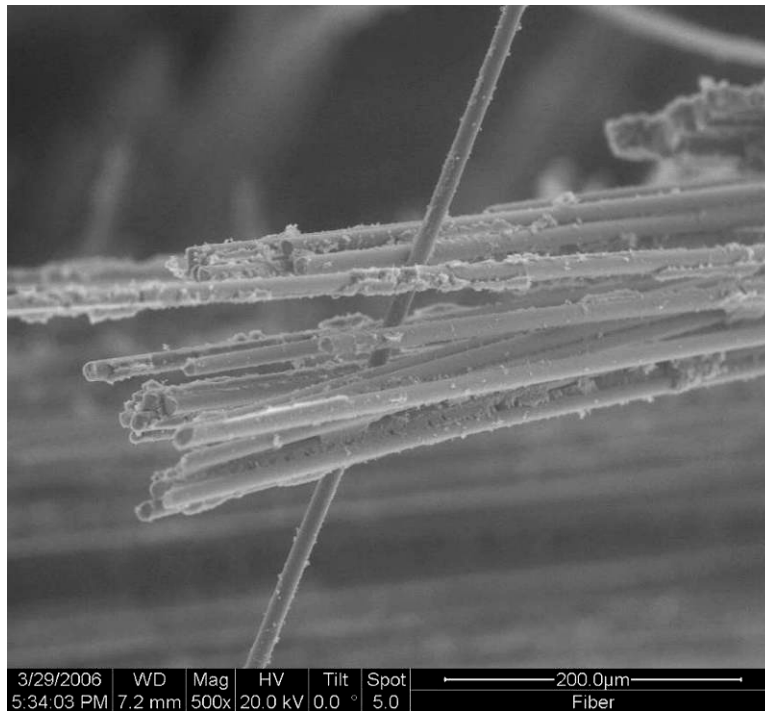


Figure 72. Fracture surface of a Nextel 720/A specimen tested in fatigue at 1200°C in steam environment (maximum stress = 170 MPa, frequency = 10 Hz) showing 90° fibers.

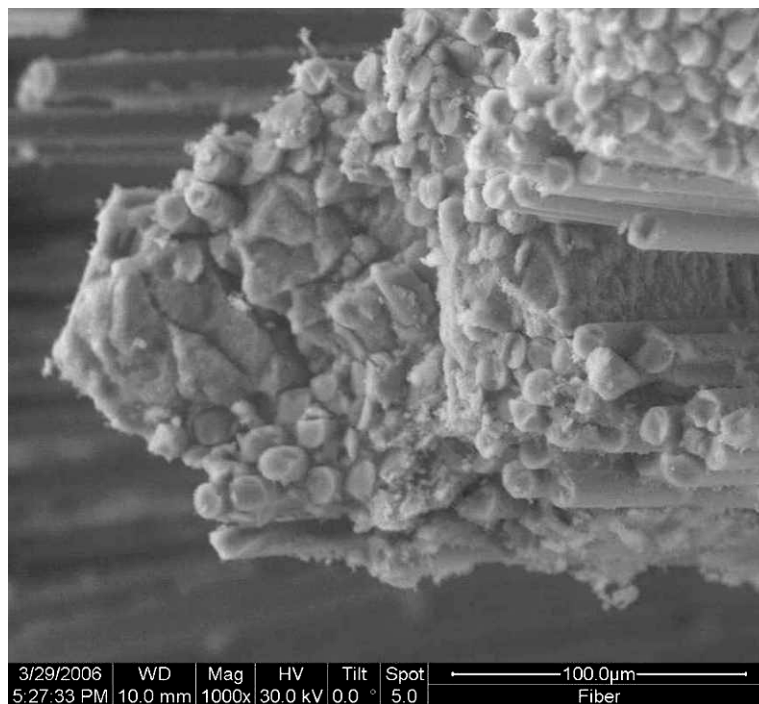


Figure 73. Fracture surface of a Nextel 720/A specimen tested in fatigue at 1200°C in steam environment (maximum stress = 170 MPa, frequency = 10 Hz) showing 90° fiber bundle.

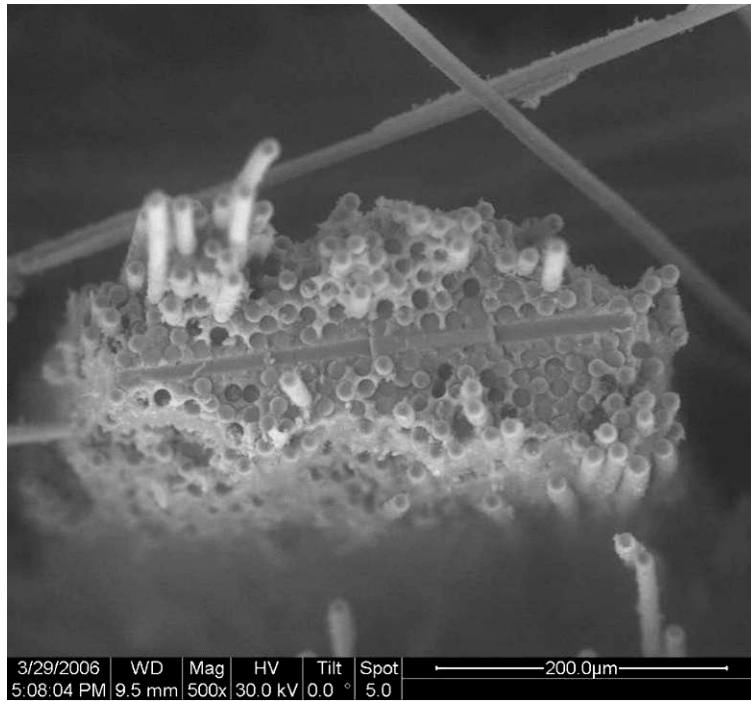


Figure 74. Fracture surface of a Nextel 720/A specimen tested in fatigue at 1200°C in steam environment (maximum stress = 170 MPa, frequency = 10 Hz) showing 0° fiber bundle.

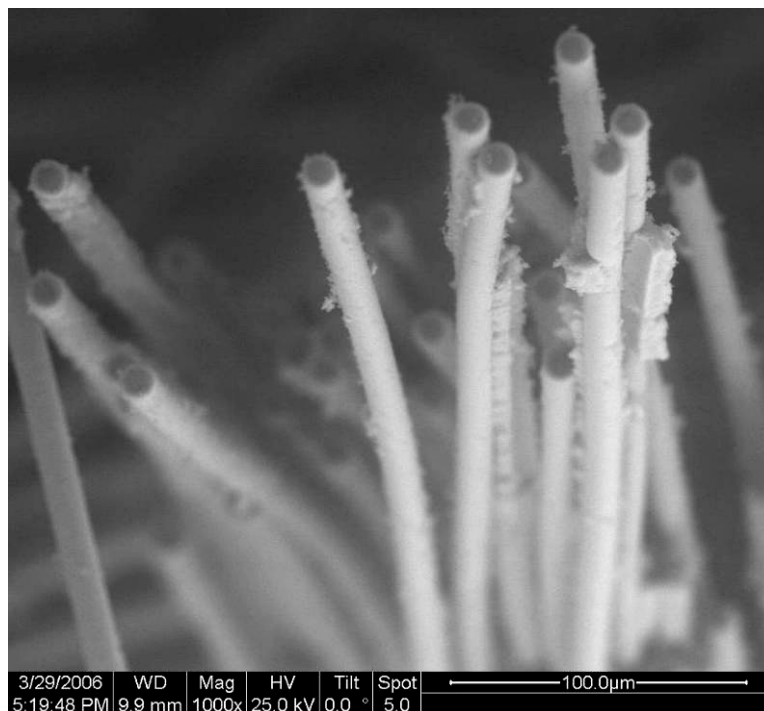


Figure 75. Fracture surface of a Nextel 720/A specimen tested in fatigue at 1200°C in steam environment (maximum stress = 170 MPa, frequency = 10 Hz) showing 0° fiber pull-out.

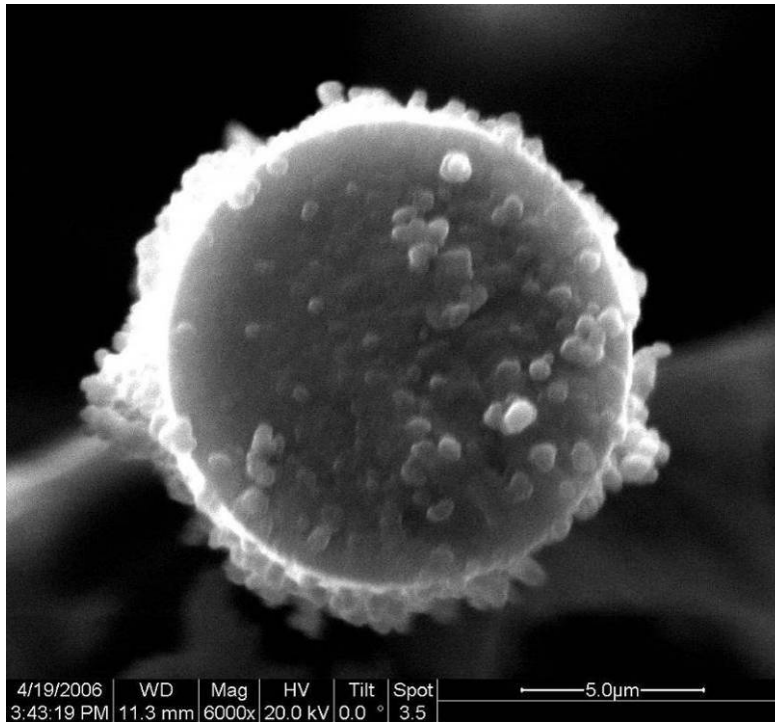


Figure 76. Fracture surface of a Nextel 720/A specimen tested in fatigue at 1200°C in steam environment (maximum stress = 170 MPa, frequency = 0.1 Hz) showing 0° fiber surface.

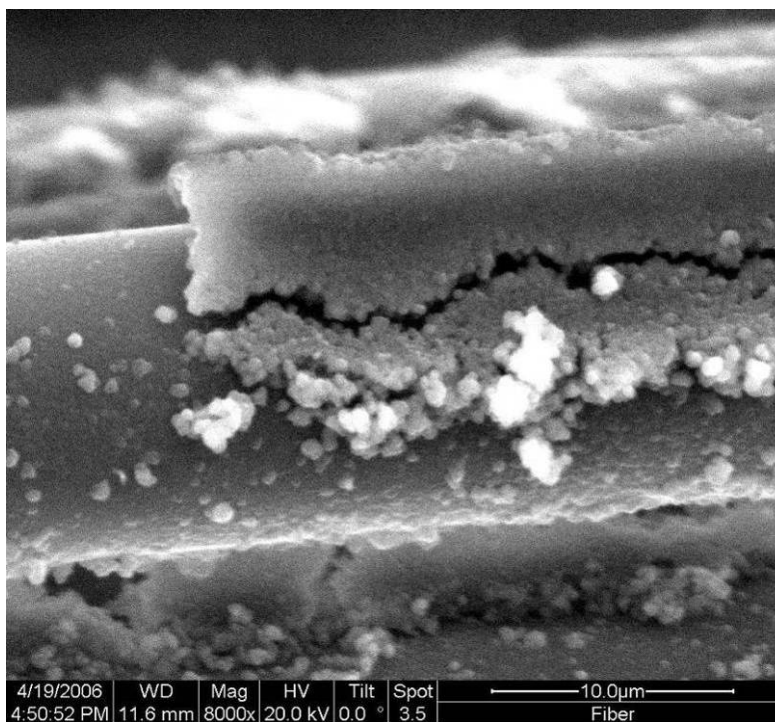


Figure 77. Fracture surface of a Nextel 720/A specimen tested in fatigue at 1200°C in steam environment (maximum stress = 170 MPa, frequency = 0.1 Hz) showing 90° fiber with pieces of matrix attached.

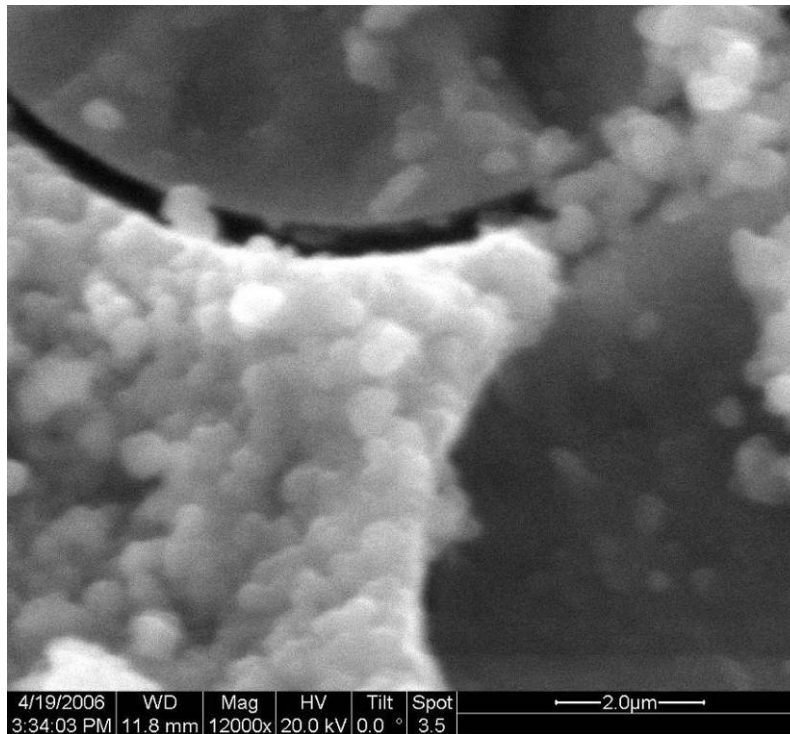


Figure 78. Fracture surface of a Nextel 720/A specimen tested in fatigue at 1200°C in steam environment (maximum stress = 170 MPa, frequency = 0.1 Hz) showing matrix infiltration between fibers in a 0° fiber tow.

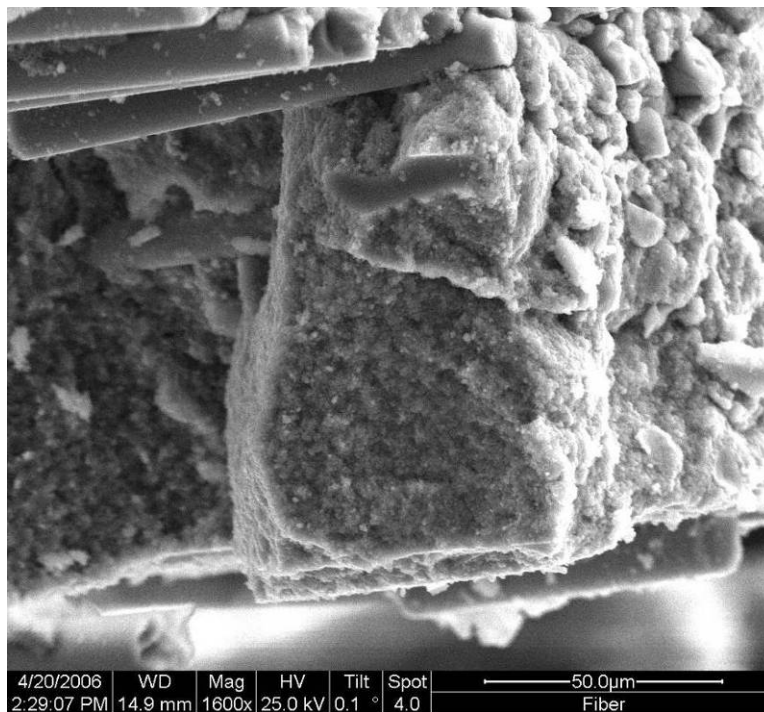


Figure 79. Fracture surface of a Nextel 720/A specimen tested in fatigue at 1200°C in steam environment (maximum stress = 170 MPa, frequency = 10 Hz) showing matrix rich area.

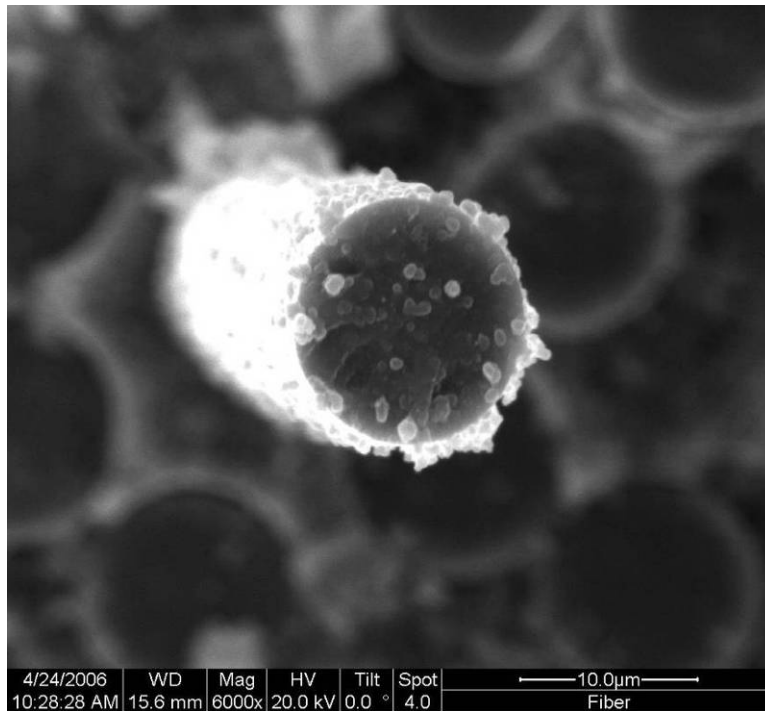


Figure 80. Fracture surface of a Nextel 720/A specimen tested in fatigue at 1200°C in steam environment (maximum stress = 170 MPa, frequency = 10 Hz) showing surface of a pulled out 0° fiber.

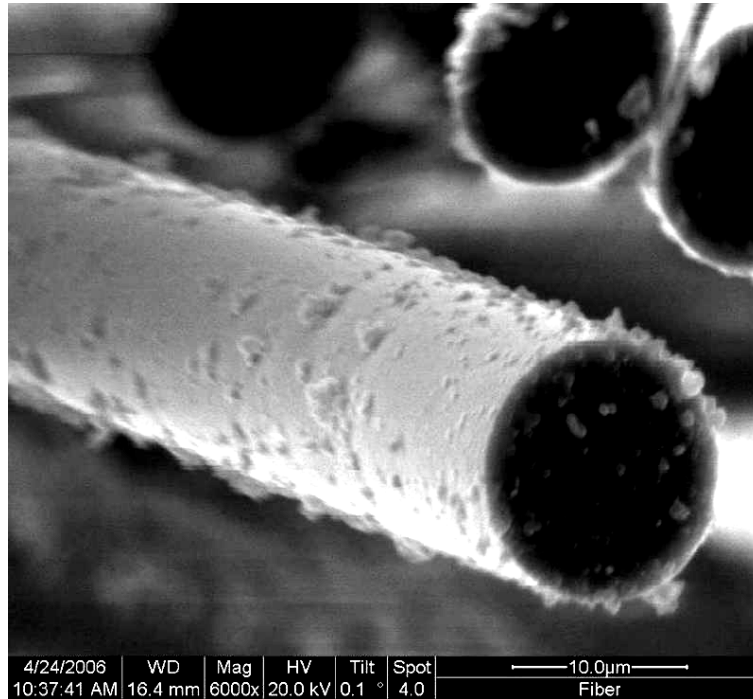


Figure 81. Fracture surface of a Nextel 720/A specimen tested in fatigue at 1200°C in steam environment (maximum stress = 170 MPa, frequency = 10 Hz) showing surface of pulled out 0° fibers.

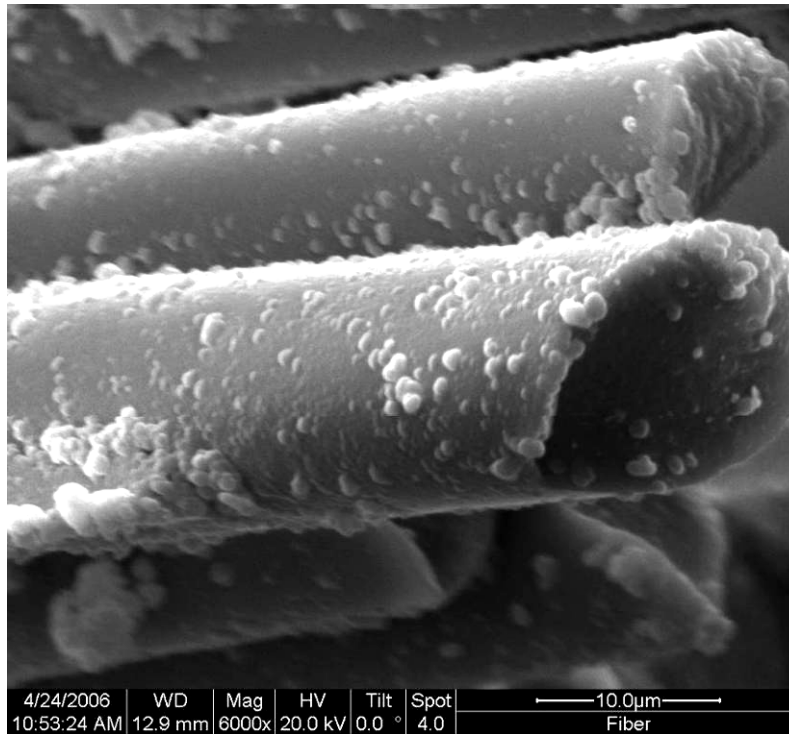


Figure 82. Fracture surface of a Nextel 720/A specimen tested in fatigue at 1200°C in steam environment (maximum stress = 170 MPa, frequency = 10 Hz) showing surface of 90° fibers.

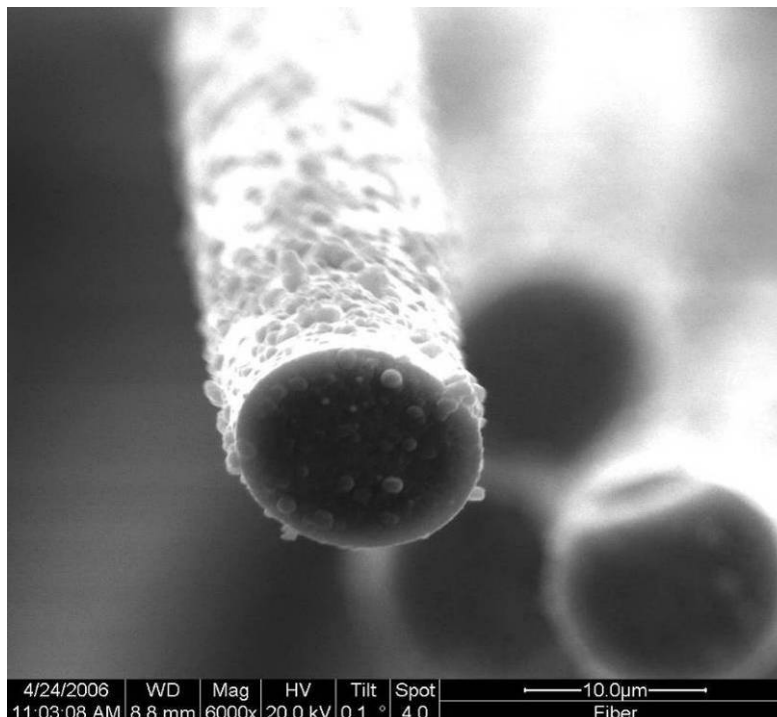


Figure 83. Fracture surface of a Nextel 720/A specimen tested in fatigue at 1200°C in steam environment (maximum stress = 170 MPa, frequency = 10 Hz) showing surface of a pulled out 0° fiber.

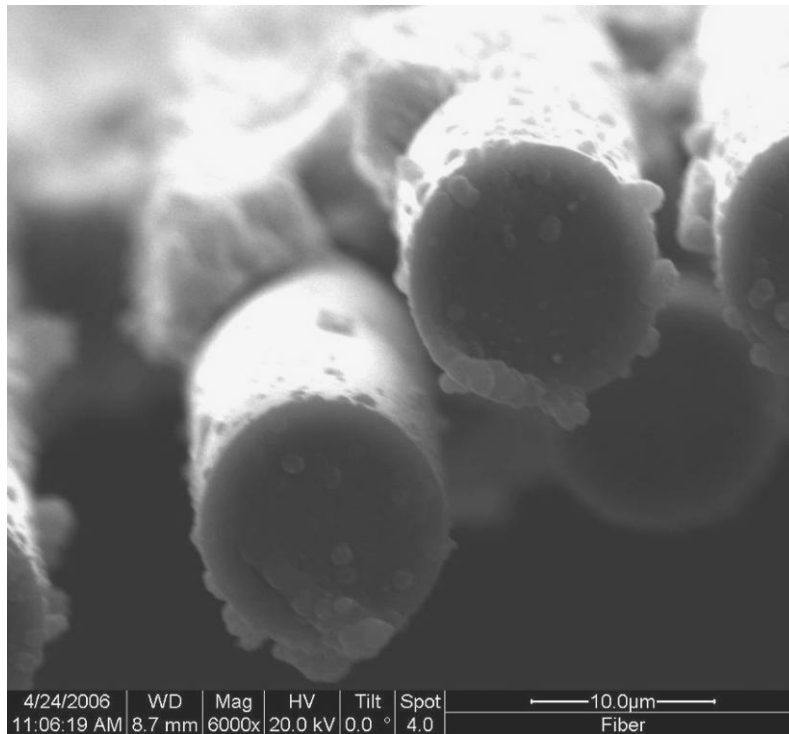


Figure 84. Fracture surface of a Nextel 720/A specimen tested in fatigue at 1200°C in steam environment (maximum stress = 170 MPa, frequency = 10 Hz) showing surface of pulled out 0° fibers.

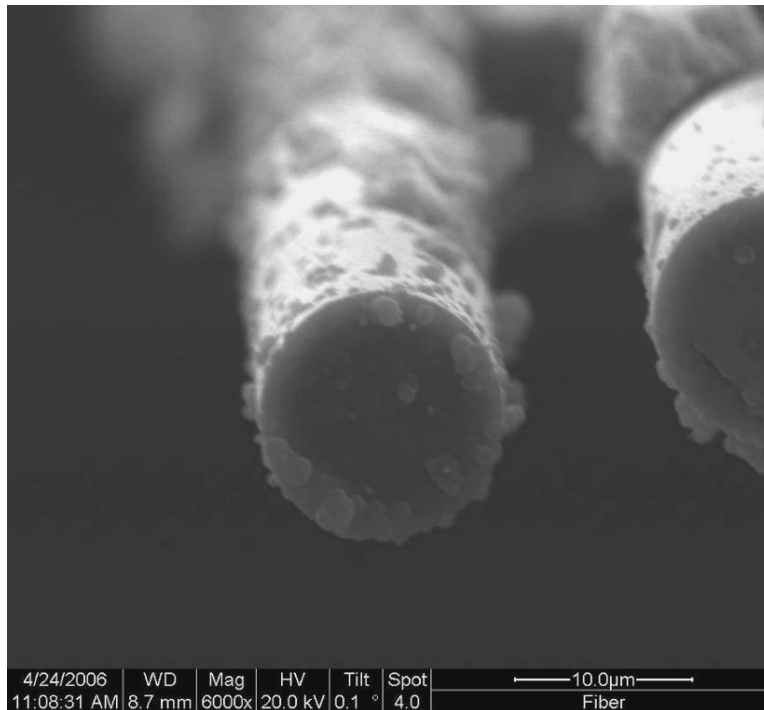


Figure 85. Fracture surface of a Nextel 720/A specimen tested in fatigue at 1200°C in steam environment (maximum stress = 170 MPa, frequency = 10 Hz) showing surface of pulled out 0° fiber

Bibliography

1. Baek, S., private communications (2006).
2. Barinov, S.M., Nikolai, V.I., Orlov, S.V., and Shevchenko, V.J. "Influence of Environment on Delayed Failure of Alumina Ceramics," *Journal of the European Ceramic Society*, 18:2057-2063 (1998).
3. Chawla, N., Kerr, M., Chawla, K.K. "Monotonic and Cyclic Fatigue Behavior of High-Performance Ceramic Fibers," *Journal of the American Ceramic Society*, 88(1):101-108 (2005).
4. Chawla, K. K. *Ceramic Matrix Composites*. London: Chapman and Hall, 1993.
5. COI Ceramics, Unpublished Data.
6. Deve, H.E. and McCullough, C. "High Performance Aluminum/Alumina Composites," *High Performance Metal and Ceramic Matrix Composites*, Upadhya, K. Ed., The Minerals, Metals, and Materials Society (1994).
7. Deleglise, F., Berger, M.H., and Bunsell, A.R., "Microstructural evolution under load and high temperature deformation mechanisms of a mullite/alumina fibre," *Journal of the European Ceramic Society*, 22:1501-1512 (2002).
8. Eber, C.A. *Effect of Temperature and Steam Environment on Fatigue Behavior of an Oxide-Oxide Continuous Fiber Ceramic Composite*. MS thesis, AFIT/GA/ENY/05-M09. School of Engineering and Management, Air Force Institute of Technology (AU), Wright-Patterson AFB, OH March 2005.
9. Gladysz, G.M. and Chawla, K.K. "Coefficients of thermal expansion of some laminated ceramic composites," *Composites: Part A*, 32:173-178 (2001).
10. Goldstein, J.I., Newbury, D.E., Echlin, P., Joy, D.C., Fiori, C., and Lifshin, E. *Scanning Electron Microscopy and X-Ray Microanalysis*. New York: Plenum Press, 1981.
11. Harlan, L.B. *Creep-Rupture Behavior of an Oxide/Oxide Ceramic Matrix Composite at Elevated Temperatures in Air and Steam Environments*. MS thesis, AFIT/GA/ENY/05-M05. School of Engineering and Management, Air Force Institute of Technology (AU), Wright-Patterson AFB, OH, March 2005.
12. Haslam, J.J., Berroth, K.E., and Lange, F.F. "Processing and Properties of an all-oxide composite with a porous matrix," *Journal of the European Ceramic Society*, 20:607-618 (2000).

13. Hazell, M. "Ceramic Matrix Composites for Industrial Gas Turbines," *Metal and Ceramic Matrix Composites*, Cantor, B., Dunne, F.P.E., and Stone, I.C. Eds., Institute of Physics Publishing (2004).
14. Holmes, J.W., Wu, X., and Sorensen, B.F. "Frequency Dependence of Fatigue Life and Internal Heating of a Fiber-Reinforced/Ceramic-Matrix Composite," *Journal of the American Ceramic Society*, 77(12):3284-3286 (1994).
15. Holmes, J.W. and Vanswijghoven, E.L. "Does a True Fatigue Limit Exist for Continuous Fiber-Reinforced Ceramic Matrix Composites?," *Journal of the American Ceramic Society*, 85(2):359-365 (2002).
16. Holmquist, M.G. and Lange, F.F. "Processing and Properties of a Porous Oxide Matrix Composite Reinforced with Continuous Oxide Fibers," *Journal of the American Ceramic Society*, 86[10]:1799-40 (2003).
17. Kaya, C., Butler, E.G., Selcuk, A., Boccaccini, A.R., and Lewis, M.H. "Mullite (Nextel™ 720) fibre-reinforced mullite matrix composites exhibiting favourable thermomechanical properties," *Journal of the European Ceramic Society*, 22: 2333-2342 (2002).
18. Kerans, R.J. and Parthasarathy, T.A. "Crack deflection in ceramic composites and fiber coating design criteria," *Composites: Part A*, 30:521-524 (1999).
19. Kooner, S., Westby, W.S., Watson, C.M.A., and Farries, P.M. "Processing of Nextel™720/mullite composition composite using electrophoretic deposition," *Journal of the European Ceramic Society*, 20:631-638 (2000).
20. Kruzic, J.J., Cannon, R.M., and Ritchie, R.O. "Effects of Moisture on Grain-Boundary Strength, Fracture, and Fatigue Properties of Alumina," *Journal of the American Ceramic Society*, 88(8): 2236-2245 (2005).
21. Mattoni, M.A., Yang, J.Y., Levi, C.G., and Zok, F.W. "Effects of Combustor Rig Exposure on a Porous-Matrix Oxide Composite," *International Journal of Applied Ceramic Technology*, 2(2):133-140 (2005).
22. Mecham, M. "Composite Power," *Aviation Week & Space Technology*, 17 April 2006.
23. Mehrman, J.M. *Effect of Hold Times on Fatigue Behavior of Nextel™ 720/Alumina Ceramic Matrix Composite at 1200°C in Air and in Steam Environment*. MS thesis, AFIT/GA/ENY/06-M23. School of Engineering and Management, Air Force Institute of Technology (AU), Wright-Patterson AFB, OH March 2006.

24. Musikant, S. *What Every Engineer Should Know About Ceramics*. New York: Marcel Dekker, 1991.
25. Nutt, S.R., "Environmental Effects on High Temperature Mechanical Behavior of Ceramic Matrix Composites," *High Temperature Mechanical Behavior of Ceramic Composites*. Newton, MA: Butterworth-Heinemann, 1995.
26. Oates, G.C. *Aerothermodynamics of Gas Turbine and Rocket Propulsion*, 3rd Ed. Reston, VA: American Institute of Aeronautics and Astronautics, Inc 1997.
27. Ohnabe, H., Masaki, S., Onozuka, M., Miyahara, K., Sasa, T. "Potential application of ceramic matrix composites to aero-engine components," *Composites: Part A*, 30:489-496 (1999).
28. Parthasarathy, T.A., Zawada, L.P., John, R., Cinibulk, M. K., Kerans, R. J., and Zelina, J. "Evaluation of Oxide-Oxide Composites in a Novel Combustor Wall Application," *International Journal of Applied Ceramic Technology*, 2 (2):122-132 (2005).
29. Parlier, M. and Ritti, M.H. "State of the art and perspectives for oxide/oxide composites," *Aerospace Science and Technology*, 7:211-221 (2003).
30. Radsick, T., Saruhan, B., and Schneider, H. "Damage tolerant oxide/oxide fiber laminate composites," *Journal of the European Ceramic Society*, 20:545-550 (2000).
31. Ramulu, M., Prasad, N.E., Malakondaiah, G. and Guo, Z. "Secondary Processing Effects and Damage Mechanisms in Continuous-Fiber Ceramic Composites," *Thermal and Mechanical Test Methods and Behavior of Continuous-Fiber Ceramic Composites*, ASTM STP 1309, Michael G. Jenkins, Stephan T. Gonczy, Edgar Lara-Curzio, Noel E. Ashbaugh, and Larry P. Zawada, Eds., American Society for Testing and Materials (1997).
32. Raymer, D.P. *Aircraft Design: A Conceptual Approach*, 3rd Ed. Reston, VA: American Institute of Aeronautics and Astronautics, Inc, 1999.
33. Reynaud, P., Dalmaz, A., Tallaron, C., Rouby, D., and Fantozzi, G. "Apparent Stiffening of Ceramic-matrix Composites Induced by Cyclic Fatigue," *Journal of the European Ceramic Society*, 18:1827-1833 (1998)
34. Rice, R.W. *Porosity of Ceramics*. New York: Marcel Dekker, 1998.
35. Ruggles-Wrenn, M.B., Mall, S., Eber, C.A., and Harlan, L.B. "Effects of Steam Environment on High-Temperature Mechanical Behavior of Nextel™720/Alumina (N720/A) Continuous Fiber Ceramic Composite", *Composites: Part A*, in press (2006).

36. Ruggles-Wrenn, M.B., Corum, J.M., and Battiste, R.L. "Short-term static and cyclic behavior of two automotive carbon-fiber composites," *Composites: Part A*, 30:731-741 (2003).
37. Ruggles-Wrenn, M.B., private communications (2006).
38. Schmidt, S., Beyer, S., Knabe, H., Immich, H., Mestring, R., and Gessler, A. "Advanced ceramic matrix composite materials for current and future propulsion technology applications," *Acta Astronautica*, 55:409-420 (2004).
39. Shi, B., Chu, W.Y., Su, Y.J., Gao, K.W., and Qiao, L.J. "Stress Corrosion Cracking and Hydrogen-Induced Cracking of an Alumina Ceramic," *Journal of the American Ceramic Society*, 88(2):353-356 (2005).
40. Simon, R. A. "Progress in Processing and Performance of Porous-Matrix Oxide/Oxide Composites," *International Journal of Applied Ceramic Technology*, 2(2):141-149 (2005).
41. Sorensen, B.F., Holmes, J.W., and Vanswijgenhoven, E.L. "Does a True Fatigue Limit Exist for Continuous Fiber-Reinforced Ceramic Matrix Composites?" *Journal of the American Ceramic Society*, 85:359-365 (2002).
42. Tressler, R.E. "Recent developments in fibers and interphases for high temperature ceramic matrix composites," *Composites: Part A*, 30:429-437 (1999).
43. Upadhy, K. "Recent Developments In Composite Materials; A Critical Review," *High Performance Metal and Ceramic Matrix Composites*, Upadhy, K., Ed., The Minerals, Metals, and Materials Society (1994).
44. Wannaparhun, S., Seal, S., and Desai, V. "Surface chemistry of Nextel-720, alumina and Nextel-720/alumina ceramic matrix composite (CMC) using XPS-A tool for nano-spectroscopy," *Applied Surface Science*, 185:183-196 (2002).
45. Watt, I.M. *The Principles and Practice of Electron Microscopy*. Cambridge: Cambridge University Press, 1989.
46. Wilson, D.M. and Visser, L.R. "High performance oxide fibers for metal and ceramic composites," *Composites: Part A*, 32:1143-1153 (2001).
47. Zawada, L.P. "Longitudinal and transthickness tensile behavior of several oxide/oxide composites," *Ceramic Science and Engineering Proceedings*, 19(3):327-340 (1998).

48. Zawada, L.P. and Lee, S.S. "The Effect of Hold Times on the Fatigue Behavior of an Oxide/Oxide Ceramic Matrix Composite," *Thermal and Mechanical Test Methods and Behavior of Continuous-Fiber Ceramic Composites, ASTM STP 1309*, Michael G. Jenkins, Stephan T. Gonczy, Edgar Lara-Curzio, Noel E. Ashbaugh, and Larry P. Zawada, Eds., American Society for Testing and Materials (1997).

Vita

Ensign Griffin Hetrick was raised in East Napa, California. He graduated from Vintage High School in Napa in 2001 and entered undergraduate studies at Rice University in Houston, Texas in the fall of the same year. In May of 2005 he graduated Magna Cum Laude as a Bachelor of Science in Mechanical Engineering. He was commissioned through the Houston Consortium Naval Reserve Officers Training Corps unit.

Ensign Hetrick's first assignment was to the Graduate School of Engineering and Management, Air Force Institute of Technology, as a participant in the Immediate Graduate Education (IGEP) program. Upon graduation in June of 2006, he will report to NAS Pensacola, Florida, for training as a student naval aviator.

REPORT DOCUMENTATION PAGE				Form Approved OMB No. 074-0188	
<p>The public reporting burden for this collection of information is estimated to average 1 hour per response, including the time for reviewing instructions, searching existing data sources, gathering and maintaining the data needed, and completing and reviewing the collection of information. Send comments regarding this burden estimate or any other aspect of the collection of information, including suggestions for reducing this burden to Department of Defense, Washington Headquarters Services, Directorate for Information Operations and Reports (0704-0188), 1215 Jefferson Davis Highway, Suite 1204, Arlington, VA 22202-4302. Respondents should be aware that notwithstanding any other provision of law, no person shall be subject to a penalty for failing to comply with a collection of information if it does not display a currently valid OMB control number.</p> <p>PLEASE DO NOT RETURN YOUR FORM TO THE ABOVE ADDRESS.</p>					
1. REPORT DATE (DD-MM-YYYY) 13-06-2006		2. REPORT TYPE Master's Thesis		3. DATES COVERED (From – To) Aug 2005 – Jun 2006	
4. TITLE AND SUBTITLE Effects of Frequency and Environment on Fatigue Behavior of an Oxide-oxide Ceramic Matrix Composite at 1200°C				5a. CONTRACT NUMBER	
				5b. GRANT NUMBER	
				5c. PROGRAM ELEMENT NUMBER	
6. AUTHOR(S) Hetrick, Griffin, Ensign, USN				5d. PROJECT NUMBER 2006-097	
				5e. TASK NUMBER	
				5f. WORK UNIT NUMBER	
7. PERFORMING ORGANIZATION NAMES(S) AND ADDRESS(S) Air Force Institute of Technology Graduate School of Engineering and Management (AFIT/EN) 2950 Hobson Way WPAFB OH 45433-7765				8. PERFORMING ORGANIZATION REPORT NUMBER AFIT/GAE/ENY/06-J05	
9. SPONSORING/MONITORING AGENCY NAME(S) AND ADDRESS(ES) AFRL/PRTC Attn: Dr. Ruth Sikorski and Dr Joseph Zelina 1950 5th Street WPAFB OH 45433-7251 DSN: 785-7268				10. SPONSOR/MONITOR'S ACRONYM(S)	
				11. SPONSOR/MONITOR'S REPORT NUMBER(S)	
12. DISTRIBUTION/AVAILABILITY STATEMENT APPROVED FOR PUBLIC RELEASE; DISTRIBUTION UNLIMITED.					
13. SUPPLEMENTARY NOTES					
14. ABSTRACT <p>Advances in aeronautical engineering in the 21st century depend upon materials that can perform well in extreme environments such as high temperatures and oxidizing conditions. Nextel™720/Alumina (N720/A) is an oxide/oxide ceramic matrix composite with a porous alumina matrix that has been identified as a candidate material for such applications. This research investigated the effects of frequency on fatigue response of N720/A at 1200°C in both air and steam environment. Prior investigation of this material by Eber [8] in 2005 studied fatigue behavior at 1200°C in air and in steam environments at the frequency of 1.0 Hz. The current research focused on fatigue response at the frequencies of 0.1 Hz and 10 Hz.</p> <p>Results of mechanical testing showed a significant decrease in fatigue performance in steam versus air. Specimens tested at 0.1 Hz exhibited shorter fatigue lives and smaller strains at failure than those tested at 10 Hz. Scanning Electron Micrographs of specimen fracture surfaces revealed higher degrees of fiber pull-out and greater variation in fiber failure locations in specimens tested at 10 Hz, indicating a weakening of the fiber/matrix interface. Qualitative assessment using Energy Dispersive Spectroscopy showed correlations between frequency and amount of silicon species migration between fiber and matrix.</p>					
15. SUBJECT TERMS Ceramic Matrix Composites, Oxide-oxide, Nextel™ 720 Fiber, Fatigue					
16. SECURITY CLASSIFICATION OF:			17. LIMITATION OF ABSTRACT	18. NUMBER OF PAGES	19a. NAME OF RESPONSIBLE PERSON
REPORT	ABSTRACT	c. THIS PAGE			Dr. Marina Ruggles-Wrenn
U	U	U	UU	118	19b. TELEPHONE NUMBER (Include area code) (937) 255-3636 x 4641; marina.ruggles-wrenn@afit.edu